Quantification of Energy Conversion Efficiency of a Micromotor System and Its Applications

Wenyu Zhang

Doshisha University

Chapter 1: Introduction 1
1.1 Micromotor System 2
1.2 Electric Micromotor System 3
1.2.1 Input 8
1.2.2 Output 8
1.2.3 Energy Conversion Efficiency 9
1.3 Future Application of the Micromotor System 9
1.4 The purpose of this Study 9
References: 11
Chapter 2: Energy Consumption and Conversion Efficiency for a Micromotor under DC Voltage 27
2.1. Introduction 28
2.2. Method 30
2.2.1 Equipment and Software 30
2.2.2 Chemical Reagent 30
2.2.3 Preparation 31
2.3. Results and Discussion 33
2.3.1. Water Droplet Motion 33
2.3.2. Electrolysis of the Water Droplet 38
2.3.3. Energy Conversion Efficiency 42
2.4. Conclusion 45
References 46
Chapter 3: Energy Flux on a Micromotor Operating under Stationary Direct Current Voltage 51
3.1. Introduction 52
3.2. Method 54
3.2.1. Equipment and Software 54
3.2.2. Chemical Reagent 54
3.2.3. Preparation 55
3.3. Result and Discussion 57
3.3.1. Microparticle Motions 57
3.3.1.1. Revolving Motion and Viscous Drag 60
3.3.1.2. Spinning Motion and Viscous Torque 63
3.3.2. Quantitative Analysis of a Micromotor Power 66

3.3.2.1. Dependency on Voltage 66
3.3.2.2. Dependency on Surfactant Concentration 68
3.3.2.3. Energy Conversion Efficiency 70
3.4. Conclusion 74
References: 75
Chapter 4: Increase in Output Power at the Cost of Lowering Energy Conversion Efficiency of a Micromotor System via the Addition of Ethanol 80
4.1. Introduction 81
4.2. Methodology 82
4.2.1 Equipment and Software 82
4.2.2 Chemical Reagent 83
4.2.3 Preparation 83
4.3. Result and Discussion 86
4.4. Conclusion 91
References: 91
Chapter 5: Future Application of the Micromotor System 95
5.1 intro 96
5.2 Method 97
5.2.1. Equipment and Software 97
5.2.2. Chemical Regent 101
5.2.3. Preparation 101
5.3 4-Pin Microelectrode System 103
5.4 Ratchet-Shaped Microparticle 109
5.5 Conclusion 115
References: 115
Chapter 6: Conclusion 120
Acknowledgement 124

Chapter 1

Introduction

1.1 Micromotor System

In recent decades, more and more attention has been focused on the development of microelectromechanical systems (MEMS)[1–7]. These systems are microdevices in micro/nano meter scale that can be applied for environmental use[8–19], medical use[20–29], etc.. A power source in micro/nano meter scale is required for these microdevices to be functional. One method to provide the power is the scale-down version of the traditional motor system. However, these microdevices are often submerged in liquid, which means that the Reynolds number is extremely low ($Re<<1$)[30]. In such cases, the viscous effect is dominant, and the traditional motor would have low efficiency due to its inertia-dependent nature. Therefore, there is a need to develop a power source for microdevices, hence, the study of the micromotor systems.

The micromotor system is defined as the motor where a particle/droplet in micro/nano meter scale, also known as a micromotor, shows mobility under certain conditions. The micromotor systems can be categorized based on their input energy types[30].

Magnetic micromotor system is the micromotor that is powered by magnetic field[22,31–39]. A typical case is a Ni nanowire showed propulsion and rotation motions under a magnetic field. These motions were precisely controlled by a uniform rotating magnetic field and can be applied to targeted drug delivery[20].

When a micromotor gains mobility from catalyzed chemical reactions, it is called a catalytic micromotor system[9,15–17,40–44]. K. Chen *et al*. reported a gold/platinum micromotor with “Z” shaped morphology shows a self-rotation motion. The mechanism was the hydrogen peroxide oxidation reduction on the surface of the gold/platinum micromotor[45].

D. Zhang *et al.* reported a phototactic liquid micromotor that was governed by white light irradiation[46]. The liquid micromotor showed propulsion motion, and the start/stop and the motion direction can be controlled by the white light. As reported, this motion may be caused by the photoisomerization of the material of the micromotor (spiropyran molecule) or the photothermal effect. Here, this type of micromotor system is called optic micromotor system[47–53].

Acoustic force can power the micromotor system as well[54,55]. Micromotors gained high velocity when an ultrasound pulse was applied, which was referred to as “microbullet” by D. Kagan *et al.*[56].

When electricity is used to power the micromotor system, it is called electric micromotor system, which was used in this study.

1.2 Electric Micromotor System

Electricity is used to power micromotor in this type of system[3,57–64]. Many motions of micromotors have been observed in electric micromotor system.

When a micromotor is oscillating between electrodes, this motion is called back-and-forth motion. Fig. 1-1 shows the schematic illustration of the geometric arrangement of electrodes reported by Kurimura *et al.* [63], where a back-and-forth motion of a liquid micromotor was observed. . This aqueous micromotor that moved between two needle-shaped electrodes was immersed in an oil phase. When a stationary direct current voltage was applied, the micromotor showed an oscillatory motion between the tips of two electrodes, hence, back-and-forth motion. This back-and-forth motion has been reported in other electric micromotor system[64], however, this motion has rarely been reported in other types of micromotor systems.

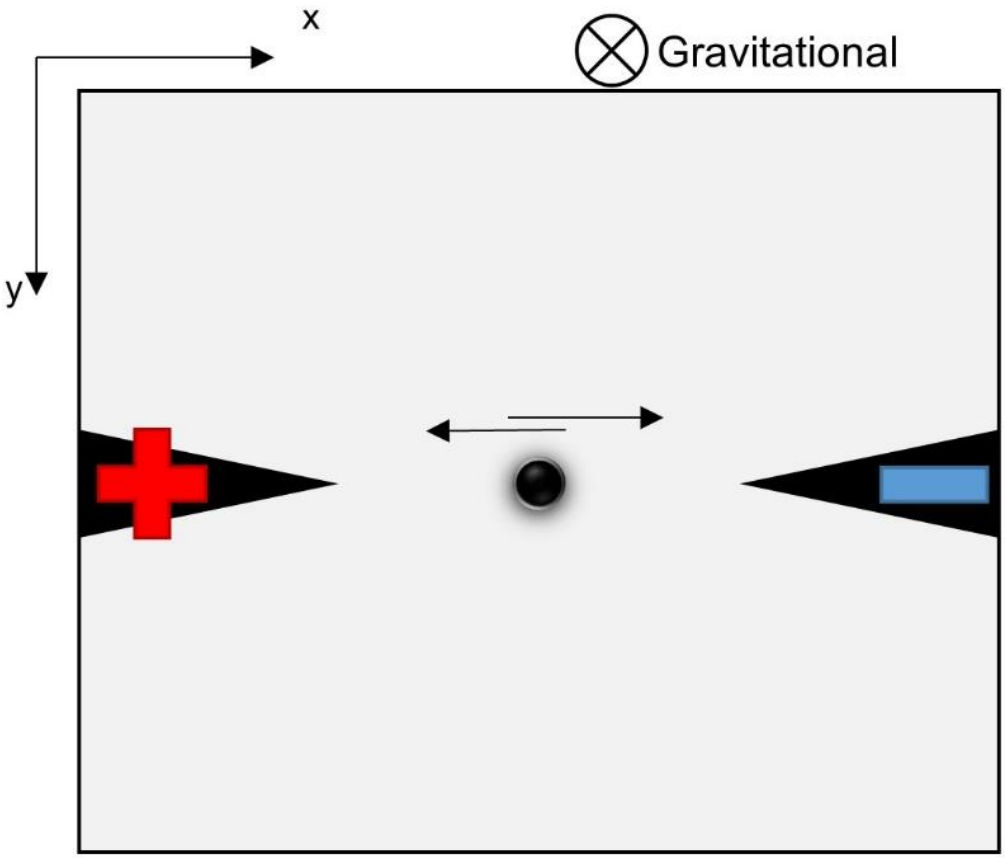

Fig.1-1 The schematic illustration of the geometric arrangement of the micromotor system used by T. Kurimura *et al*.[63]. A micromotor was moving between electrodes in a back-and-forth manner. This motion of micromotor was called back-and-forth motion.

When a micromotor revolves around an artificial point, it is defined as revolving motion here. A solid micromotor was reported by T. Kurimura *et al.* to show revolving motion in an oil phase with ionic surfactants[65]. The schematic illustration of this motion was shown in Fig. 1-2. This revolving motion was driven by the electrophoretic convection of the ionic surfactants[3,65]. The revolving motion of micromotor has been reported not only in electric micromotor system[60,61], but also other types of micromotor system as well[66].

When a micromotor rotates around its own center of mass, it is defined as spinning motion. For example, a helical microparticle, made from a type of alga, *Spirulina*[67,68], was reported to show “corkscrew rotation” under a direct current voltage[3], as shown in Fig. 1-3. This corkscrew rotation was observed as it spun around its own long axis, therefore, it fits the definition of spinning motion.

In general, the driving force of the spinning motion is the electrophoretic convection induced by the ionic surfactant[3,65]. In some cases, the motions were due to the Quincke rotor dynamics [69]. Spinning motions of electric micromotor system[61] and other micromotor systems have been reported[70,71].

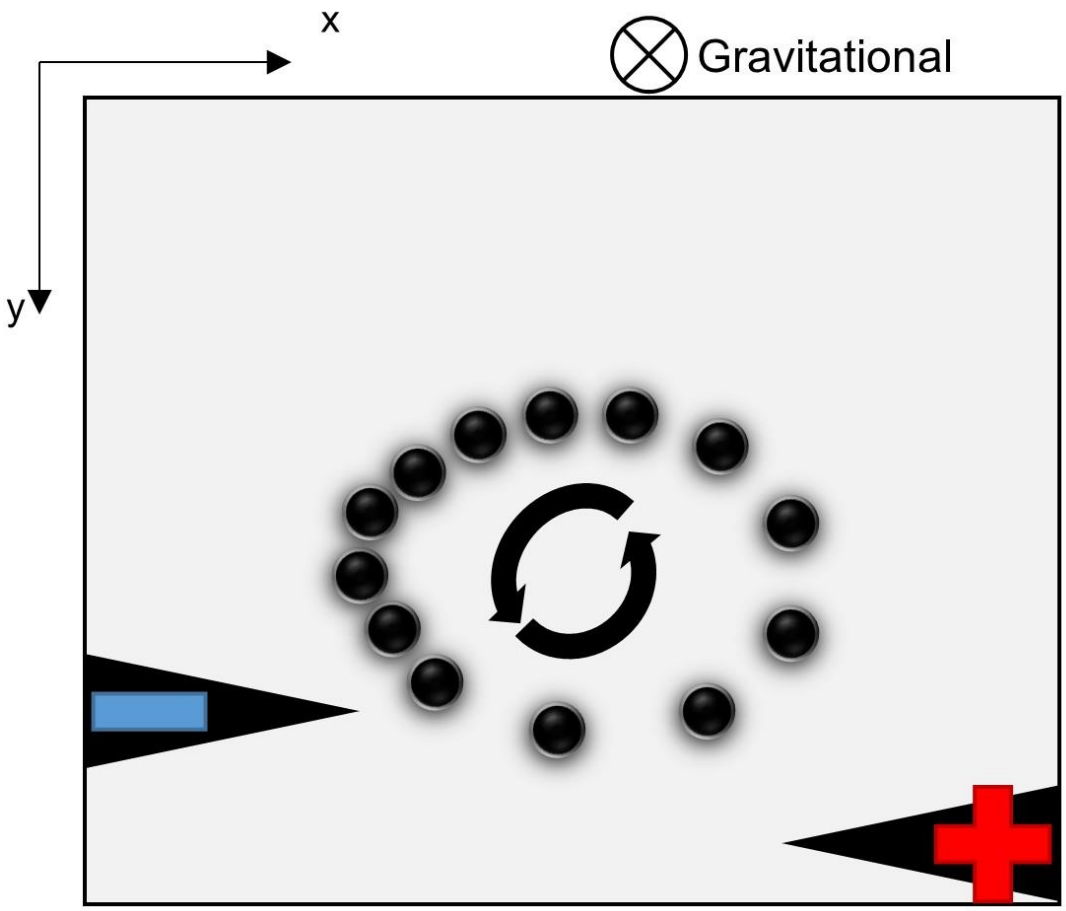

Fig. 1-2 The schematic illustration of the revolving motion of microparticle reported by T. Kurimura *et al.*[65]. Micromotor was revolving an artificial point near the electrodes.

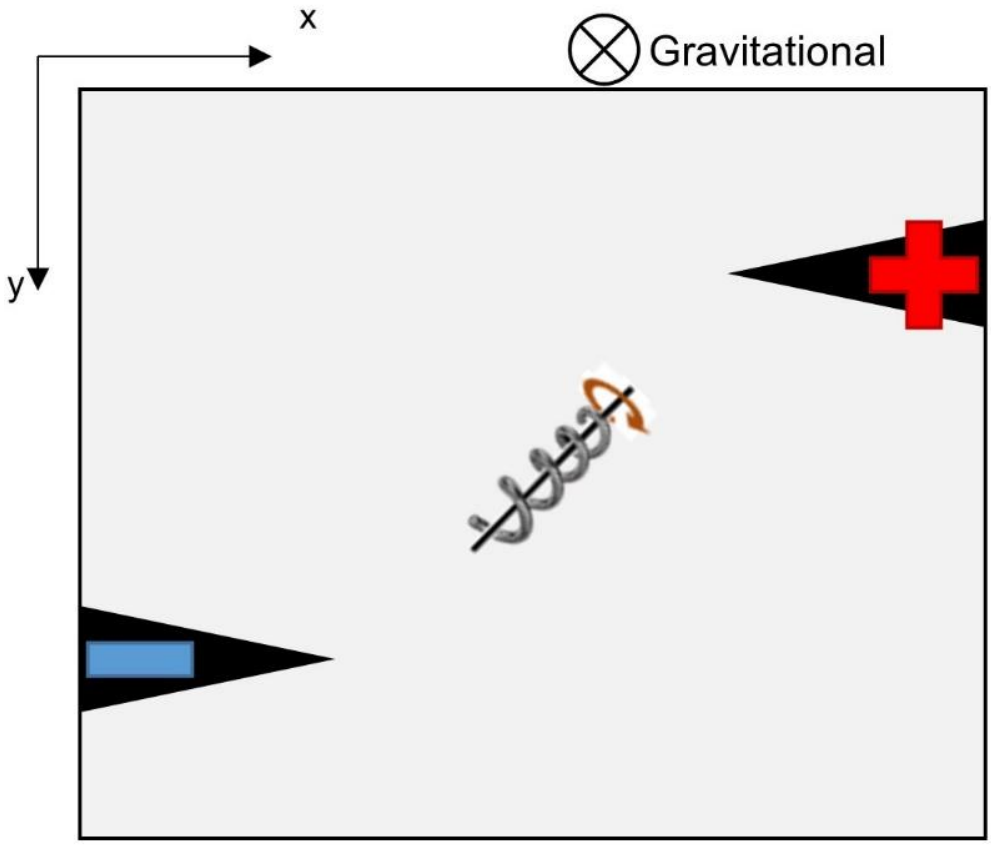

Fig. 1-3 The schematic illustration of helical micromotor “corkscrew rotation” between two needle-shaped electrodes. This motion was reported[3] that the helical microparticle span around its own long axis.

It is important to understand the energy conversion efficiency of the micromotors. To understand this, the input and the output of the electric micromotor system must be quantified first.

1.2.1 Input

For any electric devices, the electric energy input is calculated from eq.1

$$P_{in} = I \times V \quad (1)$$

where, P_{in}, I and V are the input power, the electric current and the applied voltage, respectively. In this study, the direct current voltage was measured by a voltmeter. However, the measurement of the current was difficult due to the high electric resistance of silicone oil that was used.

1.2.2 Output

In any micromotor system, the desired output is the motions of micromotors. Therefore, the mobility of micromotor should be quantified. However, until now, there was no universal parameters proposed for this quantification, and the studies on micromotors have been individually developed by different research groups. The mobility is frequently represented by the micromotor's velocity[20,32,33,40,45,54,56,72–75], angular velocity[2,62,72,76] or motion frequency[5,35,77].

The problem of the lack of universal parameter is that the output of micromotor systems in different experimental conditions are difficult to compare. For example, how one can conclude which micromotor system is better: a solid micromotor with oscillating motion in a microelectrode system [64] or a similar motion by a liquid micromotor in a two needle-shaped electrodes system[5]? A small particle with a high velocity may have the same output power as a large particle with a low velocity. Without a universal parameter, their efficiencies are different to judge.

1.2.3 Energy Conversion Efficiency

With the quantified input and output powers, the energy conversion efficiency can be calculated by eq.2

$$energy\ conversion\ efficiency = \frac{P_{out}}{P_{in}} \quad (2)$$

where, P_{out} is the output power of the micromotor system. The conversion efficiency is an essential property of electro-devices. Understanding the conversion efficiency holds significant meaning to the development of the micromotor system. Different micromotor systems from individual study can be compared in terms of the energy conversion efficiencies.

1.3 Future Application of the Micromotor System

One of the future adaptation of the electric micromotor system is to the microfluidic devices [78–80], such as the “lab-on-chips” technology. The term “lab-on-chips” means a functional analysis system that is integrated and small enough to be fit on a single glass slide [4]. These lab-on-chips microdevices provide simple, portable platforms that can work with smaller amount of samples, which benefits studies such as biosensing [81–83] and microbiology [84–88].

S. Dekker *et al.* pointed out that, at the current state of “lab-on-chips” microdevices development, the integration was limited [89]. For example, on a micro-mixing device, fluids are injected into the system by external equipment and mixed by pressure [90]. If a micromotor system is designed for and integrated into this micro-mixing device, the portability and mixing efficiency will be increased greatly.

1.4 The purpose of this Study

In this study, a quantification for the energy conversion efficiency of the micromotor system was discussed. This quantification method provides a universal tool for different micromotors to be compared, which will benefit the development of

micromotor study greatly. Moreover, a microelectrode system and a ratchet-shaped microparticle were investigated with the intention of future adaptation in microelectromechanical system. In this study, the solution mixture of silicone oil [91] and di-(2-ethylhexyl) phosphoric acid (DEHPA) was used [92–95], and additional ethanol was added when needed.

Chapter 2 proposed a quantification method of energy conversion efficiency of the micromotor system. A water microdroplet showed a back-and-forth motion between electrodes. The output power was calculated through the viscous drag force. Moreover,the electric current was successfully measured by applying an electromagnetic shield and grounding the whole system. Finally, the energy conversion efficiency of this micromotor system was able to be calculated from the input and the output power.

In chapter 3, this quantification has been further improved by analyzing the revolving motion and spinning motion of a solid microparticle. The revolving motion, similar to back-and-forth motion, was driven by the solvent flow with viscous drag. The spinning motion was analyzed, and its output power was calculated from its viscous torque[75,96–98]. The output powers calculated by the viscous drag and torque are fundamental properties to any micromotor motions. The quantification method can be applied basically to any motions of spherical micromotor.

Chapter 4 shows the result of the ethanol effect in micromotor system by comparing the energy conversion efficiencies between ethanol-added and ethanol-free micromotor system using the quantification method. The result showed that the output power of micromotor was increased with the addition of ethanol. However, since the input electric current was also increased, the energy conversion efficiency was decreased.

Chapter 5 shows that (i) in 4-pin microelectrode system, microparticle gains mobility even in low electric field intensity regions, and (ii) the ratchet-shaped microparticle showed a suspended state, oscillating and spinning motions between two needle-shaped electrodes under a direct current voltage.

Chapter 6 is the conclusion of this study. The present quantification enables micromotor systems to be compared on energy levels, irrespective of the size, velocity, angular velocity, viscosity of the solution, or types of input energy to the system. The energy conversion efficiency, as a representation of energy flux of the system, also provides guidelines for micromotor system development. The energy conversion efficiency can be a universal parameter to compare different micromotor systems in different studies, and will significantly improve the micromotor studies. The ethanol-added micromotor system showed a higher output power, but the energy conversion efficiency was lower due to the increased electric current. Both results from the four-pin microelectrode system and the ratchet-shaped microparticle benefit the future adaptation of the micromotor system in microelectromechanical systems.

The results in chapter 2 and 4 have been published in *Colloids and Surfaces A: Physicochemical and Engineering Aspects* [99] and *Chemistry Letters* [100], respectively. The result in chapter 3 has been submitted to *Colloids and Surfaces A: Physicochemical and Engineering Aspects.*

References:

[1] N.G. Dagalakis, T. LeBrun, J. Lippiatt, Micro-mirror array control of optical tweezer trapping beams, in: Proc. 2nd IEEE Conf. Nanotechnol., IEEE, 2002: pp. 177–180. https://doi.org/10.1109/NANO.2002.1032219.

[2] M. Zrínyi, M. Nakano, Toward Colloidal Motors, Period. Polytech. Chem. Eng. 61 (2017) 15. https://doi.org/10.3311/PPch.10274.

[3] D. Yamamoto, K. Kosugi, K. Hiramatsu, W. Zhang, A. Shioi, K. Kamata, T. Iyoda, K. Yoshikawa, Helical micromotor operating under stationary DC electrostatic field, J. Chem. Phys. 150 (2019) 014901. https://doi.org/10.1063/1.5055830.

[4] N. Azizipour, R. Avazpour, D.H. Rosenzweig, M. Sawan, A. Ajji, Evolution of Biochip Technology: A Review from Lab-on-a-Chip to Organ-on-a-Chip, Micromachines. 11 (2020) 599. https://doi.org/10.3390/mi11060599.

[5] M. Takinoue, Y. Atsumi, K. Yoshikawa, Rotary motion driven by a direct current electric field, Appl. Phys. Lett. 96 (2010) 104105. https://doi.org/10.1063/1.3358385.

[6] L. Hu, N. Wang, Y.D. Lim, J. Miao, Chemical reaction dependency, magnetic field and surfactant effects on the propulsion of disk - like micromotor and its application for E. coli transportation, Nano Sel. (2020) nano.202000024. https://doi.org/10.1002/nano.202000024.

[7] X.-Z. Chen, B. Jang, D. Ahmed, C. Hu, C. De Marco, M. Hoop, F. Mushtaq, B.J. Nelson, S. Pané, Small-Scale Machines Driven by External Power Sources, Adv. Mater. 30 (2018) 1705061. https://doi.org/10.1002/adma.201705061.

[8] B. Jurado-Sánchez, J. Wang, Micromotors for environmental applications: a review, Environ. Sci. Nano. 5 (2018) 1530–1544. https://doi.org/10.1039/C8EN00299A.

[9] C. Chen, E. Karshalev, J. Guan, J. Wang, Magnesium-Based Micromotors: Water-Powered Propulsion, Multifunctionality, and Biomedical and

Environmental Applications, Small. 14 (2018) 1704252. https://doi.org/10.1002/smll.201704252.

[10] H. Wang, M.G. Potroz, J.A. Jackman, B. Khezri, T. Marić, N.-J. Cho, M. Pumera, Bioinspired Spiky Micromotors Based on Sporopollenin Exine Capsules, Adv. Funct. Mater. 27 (2017) 1702338. https://doi.org/10.1002/adfm.201702338.

[11] A.K. Singh, T. Bhuyan, S. Maity, T.K. Mandal, D. Bandyopadhyay, Magnetically Actuated Carbon Soot Nanoparticle-Based Catalytic CARBOts Coated with Ni/Pt Nanofilms for Water Detoxification and Oil-Spill Recovery, ACS Appl. Nano Mater. 3 (2020) 3459–3470. https://doi.org/10.1021/acsanm.0c00199.

[12] E. Karshalev, B. Esteban-Fernández de Ávila, J. Wang, Micromotors for "Chemistry-on-the-Fly," J. Am. Chem. Soc. 140 (2018) 3810–3820. https://doi.org/10.1021/jacs.8b00088.

[13] W. Gao, J. Wang, The Environmental Impact of Micro/Nanomachines: A Review, ACS Nano. 8 (2014) 3170–3180. https://doi.org/10.1021/nn500077a.

[14] J.G.S. Moo, M. Pumera, Chemical Energy Powered Nano/Micro/Macromotors and the Environment, Chem. - A Eur. J. 21 (2015) 58–72. https://doi.org/10.1002/chem.201405011.

[15] C.-S. Lee, J. Gong, D.-S. Oh, J.-R. Jeon, Y.-S. Chang, Zerovalent-Iron/Platinum Janus Micromotors with Spatially Separated Functionalities for Efficient Water Decontamination, ACS Appl. Nano Mater. 1 (2018) 768–776. https://doi.org/10.1021/acsanm.7b00223.

[16] B. Jurado-Sánchez, M. Pacheco, R. Maria-Hormigos, A. Escarpa, Perspectives on Janus micromotors: Materials and applications, Appl. Mater. Today. 9 (2017) 407–418. https://doi.org/10.1016/j.apmt.2017.09.005.

[17] J. Parmar, K. Villa, D. Vilela, S. Sánchez, Platinum-free cobalt ferrite based micromotors for antibiotic removal, Appl. Mater. Today. 9 (2017) 605–611. https://doi.org/10.1016/j.apmt.2017.11.002.

[18] R. Wang, W. Guo, X. Li, Z. Liu, H. Liu, S. Ding, Highly efficient MOF-based self-propelled micromotors for water purification, RSC Adv. 7 (2017) 42462–42467. https://doi.org/10.1039/C7RA08127H.

[19] L. Baptista-Pires, J. Orozco, P. Guardia, A. Merkoçi, Architecting Graphene Oxide Rolled-Up Micromotors: A Simple Paper-Based Manufacturing Technology, Small. 14 (2018) 1702746. https://doi.org/10.1002/smll.201702746.

[20] L. Zhang, T. Petit, Y. Lu, B.E. Kratochvil, K.E. Peyer, R. Pei, J. Lou, B.J. Nelson, Controlled Propulsion and Cargo Transport of Rotating Nickel Nanowires near a Patterned Solid Surface, ACS Nano. 4 (2010) 6228–6234. https://doi.org/10.1021/nn101861n.

[21] J. Wang, W. Gao, Nano/Microscale Motors: Biomedical Opportunities and Challenges, ACS Nano. 6 (2012) 5745–5751. https://doi.org/10.1021/nn3028997.

[22] H. Xu, M. Medina - Sánchez, O.G. Schmidt, Magnetic Micromotors for Multiple Motile Sperm Cells Capture, Transport, and Enzymatic Release, Angew. Chemie. 132 (2020) 15139–15147. https://doi.org/10.1002/ange.202005657.

[23] I.A.B. Pijpers, S. Cao, A. Llopis-Lorente, J. Zhu, S. Song, R.R.M. Joosten, F. Meng, H. Friedrich, D.S. Williams, S. Sánchez, J.C.M. van Hest, L.K.E.A. Abdelmohsen, Hybrid Biodegradable Nanomotors through Compartmentalized Synthesis, Nano Lett. 20 (2020) 4472–4480. https://doi.org/10.1021/acs.nanolett.0c01268.

[24] R. Mundaca - Uribe, B. Esteban - Fernández de Ávila, M. Holay, P. Lekshmy Venugopalan, B. Nguyen, J. Zhou, A. Abbas, R.H. Fang, L. Zhang, J. Wang, Zinc Microrocket Pills: Fabrication and Characterization toward Active Oral Delivery, Adv. Healthc. Mater. 9 (2020) 2000900. https://doi.org/10.1002/adhm.202000900.

[25] A. Terzopoulou, X. Wang, X. Chen, M. Palacios - Corella, C. Pujante, J. Herrero - Martín, X. Qin, J. Sort, A.J. DeMello, B.J. Nelson, J. Puigmartí - Luis, S. Pané, Biodegradable Metal–Organic Framework - Based Microrobots (MOFBOTs), Adv. Healthc. Mater. 2001031 (2020) 2001031. https://doi.org/10.1002/adhm.202001031.

[26] P.L. Venugopalan, B. Esteban-Fernández de Ávila, M. Pal, A. Ghosh, J. Wang, Fantastic Voyage of Nanomotors into the Cell, ACS Nano. 14 (2020) 9423–9439. https://doi.org/10.1021/acsnano.0c05217.

[27] H. Xu, M. Medina-Sánchez, V. Magdanz, L. Schwarz, F. Hebenstreit, O.G. Schmidt, Sperm-Hybrid Micromotor for Targeted Drug Delivery, ACS Nano. 12 (2018) 327–337. https://doi.org/10.1021/acsnano.7b06398.

[28] B. Esteban-Fernández de Ávila, P. Angsantikul, J. Li, W. Gao, L. Zhang, J. Wang, Micromotors Go In Vivo: From Test Tubes to Live Animals, Adv. Funct.

Mater. 28 (2018) 1705640. https://doi.org/10.1002/adfm.201705640.

[29] A.C.H. Tsang, E. Demir, Y. Ding, O.S. Pak, Roads to Smart Artificial Microswimmers, Adv. Intell. Syst. 2 (2020) 1900137. https://doi.org/10.1002/aisy.201900137.

[30] D. Yamamoto, A. Shioi, Self-Propelled Nano/Micromotors with a Chemical Reaction: Underlying Physics and Strategies of Motion Control, KONA Powder Part. J. 32 (2015) 2–22. https://doi.org/10.14356/kona.2015005.

[31] G. Zhao, M. Pumera, Magnetotactic Artificial Self-Propelled Nanojets, Langmuir. 29 (2013) 7411–7415. https://doi.org/10.1021/la303762a.

[32] S. Tottori, L. Zhang, F. Qiu, K.K. Krawczyk, A. Franco-Obregón, B.J. Nelson, Magnetic Helical Micromachines: Fabrication, Controlled Swimming, and Cargo Transport, Adv. Mater. 24 (2012) 811–816. https://doi.org/10.1002/adma.201103818.

[33] Y. Liu, D. Ge, J. Cong, H.-G. Piao, X. Huang, Y. Xu, G. Lu, L. Pan, M. Liu, Magnetically Powered Annelid-Worm-Like Microswimmers, Small. 14 (2018) 1704546. https://doi.org/10.1002/smll.201704546.

[34] W. Gao, S. Sattayasamitsathit, K.M. Manesh, D. Weihs, J. Wang, Magnetically Powered Flexible Metal Nanowire Motors, J. Am. Chem. Soc. 132 (2010) 14403–14405. https://doi.org/10.1021/ja1072349.

[35] L. Liu, B. Chen, K. Liu, J. Gao, Y. Ye, Z. Wang, N. Qin, D.A. Wilson, Y. Tu, F. Peng, Wireless Manipulation of Magnetic/Piezoelectric Micromotors for Precise Neural Stem - Like Cell Stimulation, Adv. Funct. Mater. 30 (2020) 1910108. https://doi.org/10.1002/adfm.201910108.

[36] J. Vialetto, M. Hayakawa, N. Kavokine, M. Takinoue, S.N. Varanakkottu, S. Rudiuk, M. Anyfantakis, M. Morel, D. Baigl, Magnetic Actuation of Drops and Liquid Marbles Using a Deformable Paramagnetic Liquid Substrate, Angew. Chemie Int. Ed. 56 (2017) 16565–16570. https://doi.org/10.1002/anie.201710668.

[37] C. Calero, J. García-Torres, A. Ortiz-Ambriz, F. Sagués, I. Pagonabarraga, P. Tierno, Propulsion and energetics of a minimal magnetic microswimmer, Soft Matter. 16 (2020) 6673–6682. https://doi.org/10.1039/D0SM00564A.

[38] X. Wang, J. Law, M. Luo, Z. Gong, J. Yu, W. Tang, Z. Zhang, X. Mei, Z. Huang, L. You, Y. Sun, Magnetic Measurement and Stimulation of Cellular and Intracellular Structures, ACS Nano. 14 (2020) 3805–3821. https://doi.org/10.1021/acsnano.0c00959.

[39] Y. He, S. Dong, L. Wang, W. Rong, L. Sun, Bipedal microwalkers actuated by oscillating magnetic fields, Soft Matter. 16 (2020) 7927–7934. https://doi.org/10.1039/D0SM01228A.

[40] W.F. Paxton, K.C. Kistler, C.C. Olmeda, A. Sen, S.K. St. Angelo, Y. Cao, T.E. Mallouk, P.E. Lammert, V.H. Crespi, Catalytic Nanomotors: Autonomous Movement of Striped Nanorods, J. Am. Chem. Soc. 126 (2004) 13424–13431. https://doi.org/10.1021/ja047697z.

[41] C. Zhou, Q. Wang, X. Lv, W. Wang, Non-oscillatory micromotors “learn” to oscillate on-the-fly from oscillating Ag micromotors, Chem. Commun. 56 (2020) 6499–6502. https://doi.org/10.1039/D0CC02266G.

[42] N. Wolff, V. Ciobanu, M. Enachi, M. Kamp, T. Braniste, V. Duppel, S. Shree, S.

Raevschi, M. Medina - Sánchez, R. Adelung, O.G. Schmidt, L. Kienle, I. Tiginyanu, Advanced Hybrid GaN/ZnO Nanoarchitectured Microtubes for Fluorescent Micromotors Driven by UV Light, Small. 16 (2020) 1905141. https://doi.org/10.1002/smll.201905141.

[43] L. Chen, X. Sun, H. Wang, Z. Zhang, Preparation of dual-drive hybrid micromotors by swelling and selective surface modification of polymeric colloids, Colloid Interface Sci. Commun. 38 (2020) 100300. https://doi.org/10.1016/j.colcom.2020.100300.

[44] G. Salinas, A.L. Dauphin, S. Voci, L. Bouffier, N. Sojic, A. Kuhn, Asymmetry controlled dynamic behavior of autonomous chemiluminescent Janus microswimmers, Chem. Sci. 11 (2020) 7438–7443. https://doi.org/10.1039/D0SC02431G.

[45] K. Chen, C. Gu, Z. Yang, M. Nakajima, T. Chen, T. Fukuda, “Z”-Shaped Rotational Au/Pt Micro-Nanorobot, Micromachines. 8 (2017) 183. https://doi.org/10.3390/mi8060183.

[46] D. Zhang, Y. Sun, M. Li, H. Zhang, B. Song, B. Dong, A phototactic liquid micromotor, J. Mater. Chem. C. 6 (2018) 12234–12239. https://doi.org/10.1039/C8TC04260H.

[47] N.K. Metzger, M. Mazilu, L. Kelemen, P. Ormos, K. Dholakia, Observation and simulation of an optically driven micromotor, J. Opt. 13 (2011) 044018. https://doi.org/10.1088/2040-8978/13/4/044018.

[48] S.M. Mousavi, I. Kasianiuk, D. Kasyanyuk, S.K.P. Velu, A. Callegari, L. Biancofiore, G. Volpe, Clustering of Janus particles in an optical potential

driven by hydrodynamic fluxes, Soft Matter. 15 (2019) 5748–5759. https://doi.org/10.1039/C8SM02282H.

[49] C. Maggi, F. Saglimbeni, M. Dipalo, F. De Angelis, R. Di Leonardo, Micromotors with asymmetric shape that efficiently convert light into work by thermocapillary effects, Nat. Commun. 6 (2015) 7855. https://doi.org/10.1038/ncomms8855.

[50] M. Mijalkov, A. McDaniel, J. Wehr, G. Volpe, Engineering Sensorial Delay to Control Phototaxis and Emergent Collective Behaviors, Phys. Rev. X. 6 (2016) 011008. https://doi.org/10.1103/PhysRevX.6.011008.

[51] A. Callegari, M. Mijalkov, A.B. Gököz, G. Volpe, Computational toolbox for optical tweezers in the geometrical optics regime, in: Biophotonics Congr. Opt. Life Sci. Congr. 2019, OSA, Washington, D.C., 2019: p. AT3E.6. https://doi.org/10.1364/OMA.2019.AT3E.6.

[52] I. Buttinoni, G. Volpe, F. Kümmel, G. Volpe, C. Bechinger, Active Brownian motion tunable by light, J. Phys. Condens. Matter. 24 (2012) 284129. https://doi.org/10.1088/0953-8984/24/28/284129.

[53] F. Schmidt, B. Liebchen, H. Löwen, G. Volpe, Light-controlled assembly of active colloidal molecules, J. Chem. Phys. 150 (2019) 094905. https://doi.org/10.1063/1.5079861.

[54] J.-F. Louf, N. Bertin, B. Dollet, O. Stephan, P. Marmottant, Hovering Microswimmers Exhibit Ultrafast Motion to Navigate under Acoustic Forces, Adv. Mater. Interfaces. 5 (2018) 1800425. https://doi.org/10.1002/admi.201800425.

[55] W. Wang, L.A. Castro, M. Hoyos, T.E. Mallouk, Autonomous Motion of Metallic Microrods Propelled by Ultrasound, ACS Nano. 6 (2012) 6122–6132. https://doi.org/10.1021/nn301312z.

[56] D. Kagan, M.J. Benchimol, J.C. Claussen, E. Chuluun-Erdene, S. Esener, J. Wang, Acoustic Droplet Vaporization and Propulsion of Perfluorocarbon-Loaded Microbullets for Targeted Tissue Penetration and Deformation, Angew. Chemie Int. Ed. 51 (2012) 7519–7522. https://doi.org/10.1002/anie.201201902.

[57] P. Calvo-Marzal, S. Sattayasamitsathit, S. Balasubramanian, J.R. Windmiller, C. Dao, J. Wang, Propulsion of nanowire diodes, Chem. Commun. 46 (2010) 1623. https://doi.org/10.1039/b925568k.

[58] S. Gangwal, O.J. Cayre, M.Z. Bazant, O.D. Velev, Induced-Charge Electrophoresis of Metallodielectric Particles, Phys. Rev. Lett. 100 (2008) 058302. https://doi.org/10.1103/PhysRevLett.100.058302.

[59] T. Michálek, A. Bolopion, Z. Hurák, M. Gauthier, Control-oriented model of dielectrophoresis and electrorotation for arbitrarily shaped objects, Phys. Rev. E. 99 (2019) 053307. https://doi.org/10.1103/PhysRevE.99.053307.

[60] R. Yamamoto, D. Yamamoto, A. Shioi, S. Fujii, T. Kurimura, K. Yoshikawa, Arrangement and Periodic Motion of Microparticles in an Oil Phase under a DC Electric Field, J. Soc. Powder Technol. Japan. 51 (2014) 823–827. https://doi.org/10.4164/sptj.51.823.

[61] D. Yamamoto, R. Yamamoto, T. Kozaki, A. Shioi, S. Fujii, K. Yoshikawa, Periodic Motions of Solid Particles with Various Morphology under a DC Electrostatic Field, Chem. Lett. 46 (2017) 1470–1472.

https://doi.org/10.1246/cl.170622.

[62] L. Rodríguez-Sánchez, A. Ramos, P. García-Sánchez, Electrorotation of semiconducting microspheres, Phys. Rev. E. 100 (2019) 042616. https://doi.org/10.1103/PhysRevE.100.042616.

[63] T. Kurimura, M. Ichikawa, M. Takinoue, K. Yoshikawa, Back-and-forth micromotion of aqueous droplets in a dc electric field, Phys. Rev. E. 88 (2013) 042918. https://doi.org/10.1103/PhysRevE.88.042918.

[64] M.K. Masukawa, M. Hayakawa, M. Takinoue, Surfactant concentration modulates the motion and placement of microparticles in an inhomogeneous electric field, RSC Adv. 10 (2020) 8895–8904. https://doi.org/10.1039/D0RA00703J.

[65] T. Kurimura, S. Mori, M. Miki, K. Yoshikawa, Rotary motion of a micro-solid particle under a stationary difference of electric potential, J. Chem. Phys. 145 (2016) 034902. https://doi.org/10.1063/1.4958657.

[66] D. Yamamoto, T. Takada, M. Tachibana, Y. Iijima, A. Shioi, K. Yoshikawa, Micromotors working in water through artificial aerobic metabolism, Nanoscale. 7 (2015) 13186–13190. https://doi.org/10.1039/C5NR03300D.

[67] J. Cheng, W. Guo, K. Ameer Ali, Q. Ye, G. Jin, Z. Qiao, Promoting helix pitch and trichome length to improve biomass harvesting efficiency and carbon dioxide fixation rate by Spirulina sp. in 660 m2 raceway ponds under purified carbon dioxide from a coal chemical flue gas, Bioresour. Technol. 261 (2018) 76–85. https://doi.org/10.1016/j.biortech.2018.04.017.

[68] K. Kamata, Z. Piao, S. Suzuki, T. Fujimori, W. Tajiri, K. Nagai, T. Iyoda, A.

Yamada, T. Hayakawa, M. Ishiwara, S. Horaguchi, A. Belay, T. Tanaka, K. Takano, M. Hangyo, Spirulina-Templated Metal Microcoils with Controlled Helical Structures for THz Electromagnetic Responses, Sci. Rep. 4 (2015) 4919. https://doi.org/10.1038/srep04919.

[69] F. Peters, L. Lobry, E. Lemaire, Experimental observation of Lorenz chaos in the Quincke rotor dynamics, Chaos An Interdiscip. J. Nonlinear Sci. 15 (2005) 013102. https://doi.org/10.1063/1.1827411.

[70] A. Barbot, D. Decanini, G. Hwang, Local flow sensing on helical microrobots for semi-automatic motion adaptation, Int. J. Rob. Res. 39 (2020) 476–489. https://doi.org/10.1177/0278364919894374.

[71] L. Xie, X. Pang, X. Yan, Q. Dai, H. Lin, J. Ye, Y. Cheng, Q. Zhao, X. Ma, X. Zhang, G. Liu, X. Chen, Photoacoustic Imaging-Trackable Magnetic Microswimmers for Pathogenic Bacterial Infection Treatment, ACS Nano. 14 (2020) 2880–2893. https://doi.org/10.1021/acsnano.9b06731.

[72] R.A. Archer, J.R. Howse, S. Fujii, H. Kawashima, G.A. Buxton, S.J. Ebbens, pH - Responsive Catalytic Janus Motors with Autonomous Navigation and Cargo - Release Functions, Adv. Funct. Mater. 30 (2020) 2000324. https://doi.org/10.1002/adfm.202000324.

[73] Y. Sumino, N. Magome, T. Hamada, K. Yoshikawa, Self-Running Droplet: Emergence of Regular Motion from Nonequilibrium Noise, Phys. Rev. Lett. 94 (2005) 068301. https://doi.org/10.1103/PhysRevLett.94.068301.

[74] M.M. Alcanzare, M. Karttunen, T. Ala-Nissila, Propulsion and controlled steering of magnetic nanohelices, Soft Matter. 15 (2019) 1684–1691.

https://doi.org/10.1039/C8SM00037A.

[75] U.K. Cheang, F. Meshkati, H. Kim, K. Lee, H.C. Fu, M.J. Kim, Versatile microrobotics using simple modular subunits, Sci. Rep. 6 (2016) 30472. https://doi.org/10.1038/srep30472.

[76] T. Harada, K. Yoshikawa, Mode switching of an optical motor, Appl. Phys. Lett. 81 (2002) 4850–4852. https://doi.org/10.1063/1.1527235.

[77] M. Hase, S.N. Watanabe, K. Yoshikawa, Rhythmic motion of a droplet under a dc electric field, Phys. Rev. E. 74 (2006) 046301. https://doi.org/10.1103/PhysRevE.74.046301.

[78] S. Zhan, R.-F. Cui, L.-Y. Qiao, J.-X. Chen, Transport of nanodimers through chemical microchip, Commun. Theor. Phys. 72 (2020) 015601. https://doi.org/10.1088/1572-9494/ab544f.

[79] M. Pacheco, M.Á. López, B. Jurado-Sánchez, A. Escarpa, Self-propelled micromachines for analytical sensing: a critical review, Anal. Bioanal. Chem. 411 (2019) 6561–6573. https://doi.org/10.1007/s00216-019-02070-z.

[80] W. Li, X. Tang, L. Wang, Photopyroelectric microfluidics, Sci. Adv. 6 (2020) eabc1693. https://doi.org/10.1126/sciadv.abc1693.

[81] C. Tymm, J. Zhou, A. Tadimety, A. Burklund, J.X.J. Zhang, Scalable COVID-19 Detection Enabled by Lab-on-Chip Biosensors, Cell. Mol. Bioeng. 13 (2020) 313–329. https://doi.org/10.1007/s12195-020-00642-z.

[82] N.I. Khan, E. Song, Lab-on-a-Chip Systems for Aptamer-Based Biosensing, Micromachines. 11 (2020) 220. https://doi.org/10.3390/mi11020220.

[83] A. Tsopela, A. Laborde, L. Salvagnac, V. Ventalon, E. Bedel-Pereira, I. Séguy,

P. Temple-Boyer, P. Juneau, R. Izquierdo, J. Launay, Development of a lab-on-chip electrochemical biosensor for water quality analysis based on microalgal photosynthesis, Biosens. Bioelectron. 79 (2016) 568–573. https://doi.org/10.1016/j.bios.2015.12.050.

[84] O. Behrmann, M. Hügle, P. Bronsert, B. Herde, J. Heni, M. Schramm, F.T. Hufert, G.A. Urban, G. Dame, A lab-on-a-chip for rapid miRNA extraction, PLoS One. 14 (2019) e0226571. https://doi.org/10.1371/journal.pone.0226571.

[85] F. Nafian, B. Kamali Doust Azad, S. Yazdani, M.J. Rasaee, N. Daftarian, A lab - on - a - chip model of glaucoma, Brain Behav. (2020) 1–13. https://doi.org/10.1002/brb3.1799.

[86] G. Dame, J. Lampe, S. Hakenberg, G. Urban, Development of a Fast miRNA Extraction System for Tumor Analysis Based on a Simple Lab on Chip Approach, Procedia Eng. 120 (2015) 158–162. https://doi.org/10.1016/j.proeng.2015.08.593.

[87] M. Hügle, G. Dame, O. Behrmann, R. Rietzel, D. Karthe, F.T. Hufert, G.A. Urban, A lab-on-a-chip for preconcentration of bacteria and nucleic acid extraction, RSC Adv. 8 (2018) 20124–20130. https://doi.org/10.1039/C8RA02177E.

[88] H. Shintaku, H. Nishikii, L.A. Marshall, H. Kotera, J.G. Santiago, On-Chip Separation and Analysis of RNA and DNA from Single Cells, Anal. Chem. 86 (2014) 1953–1957. https://doi.org/10.1021/ac4040218.

[89] S. Dekker, P.K. Isgor, T. Feijten, L.I. Segerink, M. Odijk, From chip-in-a-lab to lab-on-a-chip: a portable Coulter counter using a modular platform,

Microsystems Nanoeng. 4 (2018) 34. https://doi.org/10.1038/s41378-018-0034-1.

[90] F.W.M. Ling, A.A. Khleif, H.A. Abdulbari, Investigating the effect of micro-riblets on the flow and micro-mixing behavior in micro-channel, Chem. Eng. Commun. 411 (2020) 1–14. https://doi.org/10.1080/00986445.2020.1715959.

[91] W.F. Schmidt, K. Yoshino, Ion mobilities in non-polar dielectric liquids: silicone oils, IEEE Trans. Dielectr. Electr. Insul. 22 (2015) 2424–2427. https://doi.org/10.1109/TDEI.2015.005036.

[92] S. Satpathy, S. Mishra, Investigation on molecular interaction studies of binary mixture of DEHPA and petrofin at 298.15 K, Phys. Chem. Liq. 56 (2018) 141–152. https://doi.org/10.1080/00319104.2017.1312399.

[93] R.K. Biswas, M.A. Habib, M.N. Islam, Some Physicochemical Properties of (D2EHPA). 1. Distribution, Dimerization, and Acid Dissociation Constants of D2EHPA in a Kerosene/0.10 kmol m - 3 (Na + ,H +)Cl - System and the Extraction of Mn(II), Ind. Eng. Chem. Res. 39 (2000) 155–160. https://doi.org/10.1021/ie9902535.

[94] L.R. Koekemoer, M.J.G. Badenhorst, R.C. Everson, Determination of Viscosity and Density of Di-(2-ethylhexyl) Phosphoric Acid + Aliphatic Kerosene, J. Chem. Eng. Data. 50 (2005) 587–590. https://doi.org/10.1021/je0496645.

[95] G.N. Smith, Proton transfer in nonpolar solvents: an approach to generate electrolytes in aprotic media, Phys. Chem. Chem. Phys. 20 (2018) 18919–18923. https://doi.org/10.1039/C8CP02349B.

[96] R.I. Ovseenko, Y.G. Ovseenko, Drag of a rotating sphere, Fluid Dyn. 3 (1971)

78–82. https://doi.org/10.1007/BF01016244.

[97] P. Hahn, A. Lamprecht, J. Dual, Numerical simulation of micro-particle rotation by the acoustic viscous torque, Lab Chip. 16 (2016) 4581–4594. https://doi.org/10.1039/C6LC00865H.

[98] E. Bonaccurso, H.-J. Butt, V.S.J. Craig, Surface Roughness and Hydrodynamic Boundary Slip of a Newtonian Fluid in a Completely Wetting System, Phys. Rev. Lett. 90 (2003) 144501. https://doi.org/10.1103/PhysRevLett.90.144501.

[99] W. Zhang, T. Kozaki, I. Kakimoto, D. Yamamoto, K. Yoshikawa, A. Shioi, Energy consumption and conversion efficiency for a micromotor under DC voltage, Colloids Surfaces A Physicochem. Eng. Asp. 607 (2020) 125496. https://doi.org/10.1016/j.colsurfa.2020.125496.

[100] W. Zhang, Y. Okamoto, D. Yamamoto, A. Shioi, Energy Conversion Efficiency of Micromotor System, Chem. Lett, (2021), *in press*.

Chapter 2

Energy Consumption and Conversion Efficiency for a Micromotor under DC Voltage

2.1. Introduction

Micro devices have received significant attention for decades, such as using micromotors on pollutant degradation [1]. These devices require motions of micro objects submerged in a liquid phase to be functional. However, due to nano/micrometer scale of such devices, the Reynolds number is low, implying that the inertia effect on the motions of the micromotor in such a system can be neglected and that the effect of viscosity is dominant. Thus, only inertia effect should not be considered for the motion of micro objects. Therefore, continuous provision of energy to micro objects is important for maintaining motion in a liquid phase. Micro objects that are constantly mobile are called micromotors or microswimmers.

Many methods have been reported to provide mobility to the micro-objects. Some of these methods were driven by magnetic field [2–6], catalysis [7–10] or ultrasound [11–13]. Metzger *et al*. [14] made micro particle rotate through an optical light while D. Zhang *et al*. [15] governed the motion of a liquid microdroplet by white light irradiation. Some studies on electric powered micromotor systems reported propulsion and self-spinning motions for the micro-objects in a parallel/planar electrodes system [16–19], rotation of particle in a rotating electric field [20]. When two point-shaped (needle-shaped) electrodes were introduced with a liquid droplet, a back-and-forth motion was observed [21,22]. When microparticles were used instead of a liquid droplet, other types of motions were observed, such as rotary motion for spherical particle/droplet and revolving motion for particle on a horizontal plane in liquid phase [23–25]. Another example is the cork-screw rotary motion of a helical micro particle spinning on its own long axis when put in an oil/ionic surfactant mixture [26] due to the electrophoretic convection of an ionic surfactant. Simulation models of

electric field for specific situations were built to have a better understanding of the micromotor system [26,27].

One goal in micromotor study is to increase the mobility of micromotor. However, different study groups use different parameters to represent the mobility of micromotors, frequently by micromotor's velocity [2,3,5,8,10,11,13,28–31], micromotor's angular velocity [20,29,32,33] or motion frequency [22,24,34]. Therefore, it is difficult to compare which micromotor has higher mobility, and which experiment condition is better. Moreover, the micromotor system is built for future microdevices adaptations, but there has been no report on the energy conversion efficiency of micromotor system as far as we aware.

In this study, we provide a quantification method to calculate the input and output power of micromotor system, thus, calculate the energy conversion efficiency of micromotor system. Here, back-and-forth motion of the water droplet between the needle-shaped electrodes [21,22] was comprehensively examined with the emphasis on electric current and electrochemical processes. The electric input energy was difficult to calculate due to the micrometer-scale experiment and the high electric resistant silicone oil that was used. We successfully measured the applied voltage and electric current by applying an electromagnetic shield over the experimental setup, and placing the whole system at ground level. This study quantified the input electric energy and output kinetic energy of particle motion, and reported the energy conversion efficiency of a micromotor system for the first time. The result reported here will increase our understanding on the efficiency of the micromotor system. From here, we can increase/maximise the efficiency of the system through various means in a systematic manner. This method can be the universal tool to compare different

micromotor systems developed by individual study groups. This study will significantly contribute to the development of micro electronic devices.

2.2. Method

2.2.1 Equipment and Software

Table 2-1 shows the equipment and software that were used in this study.

Table 2-1 The equipment and software that were used in this study.

Equipment and Software	Manufacturer
Ultrapure water purifier (PF3XXXXM1)	Elga
Vortex mixer (VTX-3000L)	Lms
Viscometer (HAAKE RheoStress1)	Thermofisher
Optical microscope (IX73)	Olympus
Needle type tungsten microelectrode (UJ-80-02-1.0)	Unique Medical
Power amplifier	Orix
Video recording software (FASTCAM viewer)	Photron
Image analysis software (TEMA64 4.0-008-64)	Photron
Ammeter (W32-6517A-R)	Keithley
Electromagnetic shield (DTM-888)	Toyama-Denki Building

2.2.2 Chemical Reagent

Table 2-2 shows the chemicals reagents that were used in this study.

Table 2-2 The chemicals reagents that were used in this study.

Chemical reagents	Manufacturer
silicone oil (KF-56)	Shin-Etsu Chemical Japan
di-(2-ethylhexyl)phosphoric acid (DEHPA, 97%,)	Aldrich

2.2.3 Preparation

The oil phase of the solution was prepared by mixing 100 µL silicone oil with 20 µL di-(2-ethylhexyl) phosphoric acid, in which, 0.5 µL ultra-pure water was subsequently added. The mixture was then shaken using a vortex mixer for approximately 1 min to obtain a water-in-oil droplet and afterwards, viscosity of the solution was measured.

The experimental setup prepared for droplet observation is shown in Fig. 2-1, where the solution was put on a slide glass and observed via an optical microscope. Two needle-shaped electrodes, controlled by manipulators, were inserted into the solution on the slide glass from the opposite side and DC voltage was applied by a power amplifier. The motion of the droplet was recorded using a video recording software and analysed by a software.

For measuring electric current, an ammeter was included in the electric circuit and an electromagnetic shield was applied to eliminate the noise from external sources. This shield was connected to a power amplifier and the ammeter via an alligator clip. The entire setup was placed at ground level.

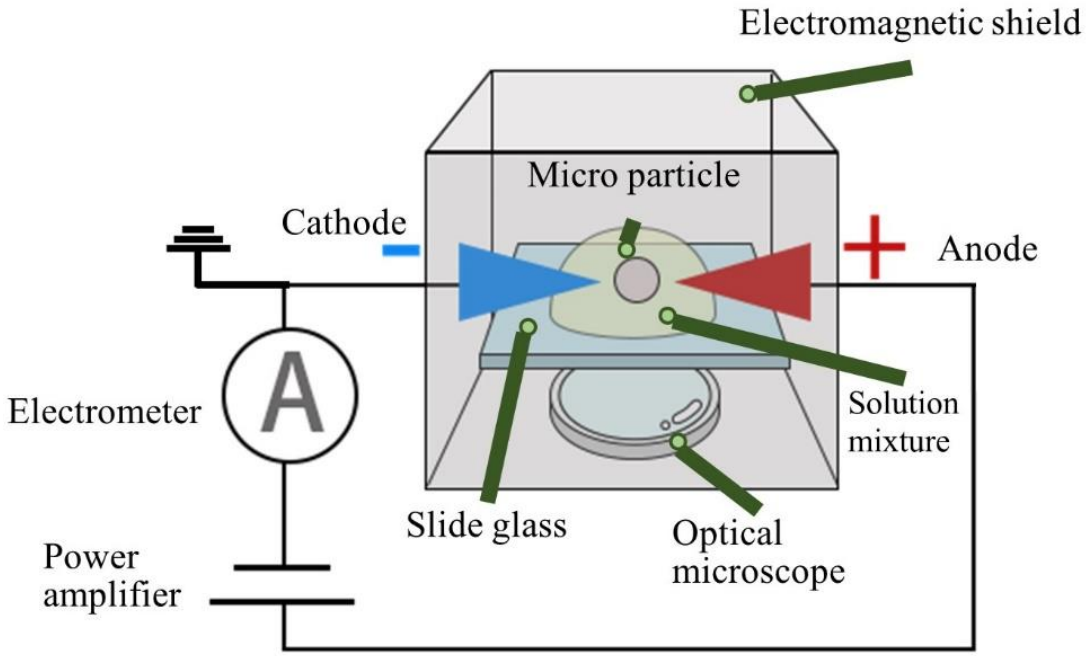

Fig. 2-1 Experimental setup prepared for micro droplet observation and electric current measurement.

2.3. Results and Discussion

2.3.1. Water Droplet Motion

When DC voltage between 50 V and 140 V was applied and the distance between the electrodes was set from 80 μm to 410 μm, only back-and-forth motion of the water droplet was observed, as reported by Kurimura, *et al.* and Hase, et al. [21,22], which was non-rotary. Rotary motion [23–25] was not observed.

Fig. 2-2 shows an example of back-and-forth motion of a water droplet ($\varnothing$ = 120 μm) under DC voltage of 55 V. The water droplet moved from the cathode to the anode along a straight line for 0.4 s and returned to the cathode along a straight line at 0.55 s after touching the anode. This motion was continuously repeated when the voltage was applied.

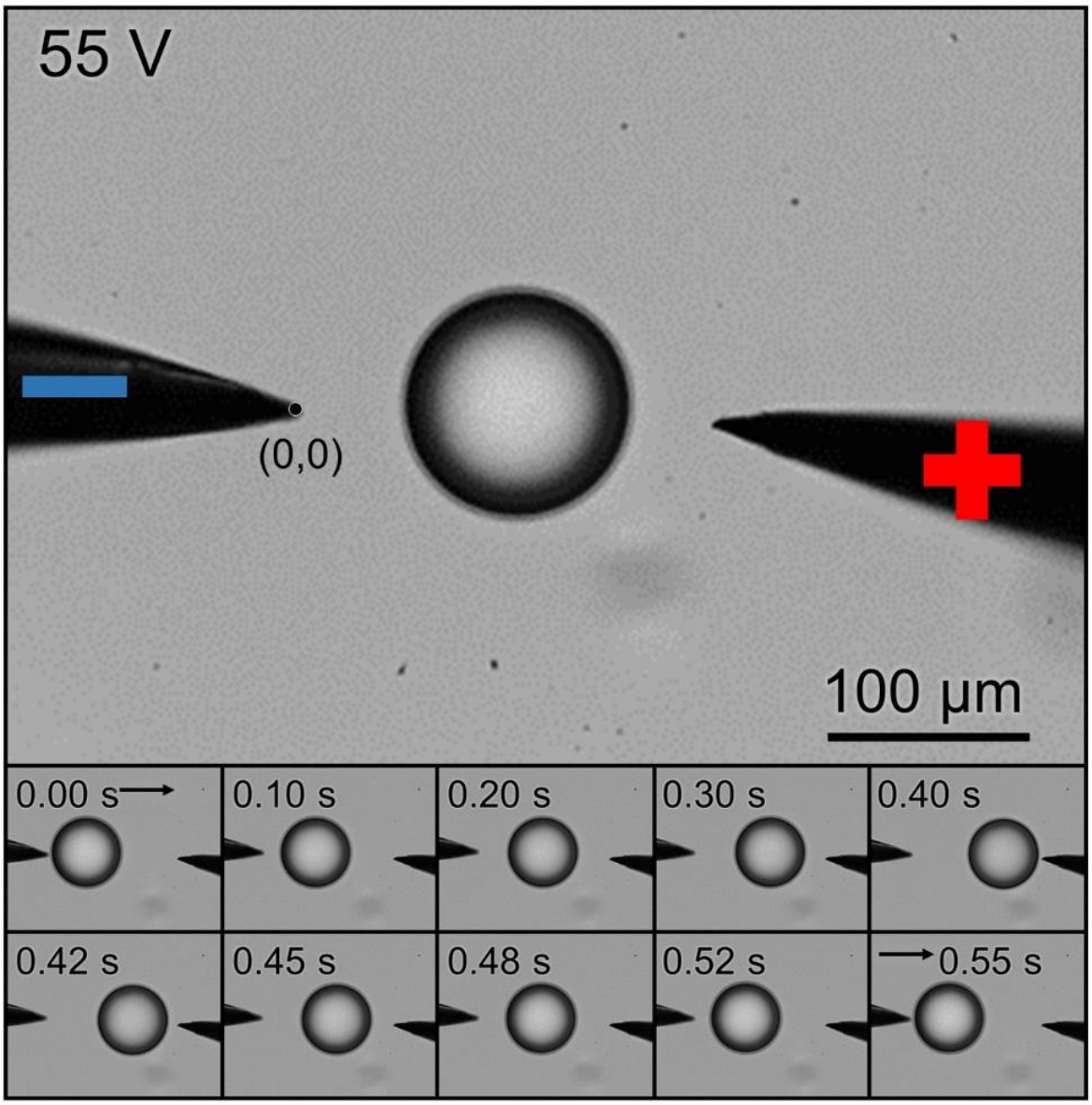

Fig. 2-2 Oscillation of the water droplet (∅= 120 μm) between the two electrodes under a voltage of 55 V DC voltage.

The tip of the cathode was set as the origin of the coordinate system and the direction from the cathode to the anode was set as positive. The mass centre of the water droplet was traced using a software. The droplet movement patterns at the applied voltage and distance between the electrodes of 50 V and 178 μm, respectively, are shown in Fig. 2-3, where *L* represents the distance between the mass centre of the water droplet and cathode. Undotted and dotted lines in Fig. 2-3 represent *L* and acceleration of the droplet, respectively. The peaks and dips in *L* represent when the water droplet reached the anode and cathode, respectively. Here, the back-and-forth motion is defined as the oscillating motion when the droplet reaches both electrodes. In the experiment carried out for Fig. 2-3(a), the water droplet ($\varnothing$ = 71 μm) oscillated with a frequency of f = 7.9 Hz. When the droplet reached the tips of the electrodes, the corresponding peaks and dips shown in the dotted line represent the abrupt decrease in its acceleration. This was due to the interruption in the droplet movement by the electrodes. A pattern of increasing acceleration was observed for the droplet as it moved near the anode/cathode. Fig. 2-3(b) shows a different water droplet ($\varnothing$ = 70 μm) under the same experimental conditions. The undotted line *L* suggests that the particle was also performing an oscillating motion at the frequency of f = 7.8 Hz. Additionally, the acceleration line can be seen to follow the same pattern as that shown in Fig. 2-3(a) (the difference in acceleration only corresponded to the difference in the movement direction).

Fig. 2-3(c) shows *L* and acceleration for another water droplet ($\varnothing$ = 22 μm) under same experimental conditions. Dips in *L* represent when the droplet reached the cathode and smooth downward curves instead of peaks represent when the droplet moved away from the cathode. These patterns suggested that the droplet did not oscillate. This type of motion can be considered to be a different type of back-and-

forth motion, defined as bouncing motion, implying the bouncing of the droplet on the cathode, without reaching the anode. Therefore, the droplet was performing a bouncing motion with a frequency of f = 3.8 Hz and this motion followed the same pattern where acceleration of the droplet increased near the electrodes. Under the experimental conditions used in this study, the modes of the motion were determined using the ratio of diameter of the droplet and distance between the electrodes. When the diameter of the droplet was larger than 20% of the distance between the electrodes, an oscillating-type back-and-forth motion was observed, otherwise, bouncing type motion was observed.

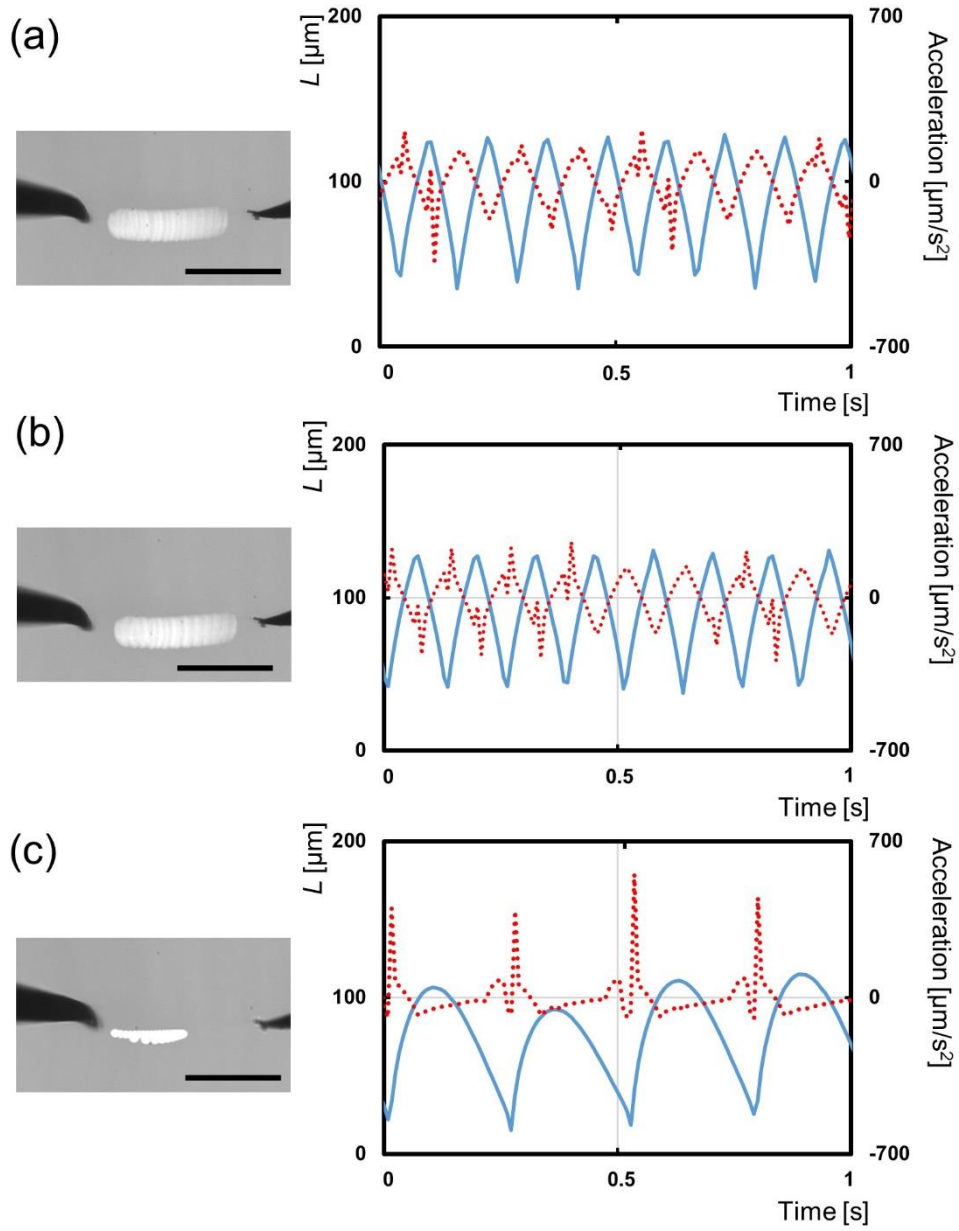

Fig. 2-3 Water droplets with (a) $\varnothing$ = 71 μm, (b) $\varnothing$ = 70 μm, and (c) $\varnothing$ = 22 μm performing back-and-forth motions under a voltage of 50 V and distance between the electrodes as 178 μm. The trajectory of the droplet movement in one period is shown in the images on the left side of the corresponding graphs, with a scale bar of 100 μm. The right side of the corresponding graphs showed the distance between the mass centre of the water droplet and cathode (*L*), and the acceleration of the droplet as undotted and dotted lines, respectively.

2.3.2. Electrolysis of the Water Droplet

A water droplet (∅ = 72 μm) was placed between the electrodes under a DC voltage of 50 V. The back-and-forth motion was observed to last for more than 508 s, until the particle disappeared. The droplet motion followed the same pattern as described in 2.3.1. Fig. 2-4 shows the electric current for this duration. The electric current was observed to be as low as a few pA due to the insulating silicone oil. It decreased over time, with several discontinuous changes observed. During this period, the volume of the water droplet kept decreasing. This could have been due the electrolysis of the water droplet. The water droplet vanished after 508 s, with the electric current showing a plateau at I = 1.72 pA. Fig. 2-4(a) and (b) display the time variation of the decrease in the volume of the water droplet over 508 s and time dependency of the droplet volume. The volume of the water droplet can be seen to linearly decreases with time.

The equation for electrolysis of water at the cathode is as follows:

$$\mathrm{H_2O} \rightarrow \frac{1}{2}\mathrm{O_2} + 2\mathrm{H^+} + 2\mathrm{e^-} \tag{2.1}$$

and the electric current for this electrolysis is expressed as:

$$I\left[{}^{C}/_{s}\right] = -F\left[{}^{C}/_{mol}\right] \times 2\,{}^{dn}/_{dt}\left[{}^{mol}/_{s}\right] \tag{2.2}$$

where I, F and n represent electric current, Faraday constant (F = 96500 C/mol) and the mole of water. Thus, the change in the volume of the water droplet is expressed as:

$${}^{dn}/_{dt}\left[{}^{mol}/_{s}\right] = {}^{dV}/_{dt}\left[{}^{m^3}/_{s}\right] \times {}^{dm}/_{dV}\left[{}^{kg}/_{m^3}\right] \times {}^{dn}/_{dm}\left[{}^{mol}/_{kg}\right] \tag{2.3}$$

where V and m represent the volume and the mass of water, respectively, and dV/dt was evaluated to be 3.97×10^{-16} m^3/s from the correlation line shown in Fig. 2-4(b). Resultantly, the electric current $I_{electrolysis} = 4.25\times10^{-6}$ A.

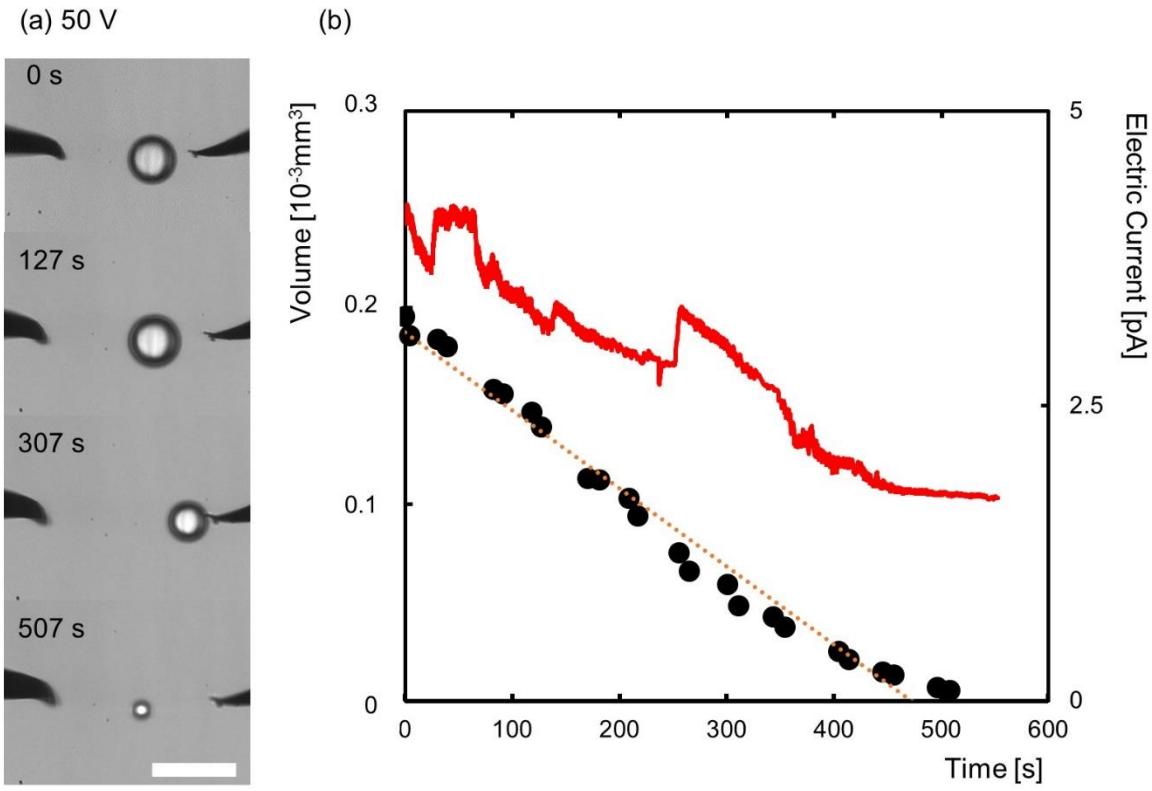

Fig. 2-4 Back-and-forth motion of the water droplet (∅ = 72 μm) over 508 s under a voltage of 50 V. (a) Photos of the water droplet at 0, 127, 307 and 507 s. The scale bar is 100 μm. (b) Black dots and red dotted line represent the droplet volumes at each time stamp and corresponding linear correlation line, respectively. Red line represents the electric current over time in a secondary axis.

Other reasons for the degradation of droplet volume could be dissolution of water into oil phase and wetting on the electrodes. To understand these effects, another set of experiments were carried out under same experimental conditions, except that silicone oil and DEHPA were saturated with ultra-pure water. This made the effect of dissolution negligible. The effects of wetting and electrolysis are discussed below.

Fig. 2-5 shows the rate of degradation of the droplet volume in a saturated solution (represented by white circles) under the applied voltage. The droplet volume decreased even when V = 0 V and in this condition, neither dissolution nor electrolysis occurred. The volume could have decreased due to the wetting effect of water on the electrodes. The degradation rate was significantly low, indicating small impact of wetting on volume reduction. Furthermore, the degradation rate was observed to linearly increase with increasing applied voltage. As the effects of dissolution and wetting were small, the increment in the degradation rate by the applied voltage was due electrolysis.

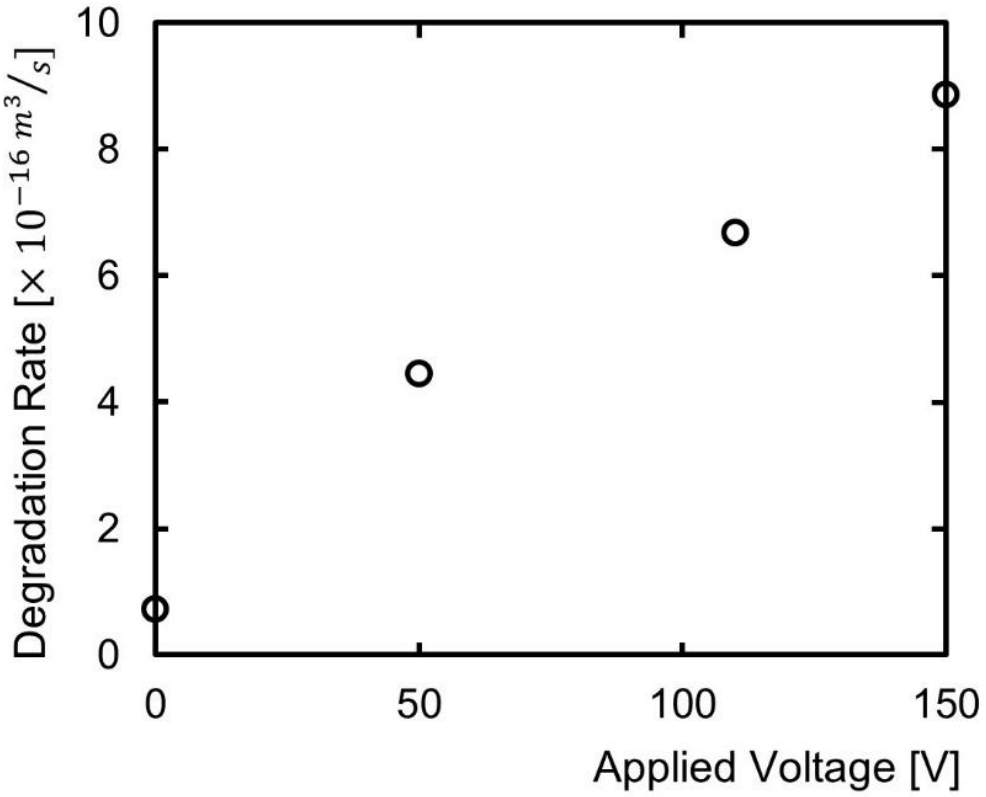

Fig. 2-5 Degradation rate of the water droplet volume under the applied voltage. White circles represent the degradation rates of the volume of the droplet in the solution saturated with water. The distance between the electrodes was set as 178 μm.

2.3.3. Energy Conversion Efficiency

The equation for the back-and-forth motion of the droplet is given as follows:

$$m\,{dv}/{dt} = F_{drive} - F_{Stokes'drag} \tag{2.4}$$

where v, F_{drive} and $F_{stoke's\ drag}$ represent the droplet velocity, driving force and Stokes' drag that exists in this silicone oil/DEHPA solution with high viscosity, respectively. Work done by F_{drive} for time interval Δt is calculated as follows:

$$W = \int_{t}^{t+\Delta t} F_{drive}\,dx \tag{2.5}$$

Using Eq. 2.4 in Eq. 2.5, we get:

$$W = \frac{1}{2}m\{v_{t+\Delta t}^2 - v_t^2\} + \int_{t}^{t+\Delta t} (F_{Stokes'drag})v\,dt \tag{2.6}$$

Thus, works done by the droplet motions shown in Fig. 2-3(a), (b) and (c) are W_a = 8.32×10^{-12} J, W_b = 2.09×10^{-12} J and W_c = 7.13×10^{-12} J, respectively. Furthermore, works (W') done by $F_{stoke's\ drag}$, shown in Fig. 2-3(a), (b) and (c), are W'_a = 8.32×10^{-12} J, W'_b = 2.09×10^{-12} J and W'_c = 7.13×10^{-12} J, respectively. The calculations show that most of the total work was done by $F_{stoke's\ drag}$, with F_{drive} having negligible effect. Therefore, the output power, as kinetic energy of the back-and-forth motion of the droplet, can be approximated by Stokes' drag as follows:

$$\text{average output power } (\mathrm{P_1}) = \frac{1}{T}\int_0^T 3\pi\eta\emptyset v(t) * v(t)\,dt \tag{2.7}$$

$$\text{instantaneous output power } (\mathrm{P_2}) = 3\pi\eta\emptyset v(t) * v(t) \tag{2.8}$$

where η, $\emptyset$ and T represent the solution viscosity, droplet diameter and time duration of the motion, respectively. The viscosity of the mixed solution was η = 1.58×10^{-2} Pas at 25 °C. Thus, the average output power, for Fig. 2-3(a), is calculated as P_1 = 2.78×10^{-12} J/s. Conversely, the instantaneous output power varied with time. To evaluate the output using Eq. 2.8, median of v (ranging from 3.0 to 737.0 μm/s) was used. Using

Eq. 2.8 was found to be easier than using Eq. 2.7. This method resulted in P_2 = 2.94×10^{-12} J/s and the results from Eq. 2.7 and 2.8 were found to be significantly close. The median of v acquired from Fig. 2-3, will be used for simplicity hereafter.

Fig. 2-6 shows the time course of the power output of the motions of the droplet, with standard deviation shown as the spans of errors. For this figure, applied voltage and distance between the electrodes were fixed as 50 V and 178 μm, respectively. Fig. 2-6 also shows the input of this system based on the measured electric current and energy conversion efficiency calculated as follows:

$$\varphi = {P_{output}}\Big/{P_{input}} \tag{2.9}$$

Where φ, P_{output} and P_{input} represent the conversion efficiency, the input and output powers of the electric and droplet kinetic energies, respectively. The average energy conversion efficiency is evaluated to be φ = 2.3 % using Eq. 2.8, with the current $I_{measured}$ measured by the ammeter being used for the calculation. This is the first study to measure the conversion efficiency of an electric micromotor.

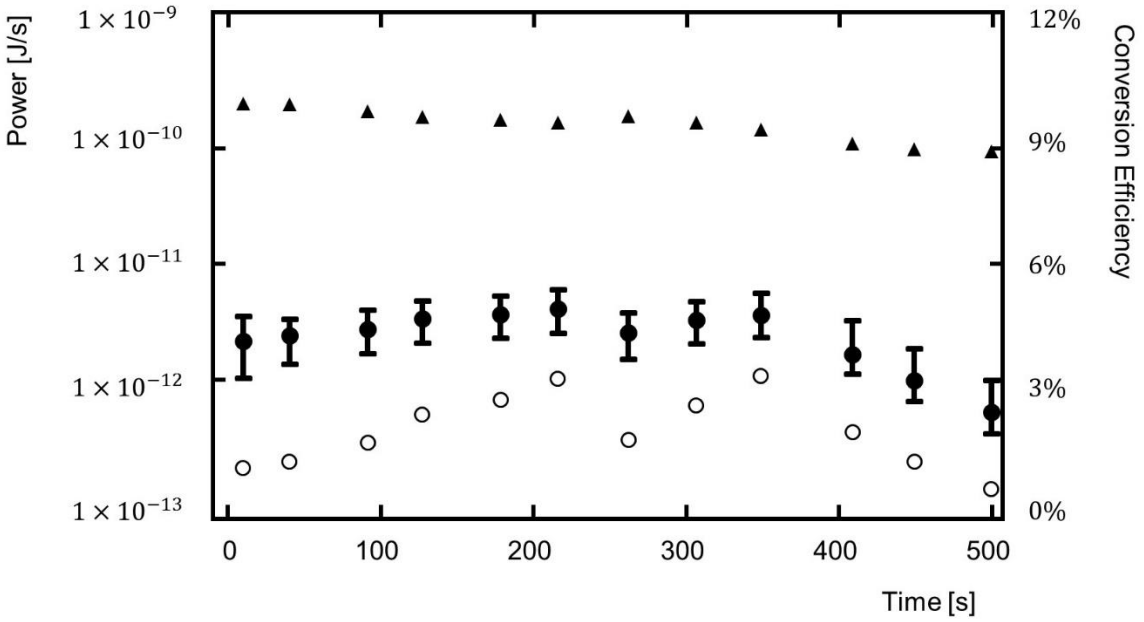

Fig. 2-6 Input (black triangles) and output (black dots) of the back-and-forth motion under 50 V and 178 μm electrodes distance. White dots represent the conversion efficiency at each measurement section.

Conversely, the electric current of electrolysis was calculated to be $I_{electrolysis}$ = 4.25×10^{-6} A, not detected by the ammeter, probably due to limited capability of the ammeter. The electrolysis occurred only when the water droplet touched the electrodes. This contact lasted for less than 8 ms. However, the time resolution of this ammeter was 156 ms, significantly longer than the contact period. Moreover, when the current drastically changed quickly, the ammeter took 2 to 5 s to respond to this change. This also complicated the detection of $I_{electrolysis}$. Therefore, the ammeter could not detect the pulse-like electric current caused by electrolysis. When the current of electrolysis $I_{electrolysis}$ was considered, the conversion efficiency $\varphi_{electrolysis}$ ~0.000001%. Considering that $I_{electrolysis} >> I_{measured}$, the energy input of this system should be calculated using $I_{electrolysis}$. Therefore, the real conversion efficiency should be $\varphi_{electrolysis}$ ~0.000001%. This efficiency was significantly low even though this was the first time that the conversion ratio was calculated for an electric micromotor.

This electrochemical process of electrolysis consumed significantly amount of electric energy, which dramatically decreased the conversion efficiency. Likewise, other energy consumption processes took place in this system: (i) fluid convection caused by DEHPA surfactant flow [25], (ii) other droplets or particles moving in or outside of observation area and (iii) Joule heating. In future studies on micromotor system, chemically inert solid particles at the electrodes should be used to increase the conversion ratio. Moreover, the electrochemical process between the particle and electrodes in the system should be reduced to avoid unnecessary energy lost.

2.4. Conclusion

A water droplet moving back-and-forth between two needle-shaped electrodes was examined in this study. Two back-and-forth motion modes were observed: oscillating and bouncing. When the diameter of the droplet was larger than 20% of

electrodes distance, oscillating-type back-and-forth motion was observed, otherwise, bouncing motion was observed. During the back-and-forth motion of the droplet, the acceleration increased when the droplet moved near the anode/cathode. The volume of the droplet was found to decrease with time when the droplet moved due to electrolysis. A quantification method was proposed to calculated the kinetic energy output of the droplet from Stokes' drag equation and the electric energy input. The energy conversion efficiency was thus quantified for the first time in micromotor study, and it has become clear that the efficiency was significantly small. This is attributable to the electrochemical process of electrolysis. In future studies, chemically inert solid particle should be used and electrochemical process between the particle and electrodes should be reduced, so as to increase the energy efficiency. The quantification method proposed in this study can become a universal tool for micromotor studies. It enables the discussion of micromotor system comparisons and can improve the development of micromotor system significantly.

References

[1] B. Jurado-Sánchez, J. Wang, Micromotors for environmental applications: a review, Environ. Sci. Nano. 5 (2018) 1530–1544. https://doi.org/10.1039/C8EN00299A.

[2] Y. Liu, D. Ge, J. Cong, H.-G. Piao, X. Huang, Y. Xu, G. Lu, L. Pan, M. Liu, Magnetically Powered Annelid-Worm-Like Microswimmers, Small. 14 (2018) 1704546. https://doi.org/10.1002/smll.201704546.

[3] S. Tottori, L. Zhang, F. Qiu, K.K. Krawczyk, A. Franco-Obregón, B.J. Nelson, Magnetic Helical Micromachines: Fabrication, Controlled Swimming, and Cargo Transport, Adv. Mater. 24 (2012) 811–816. https://doi.org/10.1002/adma.201103818.

[4] W. Gao, S. Sattayasamitsathit, K.M. Manesh, D. Weihs, J. Wang, Magnetically Powered Flexible Metal Nanowire Motors, J. Am. Chem. Soc. 132 (2010) 14403–14405. https://doi.org/10.1021/ja1072349.

[5] L. Zhang, T. Petit, Y. Lu, B.E. Kratochvil, K.E. Peyer, R. Pei, J. Lou, B.J. Nelson, Controlled Propulsion and Cargo Transport of Rotating Nickel Nanowires near a Patterned Solid Surface, ACS Nano. 4 (2010) 6228–6234. https://doi.org/10.1021/nn101861n.

[6] G. Zhao, M. Pumera, Magnetotactic Artificial Self-Propelled Nanojets, Langmuir. 29 (2013) 7411–7415. https://doi.org/10.1021/la303762a.

[7] D. Yamamoto, A. Shioi, Self-Propelled Nano/Micromotors with a Chemical Reaction: Underlying Physics and Strategies of Motion Control, KONA Powder Part. J. 32 (2015) 2–22. https://doi.org/10.14356/kona.2015005.

[8] W.F. Paxton, K.C. Kistler, C.C. Olmeda, A. Sen, S.K. St. Angelo, Y. Cao, T.E. Mallouk, P.E. Lammert, V.H. Crespi, Catalytic Nanomotors: Autonomous Movement of Striped Nanorods, J. Am. Chem. Soc. 126 (2004) 13424–13431. https://doi.org/10.1021/ja047697z.

[9] D. Yamamoto, T. Takada, M. Tachibana, Y. Iijima, A. Shioi, K. Yoshikawa, Micromotors working in water through artificial aerobic metabolism, Nanoscale. 7 (2015) 13186–13190. https://doi.org/10.1039/C5NR03300D.

[10] K. Chen, C. Gu, Z. Yang, M. Nakajima, T. Chen, T. Fukuda, “Z”-Shaped Rotational Au/Pt Micro-Nanorobot, Micromachines. 8 (2017) 183. https://doi.org/10.3390/mi8060183.

[11] D. Kagan, M.J. Benchimol, J.C. Claussen, E. Chuluun-Erdene, S. Esener, J. Wang, Acoustic Droplet Vaporization and Propulsion of Perfluorocarbon-Loaded Microbullets for Targeted Tissue Penetration and Deformation, Angew.

Chemie Int. Ed. 51 (2012) 7519–7522. https://doi.org/10.1002/anie.201201902.

[12] W. Wang, L.A. Castro, M. Hoyos, T.E. Mallouk, Autonomous Motion of Metallic Microrods Propelled by Ultrasound, ACS Nano. 6 (2012) 6122–6132. https://doi.org/10.1021/nn301312z.

[13] J.-F. Louf, N. Bertin, B. Dollet, O. Stephan, P. Marmottant, Hovering Microswimmers Exhibit Ultrafast Motion to Navigate under Acoustic Forces, Adv. Mater. Interfaces. 5 (2018) 1800425. https://doi.org/10.1002/admi.201800425.

[14] N.K. Metzger, M. Mazilu, L. Kelemen, P. Ormos, K. Dholakia, Observation and simulation of an optically driven micromotor, J. Opt. 13 (2011) 044018. https://doi.org/10.1088/2040-8978/13/4/044018.

[15] D. Zhang, Y. Sun, M. Li, H. Zhang, B. Song, B. Dong, A phototactic liquid micromotor, J. Mater. Chem. C. 6 (2018) 12234–12239. https://doi.org/10.1039/C8TC04260H.

[16] R. Yamamoto, D. Yamamoto, A. Shioi, S. Fujii, T. Kurimura, K. Yoshikawa, Arrangement and Periodic Motion of Microparticles in an Oil Phase under a DC Electric Field, J. Soc. Powder Technol. Japan. 51 (2014) 823–827. https://doi.org/10.4164/sptj.51.823.

[17] P. Calvo-Marzal, S. Sattayasamitsathit, S. Balasubramanian, J.R. Windmiller, C. Dao, J. Wang, Propulsion of nanowire diodes, Chem. Commun. 46 (2010) 1623. https://doi.org/10.1039/b925568k.

[18] S. Gangwal, O.J. Cayre, M.Z. Bazant, O.D. Velev, Induced-Charge Electrophoresis of Metallodielectric Particles, Phys. Rev. Lett. 100 (2008) 058302. https://doi.org/10.1103/PhysRevLett.100.058302.

[19] S.T. Chang, V.N. Paunov, D.N. Petsev, O.D. Velev, Remotely powered self-propelling particles and micropumps based on miniature diodes, Nat. Mater. 6 (2007) 235–240. https://doi.org/10.1038/nmat1843.

[20] L. Rodríguez-Sánchez, A. Ramos, P. García-Sánchez, Electrorotation of semiconducting microspheres, Phys. Rev. E. 100 (2019) 042616. https://doi.org/10.1103/PhysRevE.100.042616.

[21] T. Kurimura, M. Ichikawa, M. Takinoue, K. Yoshikawa, Back-and-forth micromotion of aqueous droplets in a dc electric field, Phys. Rev. E. 88 (2013) 042918. https://doi.org/10.1103/PhysRevE.88.042918.

[22] M. Hase, S.N. Watanabe, K. Yoshikawa, Rhythmic motion of a droplet under a dc electric field, Phys. Rev. E. 74 (2006) 046301. https://doi.org/10.1103/PhysRevE.74.046301.

[23] D. Yamamoto, R. Yamamoto, T. Kozaki, A. Shioi, S. Fujii, K. Yoshikawa, Periodic Motions of Solid Particles with Various Morphology under a DC Electrostatic Field, Chem. Lett. 46 (2017) 1470–1472. https://doi.org/10.1246/cl.170622.

[24] M. Takinoue, Y. Atsumi, K. Yoshikawa, Rotary motion driven by a direct current electric field, Appl. Phys. Lett. 96 (2010) 104105. https://doi.org/10.1063/1.3358385.

[25] T. Kurimura, S. Mori, M. Miki, K. Yoshikawa, Rotary motion of a micro-solid particle under a stationary difference of electric potential, J. Chem. Phys. 145 (2016) 034902. https://doi.org/10.1063/1.4958657.

[26] D. Yamamoto, K. Kosugi, K. Hiramatsu, W. Zhang, A. Shioi, K. Kamata, T. Iyoda, K. Yoshikawa, Helical micromotor operating under stationary DC electrostatic field, J. Chem. Phys. 150 (2019) 014901.

https://doi.org/10.1063/1.5055830.

[27] T. Michálek, A. Bolopion, Z. Hurák, M. Gauthier, Control-oriented model of dielectrophoresis and electrorotation for arbitrarily shaped objects, Phys. Rev. E. 99 (2019) 053307. https://doi.org/10.1103/PhysRevE.99.053307.

[28] U.K. Cheang, F. Meshkati, H. Kim, K. Lee, H.C. Fu, M.J. Kim, Versatile microrobotics using simple modular subunits, Sci. Rep. 6 (2016) 30472. https://doi.org/10.1038/srep30472.

[29] R.A. Archer, J.R. Howse, S. Fujii, H. Kawashima, G.A. Buxton, S.J. Ebbens, pH - Responsive Catalytic Janus Motors with Autonomous Navigation and Cargo - Release Functions, Adv. Funct. Mater. 30 (2020) 2000324. https://doi.org/10.1002/adfm.202000324.

[30] Y. Sumino, N. Magome, T. Hamada, K. Yoshikawa, Self-Running Droplet: Emergence of Regular Motion from Nonequilibrium Noise, Phys. Rev. Lett. 94 (2005) 068301. https://doi.org/10.1103/PhysRevLett.94.068301.

[31] M.M. Alcanzare, M. Karttunen, T. Ala-Nissila, Propulsion and controlled steering of magnetic nanohelices, Soft Matter. 15 (2019) 1684–1691. https://doi.org/10.1039/C8SM00037A.

[32] M. Zrínyi, M. Nakano, Toward Colloidal Motors, Period. Polytech. Chem. Eng. 61 (2017) 15. https://doi.org/10.3311/PPch.10274.

[33] T. Harada, K. Yoshikawa, Mode switching of an optical motor, Appl. Phys. Lett. 81 (2002) 4850–4852. https://doi.org/10.1063/1.1527235.

[34] L. Liu, B. Chen, K. Liu, J. Gao, Y. Ye, Z. Wang, N. Qin, D.A. Wilson, Y. Tu, F. Peng, Wireless Manipulation of Magnetic/Piezoelectric Micromotors for Precise Neural Stem - Like Cell Stimulation, Adv. Funct. Mater. 30 (2020) 1910108. https://doi.org/10.1002/adfm.201910108.

Chapter 3

Energy Flux on a Micromotor Operating under Stationary Direct Current Voltage

3.1. Introduction

The study of nano- and micromotors has developed rapidly over the past decade [1]. A micromotor, or microswimmer in other studies[2,3], is a particle or droplet at the nano- or micrometer scales with mobility under certain conditions. Various types of systems are being developed around such micromotors for applications such as cargo and drug delivery in the medical field [2–7] and environmental use [8,9]. Often, these micromotors must be submerged in liquids for their applications. The Reynolds number in these micro-environments is extremely low, which means the micromotor relies heavily on the effect of viscosity. Therefore, a continuous source of energy is required to maintain the motion of the micromotor.

A few methods are used to provide energy to the micromotor system. Some studies used chemical reactions for the energy source [5,9–12], and others used magnetic fields [2–4,6,13–16]. An optical light can be applied directly or indirectly to induce micromotor motions [17,18]. Some micromotors were driven using ultrasound [19,20]. Other studies used electricity, which was also used in this study.

One of the aims in the study of micromotors, being particles or droplets, is to increase their mobility in a system. The mobility is frequently represented by the micromotor's velocity [2-5,10,12,15,16,19-21], angular velocity [5,18,22,23] or motion frequency [24–26]. The mobility of these micromotors has been discussed with these parameters. Until now, studies on micromotors have been individually developed by different research groups. However, micromotors in different experimental conditions are difficult to compare. For example, how one can conclude which micromotor system is better: a solid micromotor with oscillating motion but complicated electrode configuration [27], or a similar motion by a liquid micromotor with a different motion trajectory in a two needle-shaped electrodes system [24]? A small particle with a high

velocity can have the same power as a large particle with a low velocity. Without a universal quantification method such as the quantification of energy conversion efficiency, this is very difficult to evaluate.

In this study, a two needle-shaped electrodes system was used and the micromotor was powered by an external energy supply. A direct current voltage was applied to the oil solution containing the micromotor, and hence the electric field causes the motions of any substances with electric charge. It is important to avoid the energy consumption by electric and electrochemical processes that occur at a distance from the moving micromotors. The efficiency of electric micromotor system not only shows what is the desired motion of micromotor, but also the dissipation of the system, which indicates what to improve in the future.

In this study, the micromotor was a solid polyethylene spherical particle that exhibit not only revolving but also spinning motions. The micromotor was driven by the fluidic field, which essentially was similar to other micromotor system that was governed by external field like magnetic or electric. The applied forces on the particle were analysed and their powers quantified from its viscous drag [28] and torque. With this quantification method, the mobility, in a form of mechanical energy output, can be compared to identify optimal experimental conditions.

The energy flux of the system comes from the electricity. The electricity applied to the system via power supply, dispersed onto the solutions. Solution started electrophoretic convection, which drove the particle motions. Therefore, the end of this energy flux was on the microparticles and the kinetic energy from their motions. The energy flux was discussion using the quantification method with a focus on the energy conversion efficiency from electric energy to mechanical power of the particle motion. The energy conversion efficiency, which is an essential parameter for any electric

devices, was used as a tool to compare different experimental conditions in this study. This quantification method of energy conversion efficiency can be used as a universal method to compare different micromotor systems in different studies, and will significantly improve the development of micromotor studies.

3.2. Method

3.2.1. Equipment and Software

Table 3-1 shows the equipment and software that were used in this study.

Table 3-1 The equipment and software that were used in this study.

Equipment and Software	Manufacturer
Ultrapure water purifier (PF3XXXXM1)	Elga
Vortex mixer (VTX-3000L)	Lms
Viscometer (HAAKE RheoStress1)	Thermofisher
Optical microscope (IX73)	Olympus
Needle type tungsten microelectrode (UJ-80-02-1.0)	Unique Medical
Power amplifier	Orix
Video recording software (FASTCAM viewer)	Photron
Image analysis software (TEMA64 4.0-008-64)	Photron
Ammeter (W32-6517A-R)	Keithley
Electromagnetic shield (DTM-888)	Toyama-Denki Building
Polyethylene particles (d = 175 μm, FLO-BEADS® CL-2507)	Sumitomo Seika Chemicals

3.2.2. Chemical Reagent

Table 3-2 shows the chemicals reagents that were used in this study.

Table 3-2 The chemicals reagents that were used in this study.

Chemical reagents	Manufacturer
silicone oil (KF-56)	Shin-Etsu Chemical Japan
di-(2-ethylhexyl)phosphoric acid (DEHPA, 97%,)	Aldrich

3.2.3. Preparation

The oil solution was prepared by mixing silicone oil was mixed with the anionic surfactant di-(2-ethylhexyl) phosphoric acid (DEHPA) in a plastic tube. Subsequently, sphere-shaped low-density polyethylene particles were added into the oil mixture. A vortex mixer was used to perform the mixing by placing the plastic tube in it for approximately 1 min. The viscosity of the solution was measured using a rotational viscometer.

Fig. 3-1(a) shows the experimental setup for the observation of the particle motion. The prepared solution was placed on a slide glass. Two needle-shaped electrodes were inserted into the solution via manipulators in a diagonal arrangement (Fig. 3-1(b)), and the heights of these electrodes were fixed in the experiment. A direct current voltage was applied using a power amplifier. The motion of the particle was recorded using a high-speed camera and recording software. The captured videos were analysed using software. An ammeter was used to measure the electric current.

The entire setup was set inside an electromagnetic shield to eliminate noise from external sources. The electric potential of the setup and shield was placed at ground level.

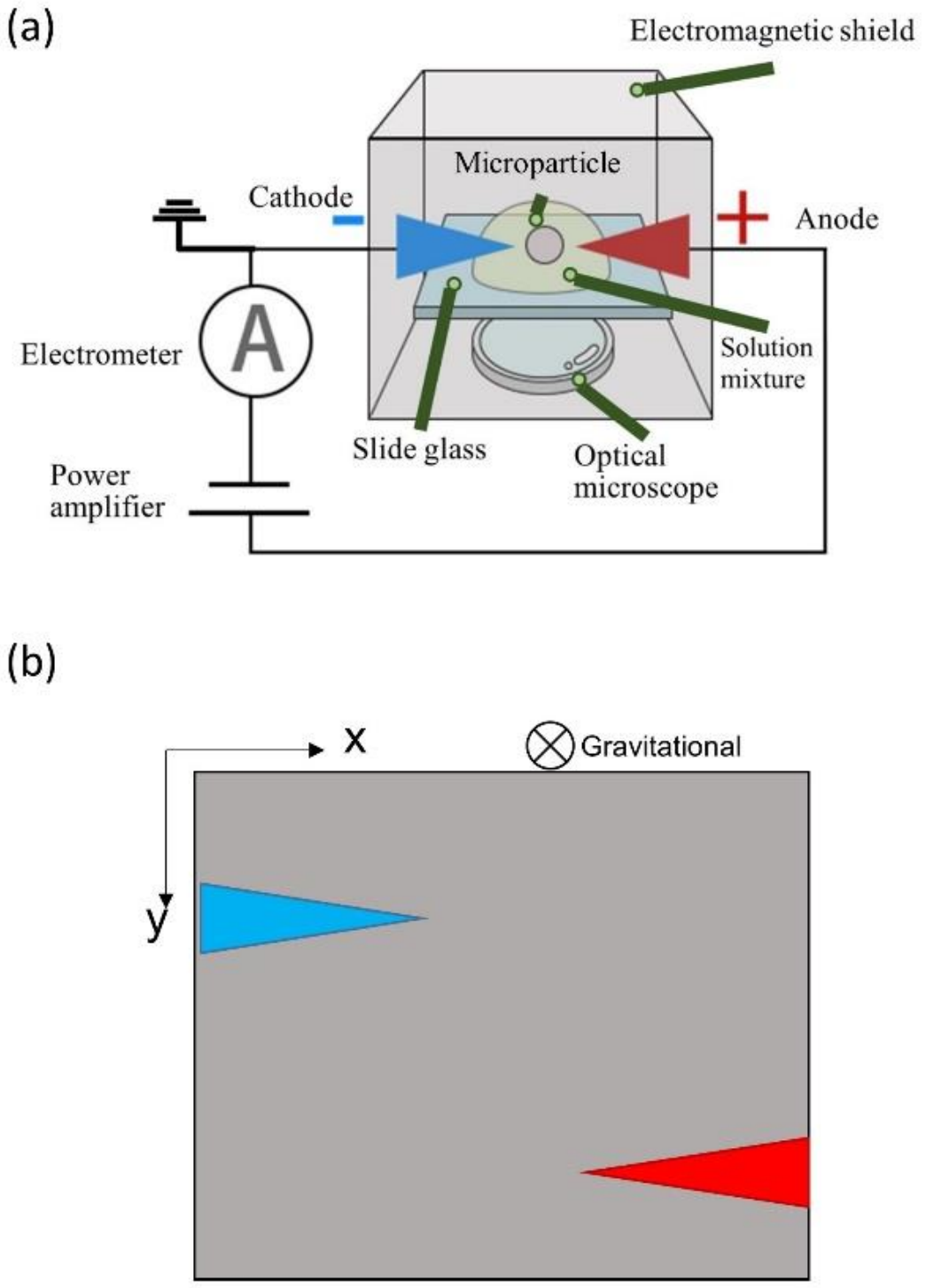

Fig. 3-1 Schematics of the experimental setup. (a) Setup of the experiment. (b) Electrode arrangements where two needle-shaped electrodes aligned diagonally.

3.3. Result and Discussion

3.3.1. Microparticle Motions

Two types of particle motions were observed: revolving and spinning, which are shown in Fig. 3-2(a) and (b), respectively. Revolving is defined as a particle moving along a circular trajectory, which is shown in Fig. 3-2(a) as a red line. The driving force for this motion was considered to be produced by the electrophoretic convection of the anionic surfactant DEHPA [29,30]. Spinning (Fig. 3-2(b)) is defined as a particle spinning around its centre of mass. In a previous study, the revolving motion was reported as the “rotary motion” of the polyethylene particle between two needle-shaped electrodes [30]. The spinning motion of this particle is first discussed in this paper.

Fig. 3-2 shows the two types of motions of the same particle ($\varnothing$ = 178 μm) under the same applied voltage (V = 200 V). The centre of mass of the particle was tracked, and the motion trajectory of the revolving motion is shown in Fig. 3-2(a) as a red line. A clockwise revolving motion was observed, which fit the direction of electrophoretic flow of DEHPA. Fig. 3-2(b) shows the time sequence of the same particle in Fig. 3-2(a). Black dots (indicated by black arrows), which were probably impurities, were observed on the particle. Using these dots, the spinning motion of the particle was tracked and the direction was clockwise.

The anionic surfactant DEHPA presumably formed inverted micelles in oil phase and were transparent to the optical light [30]. These negatively-charged inverted micelles flew from cathode to anode due to electrophoresis, created convection between electrodes [29]. This convection carried the microparticle. Therefore, microparticle moved from cathode to anode. At the beginning, the microparticle was located at the southern side of the left electrode as shown in Fig. 3-2(a). The northern

side of the microparticle was dragged by the electrophoretic flow while the southern side of the microparticle was not. Thus, the microparticle spun in a clockwise direction, which was along with the flow direction. As the microparticle moved both translationally and spun, the trajectory of the motion became curve due to the viscous effect. As a result, the revolving motion was formed with the spinning motion, and both of them were driven by the electrophoretic flow of DEHPA. The directions of revolving and spinning motions were observed to always fit the direction of DEHPA flow. The direction of the revolving motion also suggested that the particle was not charged in this study. When a conductive particle was used in a similar experimental setup, the particle was charged by the electric field. This charged particle altered the distribution of the electric field intensity, which caused the electrophoretic convection of DEHPA in a opposite direction [29]. This suggested that the spinning motion was driven by the electrophoretic flow of DEHPA as well. The directions of revolving and spinning motions were observed to always fit the direction of DEHPA flow. In this study, two motion modes of the particle were observed: (i) spinning motion with revolving motion, and (ii) spinning motion without revolving motion. Revolving motion of particle without spinning was not observed.

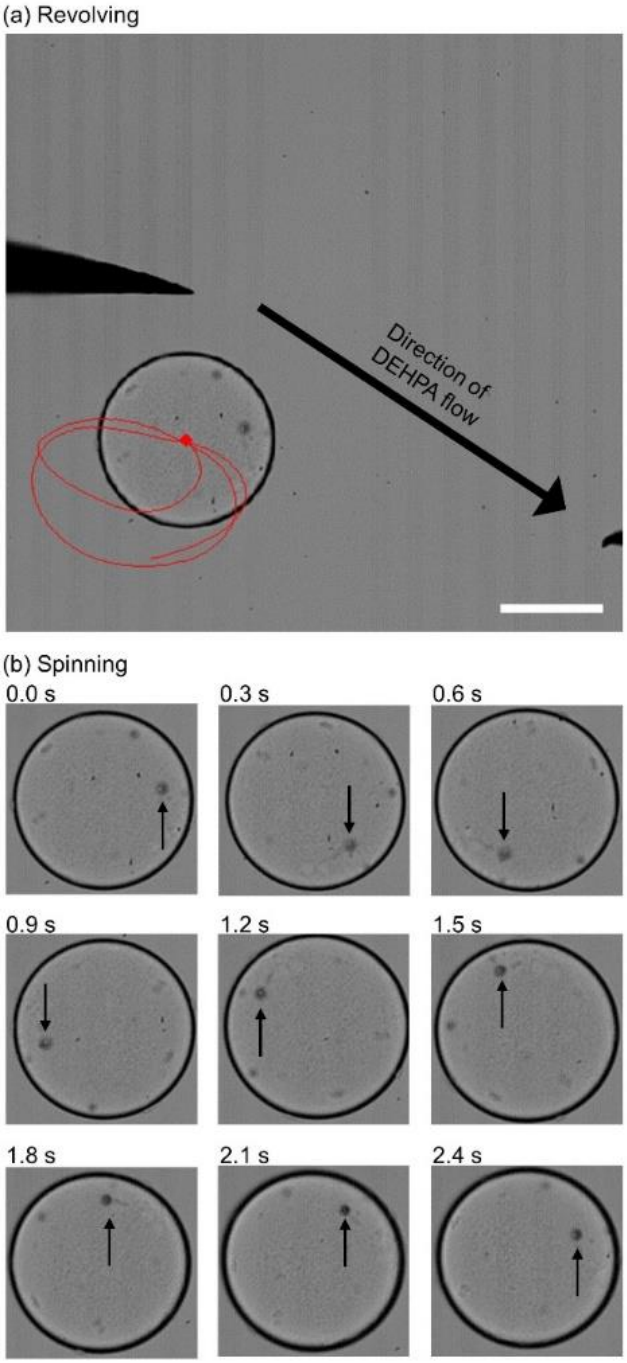

Fig. 3-2 Two types of motion when the particle was under a direct current voltage of 200 V. (a) Revolving motion of the particle. The red line indicates the trajectory of the centre of mass of the particle for 8 s. The arrow shows the direction of the supposed surfactant flow in the system. The motion direction was clockwise. (b) Spinning motion of the particle. The black dot indicated by the arrow was an impurity on the particle. The motion direction was clockwise. The scale bar is 100 μm.

3.3.1.1. Revolving Motion and Viscous Drag

When the particle in Fig. 3-2 revolves, its equation of motion is

$$m\,{dv}/{dt} = F_{drive} - F_{drag} \tag{3.1}$$

where, m, v, t, F_{drive}, and F_{drag} are the particle mass, particle velocity, time, driving force, and viscous drag, respectively. The mechanical work (W) performed by F_{drive} at a given time interval between t and $t+\Delta t$ is

$$W = \frac{1}{2}m(v_{t+\Delta t}^2 - v_t^2) + \int_t^{t+\Delta t} (3\pi\eta\emptyset v) * v\,dt \tag{3.2}$$

Where, η and $\emptyset$ are the solution viscosity and particle diameter, respectively. The Reynolds number in this study was extremely low (Re ≈ 10^{-2} << 1); therefore, the Stokes equation for viscous drag was used. For this extremely low Reynolds number, the inertia effect represented by the first term of the right-hand side of Eq. 3.2 is negligible and the work performed by the particle's revolving motion is mostly given by the second term on the right-hand side of Eq. 3.2. Therefore, the output power of the kinetic energy (P_1) caused by the revolving motion averaged over a time duration of T(<$P1$>) is approximated as

$$< P_1 >= \frac{1}{T}\int_0^T 3\pi\eta\emptyset v(t) * v(t)\,dt \tag{3.3}$$

Fig. 3-3 shows the <P_1> of different particles under different applied voltages. The particles were categorized by their diameters: <120, 121~170, and >171 μm, which are shown as crosses, circles, and diamonds. <P_1> increased monotonically with an increase in the applied voltage, and a power correlation curve is shown, irrespective of diameter, as a dotted line. The driving force was probably caused by the electrophoretic flow of DEHPA, which results in this positive correlation. The

electrode arrangement was fixed, so an increase in applied voltage increased the electric field intensity, which enhanced the effect of the DEHPA electrophoretic flow, thereby increasing the P_1 of the particle.

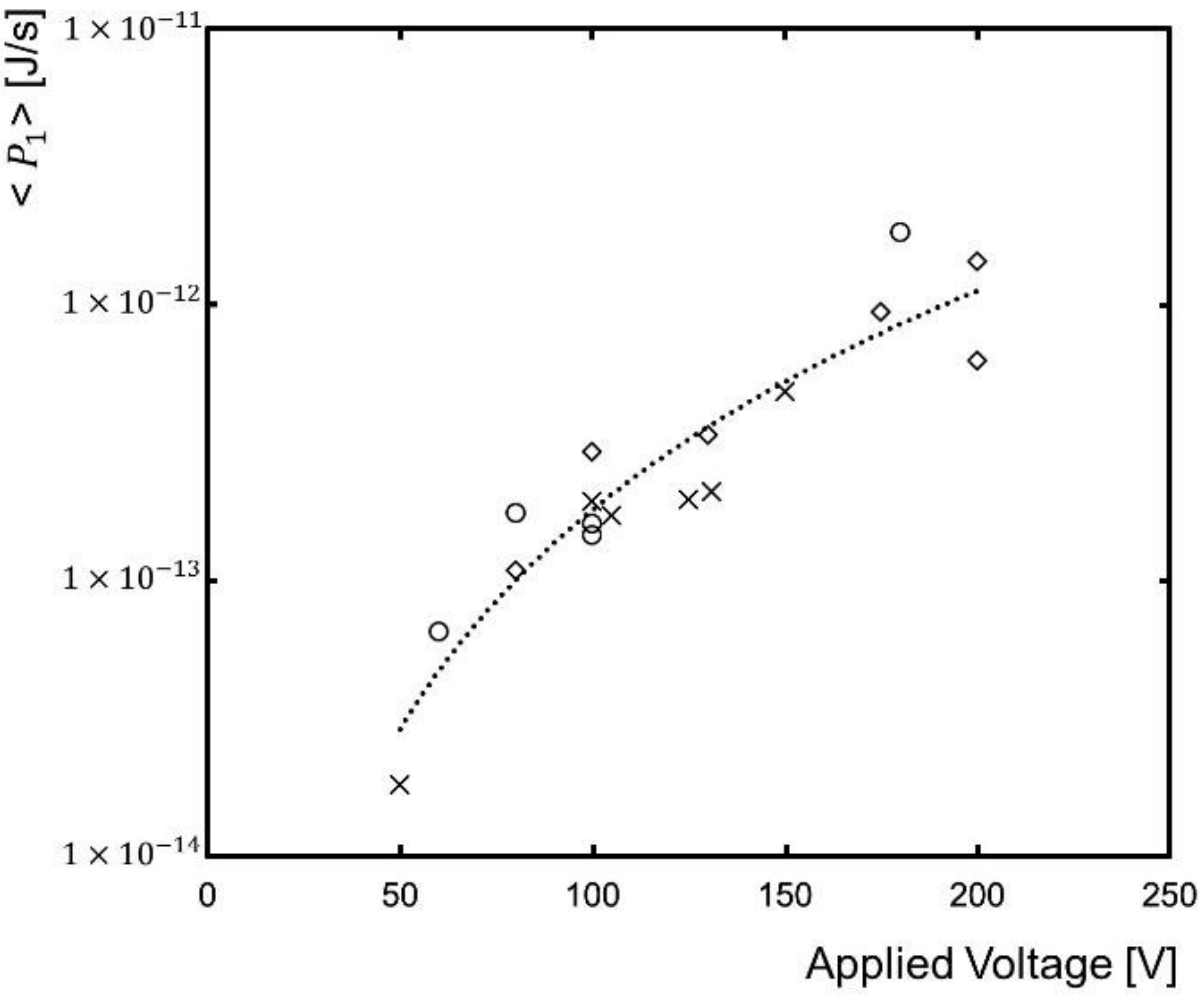

Fig. 3-3 Average output power of particles depending on applied voltage when the particle was revolving. The power correlation is indicated by a dotted line. The crosses, circles, and diamonds represent particles with the diameters of <120, 121~170, and >171 μm, respectively.

3.3.1.2. Spinning Motion and Viscous Torque

When a spherical microparticle spins in viscous solution, the mechanical work performed by the spin (W_τ) is estimated by the rotational drag [16,31,32]. The work within the time interval *t* and *t*+Δt is given as follows:

$$W_\tau = \int_t^{t+\Delta t} \pi\eta\emptyset^3\omega(t) * \omega(t)\, dt \tag{3.4}$$

where, ω is the angular velocity. Thus, the average output power (P_2) of this spinning motion over a time duration (T) is calculated as

$$< P_2 >= \frac{1}{T}\int_0^T W_\tau(t)\, dt \tag{3.5}$$

Fig. 3-4 shows the <P_2> of different particles under different applied voltages. The crosses, circles, and diamonds in the graph represent particles with diameters of <120, 121~170, and >171 μm, respectively. A tendency was observed in that the P_2 is higher at higher applied voltage. This result suggested that the electrophoretic flow of DEHPA is the driven force for spinning motion.

However, the data was relatively scattered compared with that shown in Fig. 3-3. This scattering was unrelated to particle size because even the results within the same category exhibited scatter. This difference may have been due to the surface roughness of the microparticles. The surface roughness of each particle varied; therefore, the boundary condition between DEHPA liquid flow and particle surface varied. At present, the surface roughnesses of individual particles were difficult to determine, but the impurities in or on the particle were possibly the indirect proof that surface roughness differed from particle to particle.

Moreover, particles in different size groups had similar scatteredness under same experimental conditions. Therefore, the effect of particle size was a minor factor to this study.

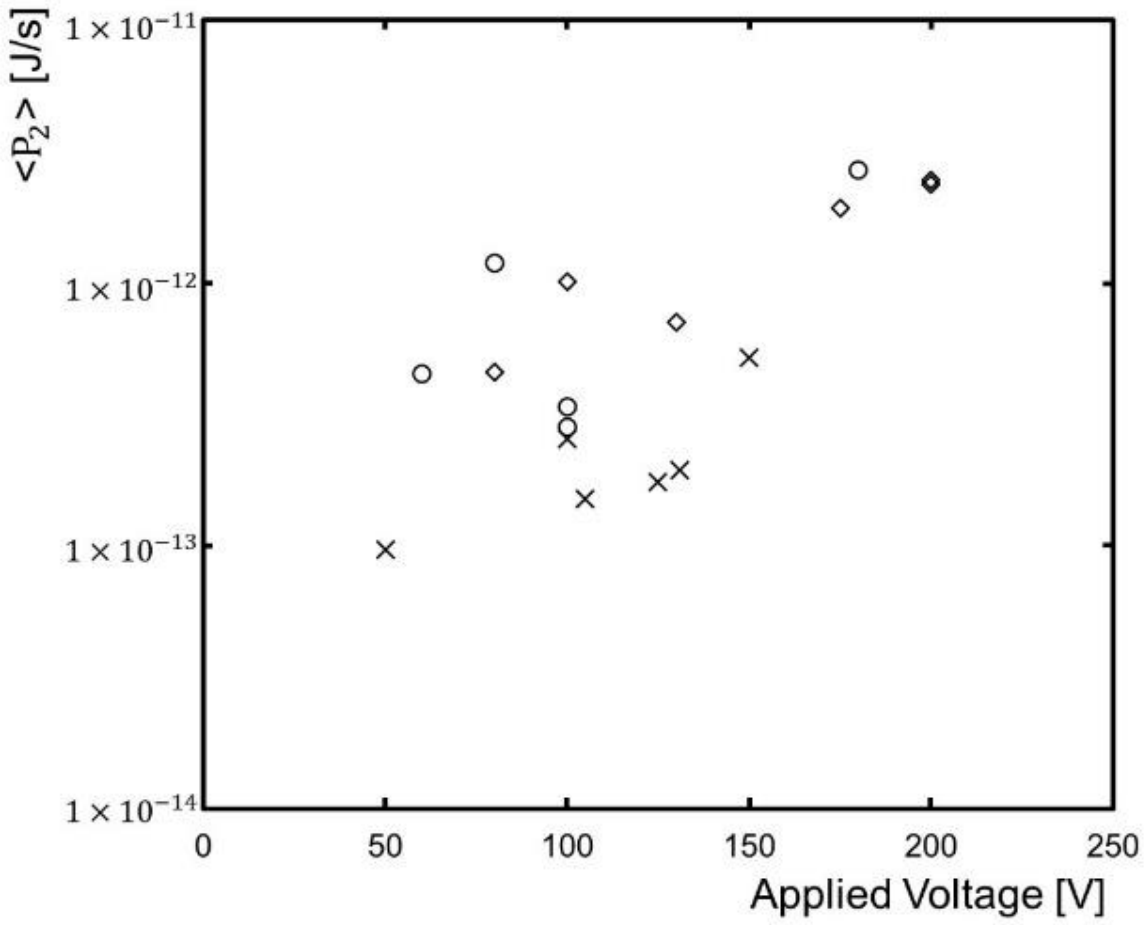

Fig. 3-4 Average output power of torque <P2> with applied voltage when the particle was spinning. The crosses, circles, and diamonds in the graph represent particles with diameters of <120, 121~170, and >171 μm, respectively.

3.3.2. Quantitative Analysis of a Micromotor Power

The kinetic energy output (P_{out}) for a particle in an oil phase under a direct current voltage may be assumed to be the sum of two outputs from two different motions, which indicates that micromotor systems can be discussed quantitatively. The calculation method is given as follows:

$$P_{out} = P_1 + P_2 \tag{3.6}$$

3.3.2.1. Dependency on Voltage

Fig. 3-5 shows the dependencies of the total power on the applied voltage, where the crosses, circles, and diamonds represent the particles with diameters of <120, 121~170, and >171 μm, respectively. A monotonous increase of output power with an increase in applied voltage was observed. This correlation was probably because both motions of the particles were driven by DEHPA flow, as shown in Fig. 3-3 and 3-4. The scattered data might have been due to particle surface roughness because the power of spinning motion was approximately 66% of total power on average.

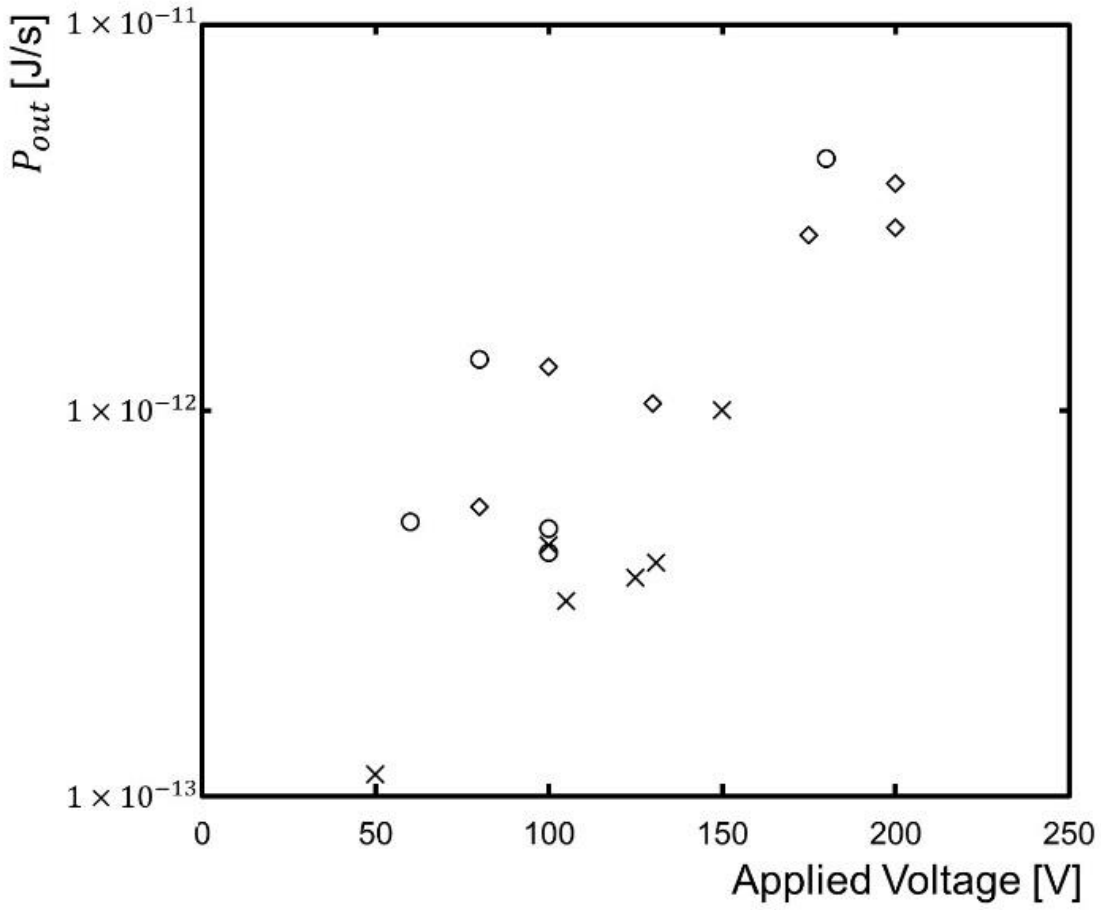

Fig. 3-5 Dependency of total output power (P_{out}) on applied voltages. The crosses, circles, and diamonds in the graph represent particles with diameters of <120, 121~170, and >171 μm, respectively.

3.3.2.2. Dependency on Surfactant Concentration

Fig. 3-6(a) shows the average output power of particles with different volume fractions of DEHPA. The error ranged from the minimum to maximum values in all experiments. The applied voltage was fixed at 150 V. The output power was observed to increase with an increase in the volume ratio of DEHPA from 10% to 30%. This increase was probably because of the effect of electrophoresis. As the concentration of DEHPA increased, more anionic surfactant was moved under the applied voltage, which enhanced the effect of electrophoresis. The electrophoretic flow was the driving force of particle motion; therefore, the output power of particles increased. However, when the volume ratio of DEHPA increased from 30% to 100%, a decrease in output power was observed. The average output power for DEHPA volume ratios at 60%, 80%, and 100% was similar.

To understand the reason for this decrease, we investigated the effect of the solution viscosity. For viscous drag, the velocity was proportional to solution viscosity, $v \sim 1/\eta$, so the output power for viscous drag was $P_1 \sim \eta \times (1/\eta)^2 = 1/\eta$. For viscous torque, the viscosity dependency was the same, which was $P_2 \sim 1/\eta$. Therefore, using the term $\eta \langle P_{out} \rangle$ can eliminate the effect of viscosity. Fig. 3-6(b) shows $\eta \langle P_{out} \rangle$ with different volume ratios of DEHPA. The error bar is the same as that in Fig. 36(a). The results were similar to those shown in Fig. 3-6(a), suggesting that the viscosity did not dominate the dependency of particle mobility.

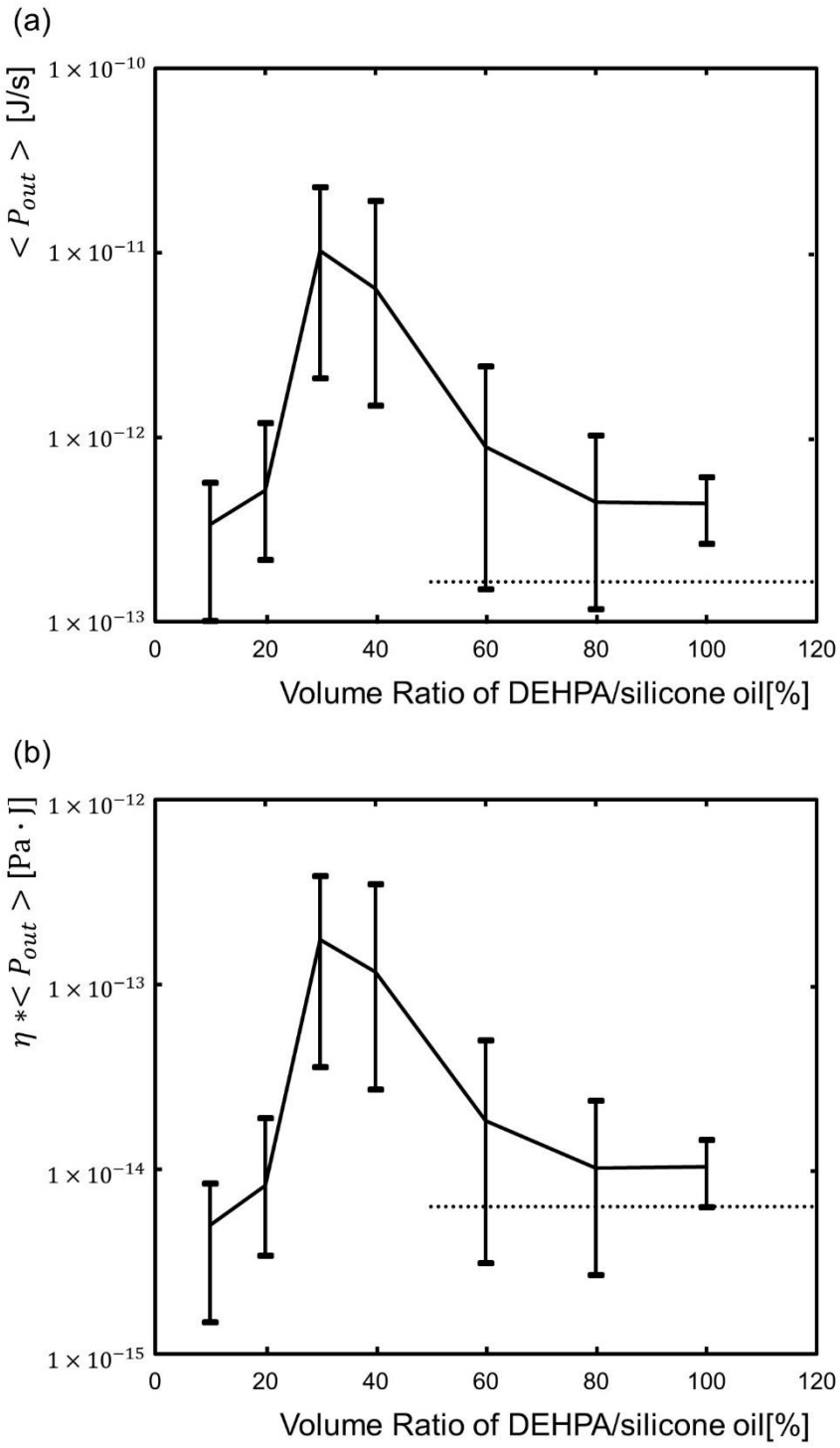

Fig. 3-6 Output power of particles and ŋ <Pout> at different volume ratios of DEHPA. The error ranged from minimum to maximum values. The applied voltage was fixed at 150 V. (a) Output power at different volume ratios of DEHPA. (b) Output power times viscosity ŋ <Pout> at different volume ratios of DEHPA. The dotted lines in (a) and (b) represent the data from the experiment on pure DEHPA solution.

Subsequently, a set of experiments was conducted to examine the effect of DEHPA, which was pure DEHPA liquid with particles under a direct current voltage of 200 V. Under these conditions, a temporal motion of a particle that moved from between the tips of electrodes to outside the observation area was observed. This motion differed from the motions in DEHPA/silicone oil solutions, which were spinning and revolving motions between or near the tips of electrodes. However, the output power of the temporal motion was $P_{out,\ DEHPA}$ = 1.65 ×10^{-13} J/s, which is indicated as a dotted line in Fig. 3-6(a) (η <P_{out}> for Fig. 3-6(b)). This output power was comparable to the output powers in solutions with >60% DEHPA volume ratio. The results of the change in the DEHPA volume ratio from 30% to 100% exhibited an asymptotic tendency compared with the result of the pure DEHPA solution. This tendency suggested that the decrease in output power was probably caused by a high DEHPA concentration. Efficient electrophoretic flow may require an appropriate mixing ratio of the two types of solutions.

3.3.2.3. Energy Conversion Efficiency

The electric energy input (P_{in}) was calculated by

$$P_{in} = I \times V \tag{3.7}$$

Where, I and V are electric current and applied voltage, respectively. Owing to the high electric resistance of silicone oil in the solution, the electric current measurement required an electromagnetic shield to eliminate internal and external noise. An ammeter was used in the experiment to measure the electric current. The energy conversion efficiency (φ) is given as follows:

$$\varphi = {P_{out}}/{P_{in}} \tag{3.8}$$

Fig. 3-7 shows the output and input powers of a micromotor. The undotted line indicates 100% of energy conversion efficiency. The data was collected from different particles whose diameters are marked next to the corresponding data point (squares). The average conversion ratio was φ = 2.8%, which is indicated by a dotted line. The energy conversion efficiency can be used as a parameter to compare micromotor systems for various studies. For example, a water droplet between two needle-shaped electrodes exhibits a back-and-forth motion under a direct current voltage [28]. Without the proposed quantification method, the comparison of these two systems is difficult, because the micromotors were made from different materials (water vs. polyethylene) and with different diameters. Moreover, their motions were different (back-and-forth oscillating vs. revolving/spinning), as was the and the electrode arrangements and applied voltage that provided the highly motile conditions. However, the quantification method clearly indicates that a solid-particle micromotor system has a higher energy conversion efficiency than a water-droplet micromotor system (φ_{water} ~0.000001%). (The water droplet was electrolysed [28], which consumed the most electric energy). By using a chemically inert particle in this study, the micromotor system energy conversion ratio became approximately more than 10^5 times greater.

Another possible approach was to evaluate the efficiency from the effective size of the convection to the micromotor volume. Case in point, the electrophoretic convection of anionic surfactant and a particle image velocimetry (PIV) of the convection flow that was reported [29]. The PIV result suggested that the velocity of flows rapidly decayed with the distance from the line connecting the two electrodes. However, precise evaluation of the flow area was difficult because the weak convection extended the observation area. This method can be applied only when the area of convection was restricted to an observable size.

This quantification of energy conversion efficiency of micromotor system will be an essential tool for the study of micromotors in the future. This method focuses micromotor mobility on the energy level, regardless of the material, size, motion type, type of input energy (electricity, or non-electrical such as magnetic energy), etc. A future study on micromotors will focus on two aspects: (i) increasing the conversion efficiency of the system by minimizing the energy waste in the system; (ii) increasing the output power by increasing the mobility of the micromotor. Considering that we are still in the early stages of micromotor system development, an increase in micromotor mobility at the expense of energy conversion efficiency might be necessary.

To increase the conversion efficiency of the micromotor system in this study, three methods may be proposed. First, the electrophoretic flow that is not associated with particle motion can be reduced. The electrophoresis of ionic surfactants consumes energy, and only the flow around the micromotor is useful. Second, diminishing excess particle motion that cannot be utilized for the micromotor. Third, reducing the joule heating in the system. To increase the output power, alternating solution reagents may be beneficial. The future solution should contain these properties: (1) should include ionic surfactant, which is the key to electrophoretic convection that drives the particle; (2) should be a surfactant/other liquid mixture, which allows efficient electrophoretic flow; (3) should have relatively higher electric conductivity. The last point was based on a similar study which used an ethanol-added solution (discuss in Chapter 4) the output power increased significantly with the sacrifice of energy conversion efficiency.

Considering that we are still in the early stages of micromotor system development, an increase in micromotor mobility at the expense of energy conversion efficiency might be necessary.

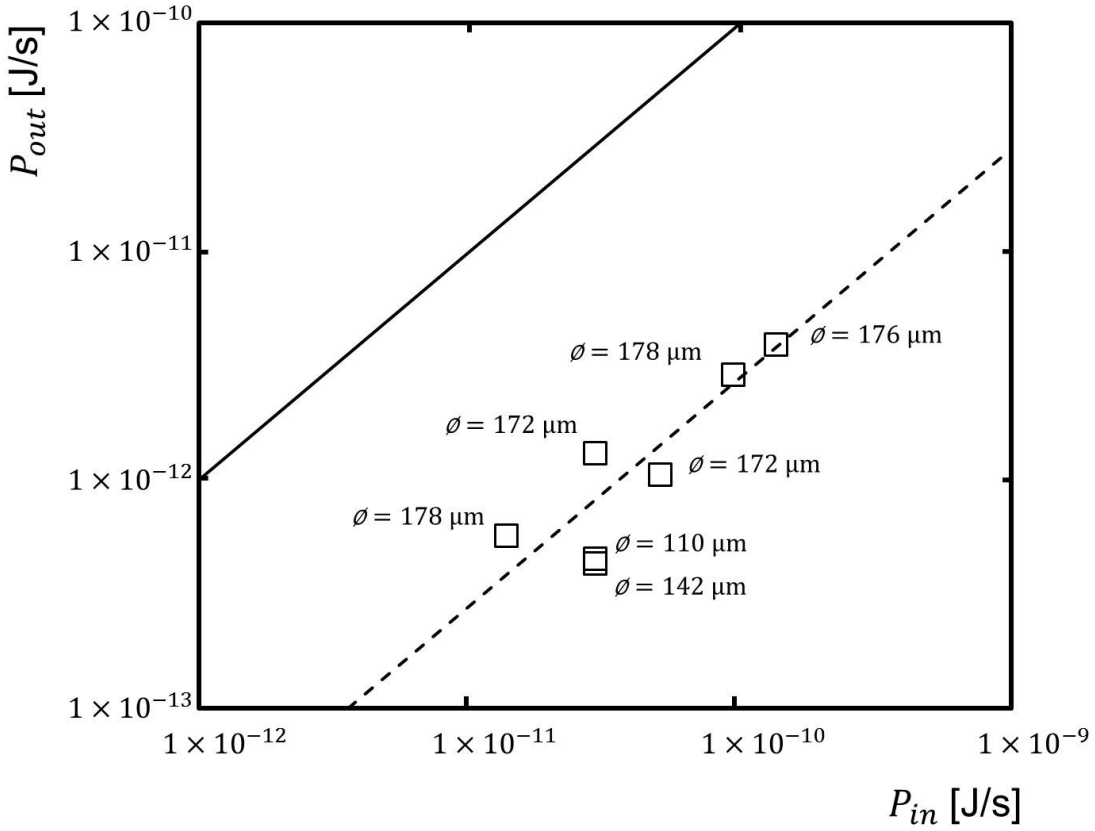

Fig. 3-7 Output power of different particles with the input power to the micromotor system. The diameter of each particle is marked next to the data point.

3.4. Conclusion

A solid, spherical polyethylene micromotor in an oil solution with anionic surfactant was placed between two needle-shaped electrodes and under a direct current voltage. Revolving and spinning motions were observed for this micromotor. The output power of the revolving and spinning motions was calculated based on viscous drag and viscous torque, respectively. The total output power of a spherical micromotor was assumed to be the sum of these two output powers. The dependency of the output power on the applied voltage demonstrated that the output power increased with an increase in applied voltage. The dependency of the output power on the surfactant concentration indicated an increase in output power in low concentration solutions but a decrease was observed in high concentration solutions. The increment in the output power of the micromotors was probably due to the effect of surfactant electrophoretic flow, which was enhanced by higher voltage and higher surfactant concentration. The diminution was considered not to be the result of the increased viscosity of solutions. An asymptotic tendency of the output power was observed in a highly concentrated surfactant solution compared with the pure surfactant solution, suggesting that the decrease was caused by the high surfactant ratio. Moreover, the electric energy input to the system was calculated. As a result, the energy conversion efficiency of a spherical micromotor system was quantified. This quantification can enable micromotor systems to be compared on energy levels, irrespective of the size, velocity, angular velocity of the micromotors, viscosity of the solution, or types of input energy to the system. The energy conversion efficiency, as a representation of energy flux of the system, also provides guidelines for micromotor system development and will improve the progress of micromotor systems.

References:

[1] D. Yamamoto, A. Shioi, Self-Propelled Nano/Micromotors with a Chemical Reaction: Underlying Physics and Strategies of Motion Control, KONA Powder Part. J. 32 (2015) 2–22. https://doi.org/10.14356/kona.2015005.

[2] S. Tottori, L. Zhang, F. Qiu, K.K. Krawczyk, A. Franco-Obregón, B.J. Nelson, Magnetic Helical Micromachines: Fabrication, Controlled Swimming, and Cargo Transport, Adv. Mater. 24 (2012) 811–816. https://doi.org/10.1002/adma.201103818.

[3] L. Zhang, T. Petit, Y. Lu, B.E. Kratochvil, K.E. Peyer, R. Pei, J. Lou, B.J. Nelson, Controlled Propulsion and Cargo Transport of Rotating Nickel Nanowires near a Patterned Solid Surface, ACS Nano. 4 (2010) 6228–6234. https://doi.org/10.1021/nn101861n.

[4] Y. Liu, D. Ge, J. Cong, H.-G. Piao, X. Huang, Y. Xu, G. Lu, L. Pan, M. Liu, Magnetically Powered Annelid-Worm-Like Microswimmers, Small. 14 (2018) 1704546. https://doi.org/10.1002/smll.201704546.

[5] R.A. Archer, J.R. Howse, S. Fujii, H. Kawashima, G.A. Buxton, S.J. Ebbens, pH‐Responsive Catalytic Janus Motors with Autonomous Navigation and Cargo‐Release Functions, Adv. Funct. Mater. 30 (2020) 2000324. https://doi.org/10.1002/adfm.202000324.

[6] A. Barbot, D. Decanini, G. Hwang, Local flow sensing on helical microrobots for semi-automatic motion adaptation, Int. J. Rob. Res. 39 (2020) 476–489. https://doi.org/10.1177/0278364919894374.

[7] J. Wang, W. Gao, Nano/Microscale Motors: Biomedical Opportunities and Challenges, ACS Nano. 6 (2012) 5745–5751. https://doi.org/10.1021/nn3028997.

[8] B. Jurado-Sánchez, J. Wang, Micromotors for environmental applications: a review, Environ. Sci. Nano. 5 (2018) 1530–1544. https://doi.org/10.1039/C8EN00299A.

[9] C. Chen, E. Karshalev, J. Guan, J. Wang, Magnesium-Based Micromotors: Water-Powered Propulsion, Multifunctionality, and Biomedical and Environmental Applications, Small. 14 (2018) 1704252. https://doi.org/10.1002/smll.201704252.

[10] W.F. Paxton, K.C. Kistler, C.C. Olmeda, A. Sen, S.K. St. Angelo, Y. Cao, T.E. Mallouk, P.E. Lammert, V.H. Crespi, Catalytic Nanomotors: Autonomous Movement of Striped Nanorods, J. Am. Chem. Soc. 126 (2004) 13424–13431. https://doi.org/10.1021/ja047697z.

[11] D. Yamamoto, T. Takada, M. Tachibana, Y. Iijima, A. Shioi, K. Yoshikawa, Micromotors working in water through artificial aerobic metabolism, Nanoscale. 7 (2015) 13186–13190. https://doi.org/10.1039/C5NR03300D.

[12] K. Chen, C. Gu, Z. Yang, M. Nakajima, T. Chen, T. Fukuda, “Z”-Shaped Rotational Au/Pt Micro-Nanorobot, Micromachines. 8 (2017) 183. https://doi.org/10.3390/mi8060183.

[13] W. Gao, S. Sattayasamitsathit, K.M. Manesh, D. Weihs, J. Wang, Magnetically Powered Flexible Metal Nanowire Motors, J. Am. Chem. Soc. 132 (2010) 14403–14405. https://doi.org/10.1021/ja1072349.

[14] G. Zhao, M. Pumera, Magnetotactic Artificial Self-Propelled Nanojets, Langmuir. 29 (2013) 7411–7415. https://doi.org/10.1021/la303762a.

[15] M.M. Alcanzare, M. Karttunen, T. Ala-Nissila, Propulsion and controlled steering of magnetic nanohelices, Soft Matter. 15 (2019) 1684–1691. https://doi.org/10.1039/C8SM00037A.

[16] U.K. Cheang, F. Meshkati, H. Kim, K. Lee, H.C. Fu, M.J. Kim, Versatile microrobotics using simple modular subunits, Sci. Rep. 6 (2016) 30472. https://doi.org/10.1038/srep30472.

[17] N.K. Metzger, M. Mazilu, L. Kelemen, P. Ormos, K. Dholakia, Observation and simulation of an optically driven micromotor, J. Opt. 13 (2011) 044018. https://doi.org/10.1088/2040-8978/13/4/044018.

[18] T. Harada, K. Yoshikawa, Mode switching of an optical motor, Appl. Phys. Lett. 81 (2002) 4850–4852. https://doi.org/10.1063/1.1527235.

[19] D. Kagan, M.J. Benchimol, J.C. Claussen, E. Chuluun-Erdene, S. Esener, J. Wang, Acoustic Droplet Vaporization and Propulsion of Perfluorocarbon-Loaded Microbullets for Targeted Tissue Penetration and Deformation, Angew. Chemie Int. Ed. 51 (2012) 7519–7522. https://doi.org/10.1002/anie.201201902.

[20] J.-F. Louf, N. Bertin, B. Dollet, O. Stephan, P. Marmottant, Hovering Microswimmers Exhibit Ultrafast Motion to Navigate under Acoustic Forces, Adv. Mater. Interfaces. 5 (2018) 1800425. https://doi.org/10.1002/admi.201800425.

[21] Y. Sumino, N. Magome, T. Hamada, K. Yoshikawa, Self-Running Droplet: Emergence of Regular Motion from Nonequilibrium Noise, Phys. Rev. Lett. 94 (2005) 068301. https://doi.org/10.1103/PhysRevLett.94.068301.

[22] M. Zrínyi, M. Nakano, Toward Colloidal Motors, Period. Polytech. Chem. Eng. 61 (2017) 15. https://doi.org/10.3311/PPch.10274.

[23] L. Rodríguez-Sánchez, A. Ramos, P. García-Sánchez, Electrorotation of semiconducting microspheres, Phys. Rev. E. 100 (2019) 042616. https://doi.org/10.1103/PhysRevE.100.042616.

[24] M. Takinoue, Y. Atsumi, K. Yoshikawa, Rotary motion driven by a direct current electric field, Appl. Phys. Lett. 96 (2010) 104105. https://doi.org/10.1063/1.3358385.

[25] M. Hase, S.N. Watanabe, K. Yoshikawa, Rhythmic motion of a droplet under a dc electric field, Phys. Rev. E. 74 (2006) 046301. https://doi.org/10.1103/PhysRevE.74.046301.

[26] L. Liu, B. Chen, K. Liu, J. Gao, Y. Ye, Z. Wang, N. Qin, D.A. Wilson, Y. Tu, F. Peng, Wireless Manipulation of Magnetic/Piezoelectric Micromotors for Precise Neural Stem - Like Cell Stimulation, Adv. Funct. Mater. 30 (2020) 1910108. https://doi.org/10.1002/adfm.201910108.

[27] M.K. Masukawa, M. Hayakawa, M. Takinoue, Surfactant concentration modulates the motion and placement of microparticles in an inhomogeneous electric field, RSC Adv. 10 (2020) 8895–8904. https://doi.org/10.1039/D0RA00703J.

[28] W. Zhang, T. Kozaki, I. Kakimoto, D. Yamamoto, K. Yoshikawa, A. Shioi, Energy consumption and conversion efficiency for a micromotor under DC voltage, Colloids Surfaces A Physicochem. Eng. Asp. 607 (2020) 125496. https://doi.org/10.1016/j.colsurfa.2020.125496.

[29] D. Yamamoto, K. Kosugi, K. Hiramatsu, W. Zhang, A. Shioi, K. Kamata, T. Iyoda, K. Yoshikawa, Helical micromotor operating under stationary DC electrostatic field, J. Chem. Phys. 150 (2019) 014901. https://doi.org/10.1063/1.5055830.

[30] T. Kurimura, S. Mori, M. Miki, K. Yoshikawa, Rotary motion of a micro-solid particle under a stationary difference of electric potential, J. Chem. Phys. 145 (2016) 034902. https://doi.org/10.1063/1.4958657.

[31] R.I. Ovseenko, Y.G. Ovseenko, Drag of a rotating sphere, Fluid Dyn. 3 (1971) 78–82. https://doi.org/10.1007/BF01016244.

[32] P. Hahn, A. Lamprecht, J. Dual, Numerical simulation of micro-particle rotation by the acoustic viscous torque, Lab Chip. 16 (2016) 4581–4594. https://doi.org/10.1039/C6LC00865H.

Chapter 4

Increase in Output Power at the Cost of Lowering Energy Conversion Efficiency of a Micromotor System via the Addition of Ethanol

4.1. Introduction

The study of micromotor systems has developed rapidly in recent years. These systems receive energy input, generating the micromotor motion, and output mechanical energy [1]. The micromotor is a particle/droplet with various morphologies, such as spherical, helical [2–4], or “worm-like” [5], on the micro-/nano-meter scale. Based on the input energy to the system, the micromotor system can be categorized as a [6]: magnetic micromotor [4,7,8], optical micromotor [9], catalytic micromotor [10,11], or electric micromotor system [2,12,13]. These systems are often submerged in liquid to be functional. Therefore, the Reynolds’ number is low; i.e., viscous effects dominate the motion of the micromotor.

In our previous research, we identified the forces applied to a spherical micromotor: viscous drag and viscous torque. Here, viscous drag is the force driving the directional motion, such as the back-and-forth and revolving motions, where the micromotor revolves about an artificial center. The viscous torque is the driving force of the spinning motion, whereby the micromotor spins around its center of mass.

After we identified the applied forces, we were able to quantify the energy conversion efficiency of a spherical microparticle in the oil phase via the following:

$$\text{energy conversion efficiency} = \frac{\frac{1}{T}\int_0^T (W_d + W_\tau)\, dt}{I * V} \quad (1)$$

where, T, W_d, W_t, t, I, and V are the duration of microparticle motions, work of viscous drag, work of viscous torque, time, electric current, and applied direct current voltage, respectively. The numerator is the kinetic energy output derived from the two types of motions: translational and spinning motions. The denominator calculates the electric energy input to the micromotor system. The reported output power was in the range of 1.06×10^{-13} – 4.16×10^{-12} J/s and the average energy conversion efficiency was 2.8%.

This method enables an efficient comparison between different micromotor systems. Ideally, the higher energy conversion efficiency indicates a higher output for the same direct current voltage applied to the system. However, the additive chemicals in the micromotor system significantly affect the electrical and mechanical properties of the liquid, thus changing both the numerator and denominator of Eq.1. Therefore, the effect of the additives on the micromotor performance is not simple, i.e., the larger output power may come with the cost of lowering energy conversion efficiency.

In this study, the effect of an additional solvent, ethanol, on the micromotor was examined at an applied direct current (DC) voltage, from 50 – 190 V. The microparticle was driven by the electrophoretic convection caused by the ionic surfactant dissolved in the system. The results demonstrate an increase in the output power of the micromotor; however, the electric current also increased and the energy conversion efficiency was thus lower.

4.2. Methodology

4.2.1 Equipment and Software

Table 4-1 shows the equipment and software that were used in this study.

Table 4-1 The equipment and software that were used in this study.

Equipment and Software	Manufacturer
Ultrapure water purifier (PF3XXXXM1)	Elga
Vortex mixer (VTX-3000L)	Lms
Viscometer (HAAKE RheoStress1)	Thermofisher
Optical microscope (IX73)	Olympus
Needle type tungsten microelectrode (UJ-80-02-1.0)	Unique Medical
Power amplifier	Orix
Video recording software (FASTCAM viewer)	Photron
Image analysis software (TEMA64 4.0-008-64)	Photron
Ammeter (W32-6517A-R)	Keithley
Electromagnetic shield (DTM-888)	Toyama-Denki Building
Polyethylene particles (*d* = 175 μm, FLO-BEADS® CL-2507)	Sumitomo Seika Chemicals

4.2.2 Chemical Reagent

Table 4-2 shows the chemicals reagents that were used in this study.

Table 4-2 The chemicals reagents that were used in this study.

Chemical reagents	Manufacturer
silicone oil (KF-56)	Shin-Etsu Chemical Japan
di-(2-ethylhexyl)phosphoric acid (DEHPA, 97%,)	Aldrich
Ethanol(99.5%)	Wako Chemical Japan

4.2.3 Preparation

This study inherits the experimental setup of our previous study. The oil solution was a mixture of silicone oil, the anionic surfactant di-(2-Ethylhexyl) phosphoric acid (DEHPA), and ethanol at a volume ratio of 10:2:1, respectively. This mixture was

added in a plastic tube with sphere-shaped low-density polyethylene particles. Then, the plastic tube was placed on a vortex mixer for approximately 1 min. A rotational viscometer was used to measure the viscosity of the solution.

Fig. 4-1 shows a schematic illustration of the experimental setup. The solution mixture was placed on a glass slide. Two needle-shaped electrodes were inserted into the solution. The geometric arrangement of electrodes and the distance between the electrode tips were fixed during the experiment. A DC voltage was applied by a power amplifier. An ammeter was used to measure the electric current. An electromagnetic shield was used to cover the experimental setup to eliminate noise from the external environment. The setup and the shield were grounded. A high-speed microscope and recording software were used to record the motion of the microparticle and the recorded video was analyzed by software.

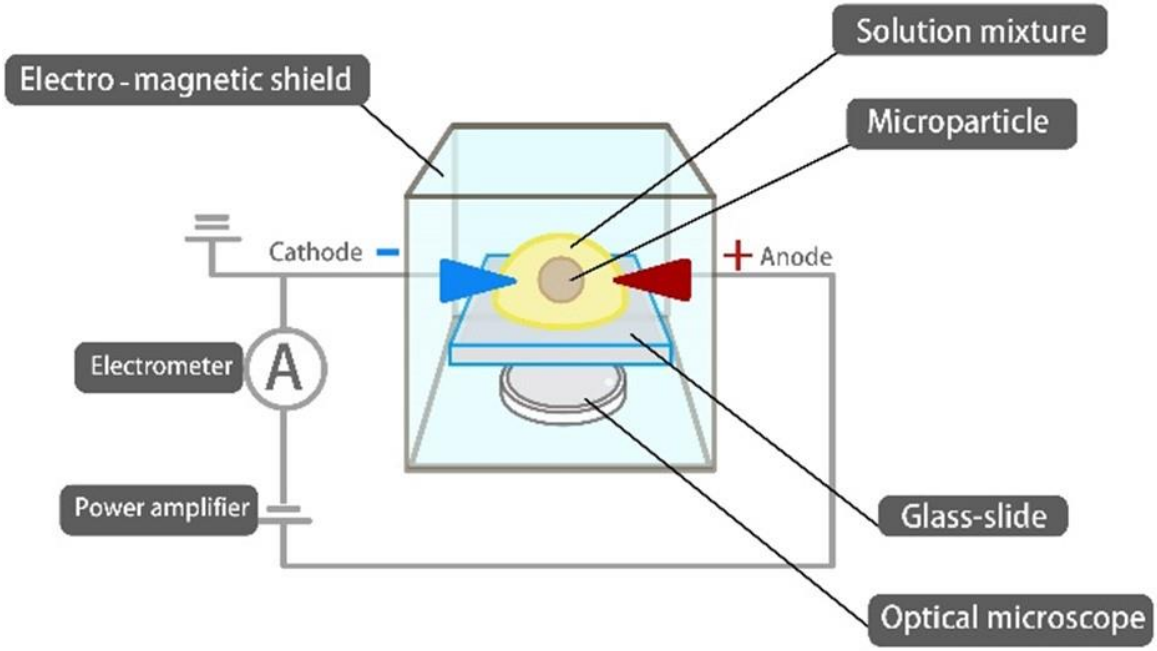

Fig. 4-1 Schematic illustration of the experimental setup.

4.3. Result and Discussion

Two types of motion were observed when a DC voltage was applied: revolving and spinning motions. Fig. 4-2 shows a microparticle exhibiting these motions ($\varnothing$ = 187 μm) near the cathode, under 50 V. Fig. 4-2(a) shows the trajectory of the counter-clockwise revolving motion. Fig. 4-2(b) is a sequence of photos of the spinning motion after adjusting the camera focus. The spinning motion was observed by tracking the black dots (presumably impurities, indicated by the black arrows) on the microparticle; the direction was also counter-clockwise. The directions of both motions agree with that of the electrophoretic convection flow of the surfactant [2,13].

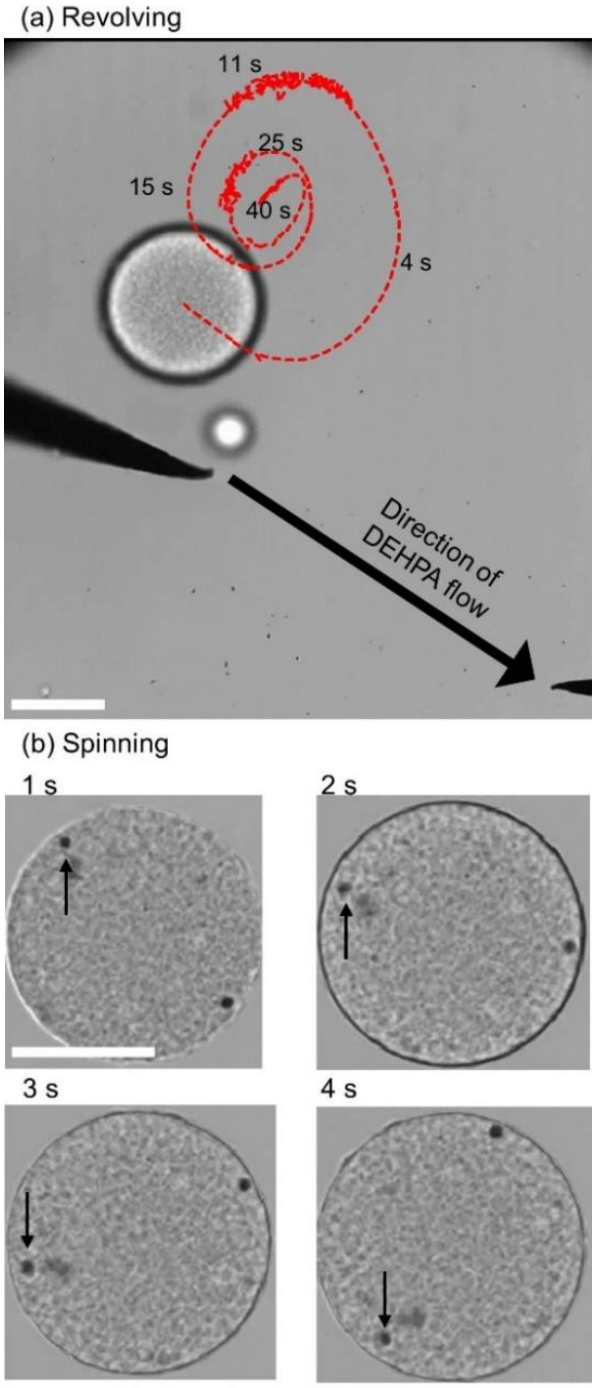

Fig. 4-2 Photos of a microparticle (∅ = 187 μm) under a stationary DC voltage of 50 V. (a) This microparticle was revolving and its trajectory was shown as a red dotted line. (b) A series of photos indicates the spinning motion of the microparticle of (a), after adjusting the camera focus on the microparticle. The motion is identified by tracking the black dot (indicated by the black arrows). Both the revolving and spinning motion directions were counter-clockwise. Both scale bars indicate 100 μm.

The output power of the microparticles were calculated via Eq. 1. Fig. 4-3 shows the output power (P_{out}) of the microparticles in the ethanol-added solution and the corresponding correlation line is indicated by the dotted line. The correlation line of the ethanol-free-solution is also shown as a dashed line. The output power of the microparticles significantly increases with the addition of ethanol, although the data appears to be scattered; this may be due to the difference in surface roughness of each microparticle, as previously reported.

However, this improvement to the output power is achieved at the cost of energy conversion efficiency. Fig. 4-4 shows the output (P_{out}) vs. the input power ($I \times V$) of the ethanol-added micromotor system. The dotted line (0.3%) corresponds to the average conversion efficiency of ethanol-added system. The decrement in energy conversion efficiency was due to the increment in electric current, which ranged from 2.59×10^{-12} – 2.64×10^{-10} A in the ethanol-added solution. Comparatively, the electric current was 10^{-13} A in the ethanol-free micromotor system.

The increase in the electric current may be due to the lower electrical resistance of the solution mixture. The addition of ethanol increases the conductivity of the silicone oil and DEHPA mixture, as shown in the supporting information; this caused the increase in electric current and, therefore, the increase in the denominator of Eq.1. Resultantly, the energy conversion efficiency decreased in the ethanol-added micromotor system.

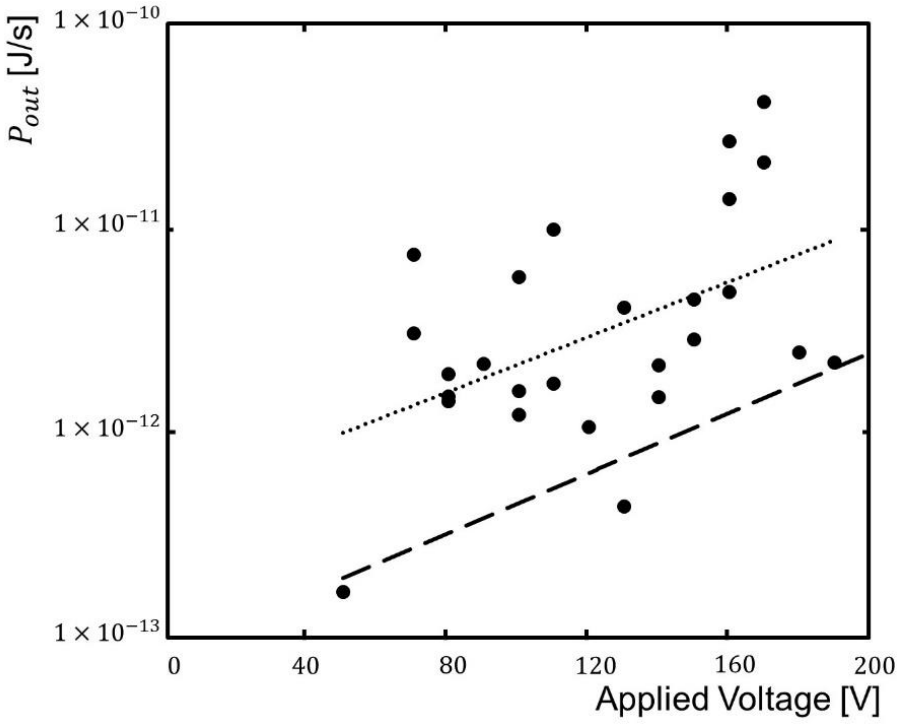

Fig. 4-3 The output power (P_{out}) over the applied voltage for microparticles under a stationary DC voltage. The black dots and dotted line indicate the output power of microparticles in the ethanol-added solution and their corresponding exponential correlation line, respectively. The dashed line is the power correlation line of the output power in an ethanol-free micromotor system.

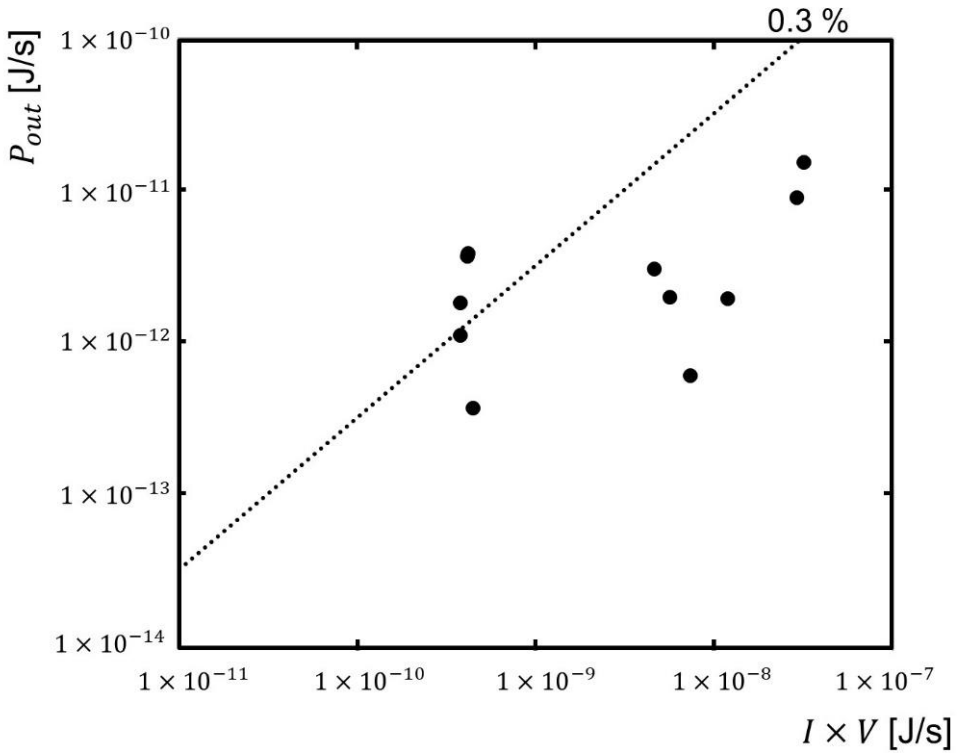

Fig. 4-4 The output power (P_{out}) vs. the input power ($I \times V$) of the micromotor system in the ethanol-added solution. The dotted line corresponds to the average conversion efficiency of ethanol-added system.

4.4. Conclusion

The effect of the additional solvent, ethanol, on the output power and energy conversion efficiency of a spherical micromotor was studied. The output power of the microparticle in the ethanol-added system increased compared to that in the ethanol-free system. However, the electric current increased, which was caused by the higher conductivity of the solution. As a result, the energy conversion efficiency was lower, compared to the ethanol-free micromotor system. In the liquid micromotor system, the lower conversion efficiency does not necessarily correspond to lower output power. The results of this study pave the way for future studies on micromotor development through the control of solvent properties.

References:

[1] W. Zhang, T. Kozaki, I. Kakimoto, D. Yamamoto, K. Yoshikawa, A. Shioi, Energy consumption and conversion efficiency for a micromotor under DC voltage, Colloids Surfaces A Physicochem. Eng. Asp. 607 (2020) 125496. https://doi.org/10.1016/j.colsurfa.2020.125496.

[2] D. Yamamoto, K. Kosugi, K. Hiramatsu, W. Zhang, A. Shioi, K. Kamata, T. Iyoda, K. Yoshikawa, Helical micromotor operating under stationary DC electrostatic field, J. Chem. Phys. 150 (2019) 014901. https://doi.org/10.1063/1.5055830.

[3] A. Barbot, D. Decanini, G. Hwang, Local flow sensing on helical microrobots for semi-automatic motion adaptation, Int. J. Rob. Res. 39 (2020) 476–489. https://doi.org/10.1177/0278364919894374.

[4] M.M. Alcanzare, M. Karttunen, T. Ala-Nissila, Propulsion and controlled steering of magnetic nanohelices, Soft Matter. 15 (2019) 1684–1691. https://doi.org/10.1039/C8SM00037A.

[5] Y. Liu, D. Ge, J. Cong, H.-G. Piao, X. Huang, Y. Xu, G. Lu, L. Pan, M. Liu, Magnetically Powered Annelid-Worm-Like Microswimmers, Small. 14 (2018) 1704546. https://doi.org/10.1002/smll.201704546.

[6] D. Yamamoto, A. Shioi, Self-Propelled Nano/Micromotors with a Chemical Reaction: Underlying Physics and Strategies of Motion Control, KONA Powder Part. J. 32 (2015) 2–22. https://doi.org/10.14356/kona.2015005.

[7] L. Liu, B. Chen, K. Liu, J. Gao, Y. Ye, Z. Wang, N. Qin, D.A. Wilson, Y. Tu, F. Peng, Wireless Manipulation of Magnetic/Piezoelectric Micromotors for Precise Neural Stem‐Like Cell Stimulation, Adv. Funct. Mater. 30 (2020) 1910108. https://doi.org/10.1002/adfm.201910108.

[8] C. Calero, J. García-Torres, A. Ortiz-Ambriz, F. Sagués, I. Pagonabarraga, P. Tierno, Propulsion and energetics of a minimal magnetic microswimmer, Soft Matter. 16 (2020) 6673–6682. https://doi.org/10.1039/D0SM00564A.

[9] S.M. Mousavi, I. Kasianiuk, D. Kasyanyuk, S.K.P. Velu, A. Callegari, L. Biancofiore, G. Volpe, Clustering of Janus particles in an optical potential driven by hydrodynamic fluxes, Soft Matter. 15 (2019) 5748–5759. https://doi.org/10.1039/C8SM02282H.

[10] R.A. Archer, J.R. Howse, S. Fujii, H. Kawashima, G.A. Buxton, S.J. Ebbens, pH‐Responsive Catalytic Janus Motors with Autonomous Navigation and Cargo‐Release Functions, Adv. Funct. Mater. 30 (2020) 2000324. https://doi.org/10.1002/adfm.202000324.

[11] C. Zhou, Q. Wang, X. Lv, W. Wang, Non-oscillatory micromotors “learn” to oscillate on-the-fly from oscillating Ag micromotors, Chem. Commun. 56 (2020) 6499–6502. https://doi.org/10.1039/D0CC02266G.

[12] M.K. Masukawa, M. Hayakawa, M. Takinoue, Surfactant concentration

modulates the motion and placement of microparticles in an inhomogeneous electric field, RSC Adv. 10 (2020) 8895–8904. https://doi.org/10.1039/D0RA00703J.

[13] T. Kurimura, S. Mori, M. Miki, K. Yoshikawa, Rotary motion of a micro-solid particle under a stationary difference of electric potential, J. Chem. Phys. 145 (2016) 034902. https://doi.org/10.1063/1.4958657.

Supporting information

The measurement of solution conductivity.

In this study, the conductivity of a solution mixture is measured via a conductivity meter (Portavo 907 Multi, Knick, Germany), with an attached SE 605 H sensor. The measuring range is from 1 nS/cm – 1000 μS/cm. The solution mixture comprises silicone oil and DEHPA at a volume ratio of 10:2, respectively. Then, ethanol at a volume ratio of x% (x=0, 5, 10, …, 50) was added and the mixture was measured while stirring. Fig. S1 shows the measured conductivity of the solution mixture vs. the volume ratio of ethanol. The conductivity showed an increment with the increase in the ethanol volume ratio. This result proves that the addition of ethanol increases the conductivity of the silicone oil/DEHPA solution. The measurements at a low volume ratio of ethanol ($x \leq 10$) was difficult because of their extremely low values.

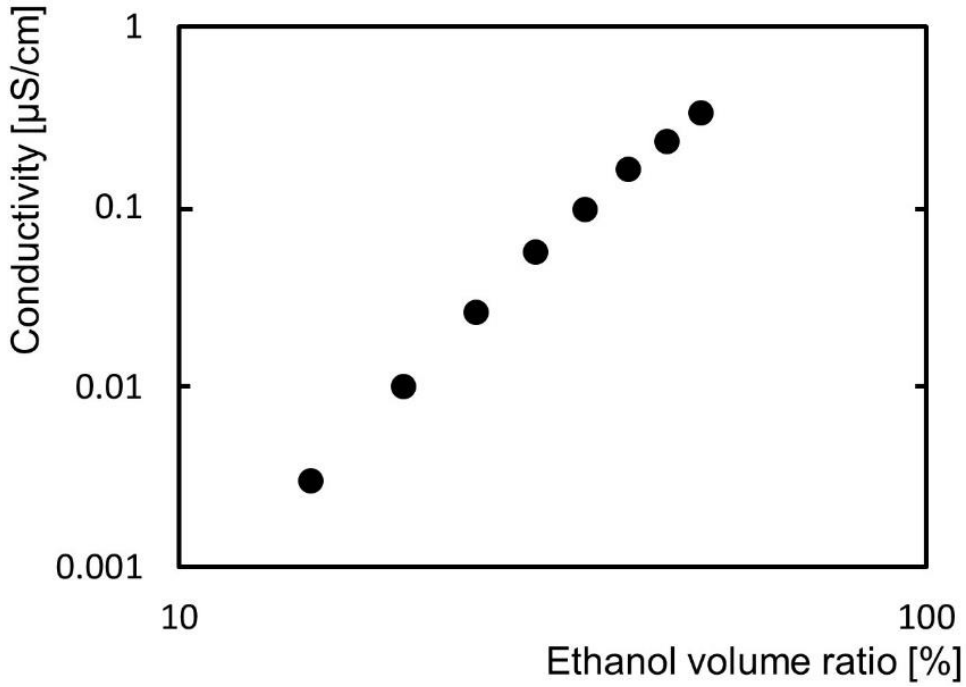

Fig. S1. The conductivity of silicone oil/DEHPA/ethanol solution mixture vs. ethanol volume ratio.

Chapter 5

Future Application of the Micromotor System

5.1 intro

In the past few decades, more and more focus has been devoted onto the development and applications of microelectromechanical systems (MEMS)[1,2] in environmental [3,4] and medical use[5–8]. These systems are microdevices that is integrated from small elements. A motor system can be integrated into MEMS to provide power. One possibility is the scale down of the ordinary motor system to micro/nano meter scale. However, due to the small scale of such microdevices to the liquid environment, the Reynolds' number is extremely low[9,10]. Therefore, a new type of motor, the micromotor, system is needed for the development of MEMS.

Currently, there are different types of micromotor system developed by several research groups, such as magnetic [5], optical [11], and catalytic micromotor systems[12]. In chapter 3, a quantification method was proposed for the electric micromotor system[9]. This quantification method is expected to play a key role in the development of electric micromotor system, and to find the optimum experimental conditions that increase the output power while decrease the input power to the micromotor system.

In this chapter, the future application for the electric micromotor system is discussed. One of the possible adaptations would be to the microfluidic devices[12–14], such as the "lab-on-chips" technology. "Lab-on-chips" means a integration of analytical systems that are in small scale , such as a "lab-on-chips" on a glass slide [15]. These microdevices have wide application fields, commonly for biosensing[16–18] and microbiology[19–23].

It has been pointed out by S. Dekker *et al.* that the integration of microdevices was limited currently[24]. Considering a micro-mixing device, for example, fluids are injected into the system by external pressure [25], which limits the portability of the

micro-mixing devices. If a micromotor system is designed for the integration in micro-mixing device, not only the portability but also the mixing efficiency will be increased dramatically.

In this study, a 4-pin microelectrodes system was designed and investigated. The revolving and spinning motions of microparticles were observed. The motions appeared at the low electric field intensity region. The micromotors are expected to have higher mobility especially in a high electric field intensity region. Moreover, a ratchet-shaped “shuriken” microparticle was studied. Under a direct current voltage, back-and-forth and spinning motion were observed. The spinning motion of micropaticle with ratchet shape may be adapted for micro-mixing.

5.2 Method

5.2.1. Equipment and Software

Table 5-1 shows the equipment and software that were used in this study.

Table 5-1 The equipment and software that were used in this study.

Equipment and Software	Manufacturer
Vortex mixer (VTX-3000L)	Lms
Viscometer (HAAKE RheoStress1)	Thermofisher
Optical microscope (IX73)	Olympus
Needle type tungsten microelectrode (UJ-80-02-1.0)	Unique Medical
Power amplifier	Orix
Video recording software (FASTCAM viewer)	Photron
Image analysis software (TEMA64 4.0-008-64)	Photron
Ammeter (W32-6517A-R)	Keithley
Electromagnetic shield (DTM-888)	Toyama-Denki Building
Polyethylene particles (d = 175 μm, FLO-BEADS® CL-2507)	Sumitomo Seika Chemicals
4-pin microelectrodes system	Original design. Fabricated in Takinoue Lab, Tokyo Institute of Technology
Ratchet-shaped particle	Masuda Ikakikai

The 4-pin microelectrodes system was an original design, fabricated with the helps from Takinoue Lab, Tokyo Institute of Technology. Its photos are shown in Fig. 5-1. Fig. 5-1(a) shows that, on a glass slide, three sets of 4-pin microelectrodes were printed by the method reported by M. Masukawa *et al.*[26]. Fig.5-1(b) shows its microscopic image, where the center was marked by a black dot. The distance between tips of the four-pin microelectrodes system was around 500 μm and the thickness is within 10 μm.

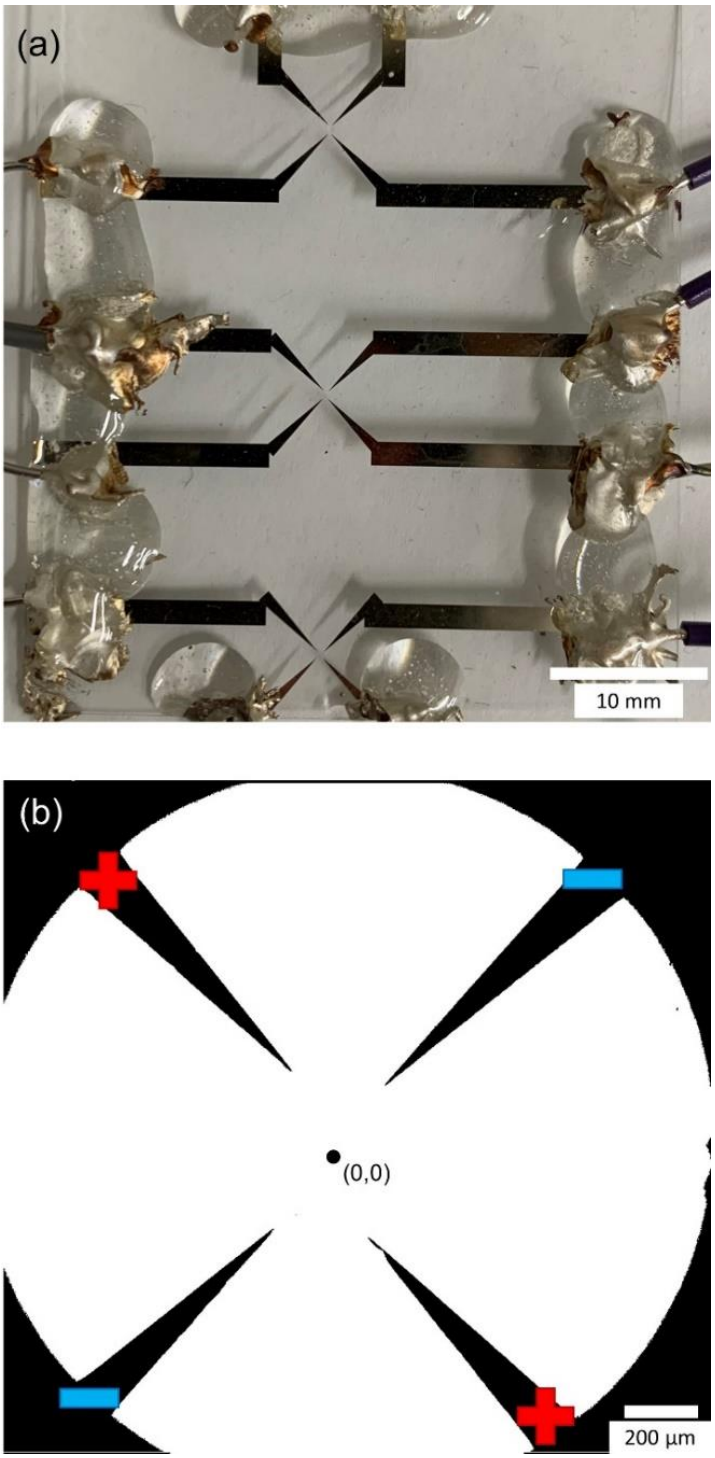

Fig. 5-1 Photos of the 4-pin microelectrode system. (a) Three sets of microelectrode system on a glass slide. (b) The microscopic photo of one set of microelectrode system. The black dot marked the center of the four electrodes. The scale bars were shown in the figure.

5.2.2. Chemical Regent

Table 5-2 shows the chemicals reagents that were used in this study.

Table 5-2 The chemicals reagents that were used in this study.

Chemical reagents	Manufacturer
silicone oil (KF-56)	Shin-Etsu Chemical Japan
di-(2-ethylhexyl)phosphoric acid (DEHPA, 97%,)	Aldrich
Ethanol(99.5%)	Wako Chemical Japan

5.2.3. Preparation

The solution mixture was prepared from silicone oil and the anionic surfactant di-(2-ethylhexyl) phosphoric acid (DEHPA) in a plastic tube. Ethanol was added as needed. The spherical low-density polyethylene particles were added into the mixture. A vortex mixer was used for approximately 1 min. The viscosity of the solution was measured using a rotational viscometer.

For the experiment of ratchet-shaped microparticle, as shown in Fig. 5-2(a), a two needle-shaped electrodes system shown in Fig.5.2(b) was used. The prepared solution was placed on a slide glass. Two needle-shaped electrodes were inserted into the solution via manipulators. A direct current voltage was applied. The motion of the particle was recorded using a high-speed camera and analysed by software. The entire setup was set inside an electromagnetic shield to eliminate noise from external sources. The electric potential of the setup and shield was set at ground level. The electric current was measured by an ammeter.

For the experiment of 4-pin microelectrodes system, the microelectrodes system was connected to the experimental setup instead of the two needle-shaped electrodes.

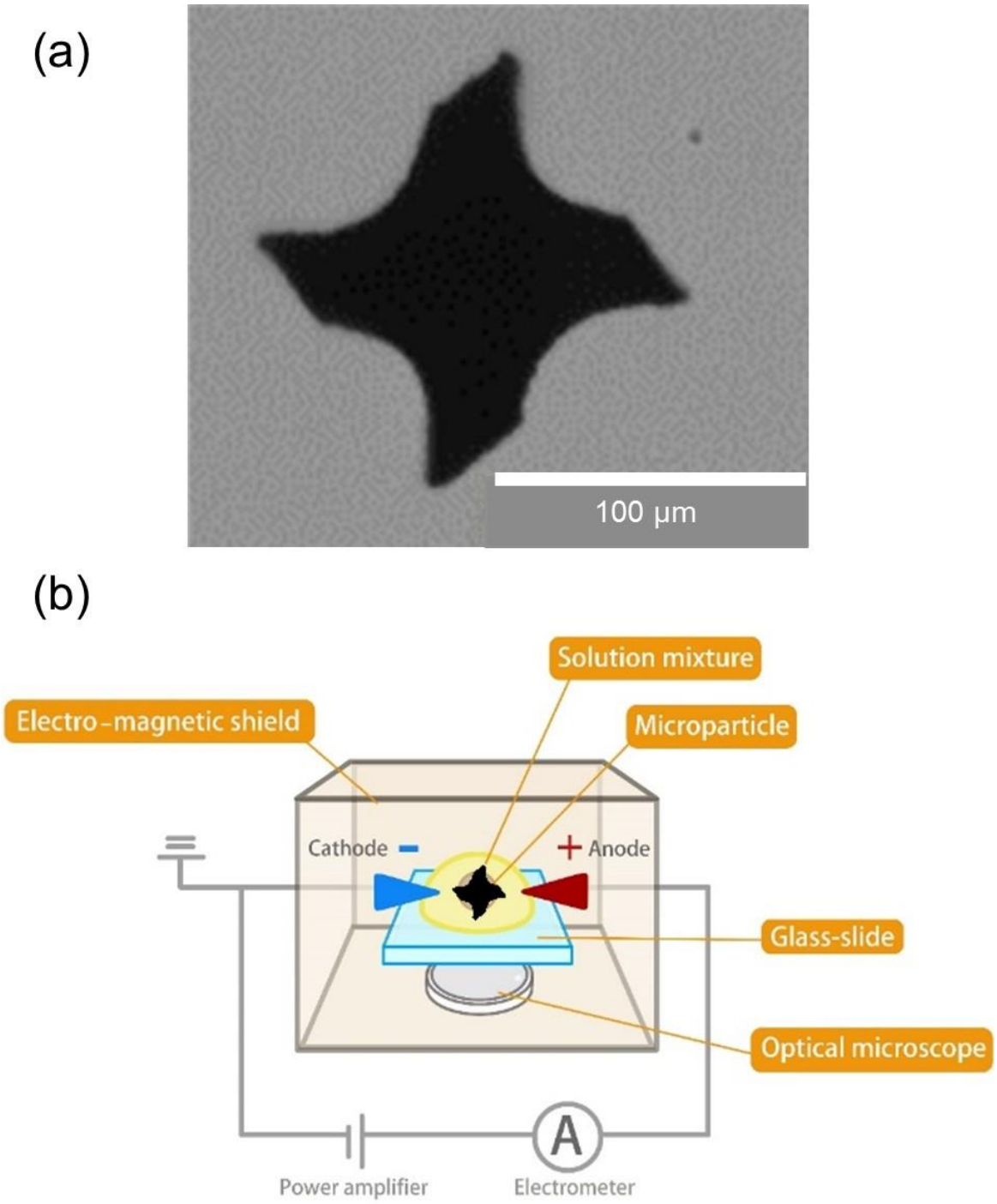

Fig. 5-2 The photo of ratchet-shaped microparticle and the schematic illustration of the experimental setup are shown in (a) and (b), respectively. When the 4-pin microelectrodes system was used, it was connected to the setup by replacing the two needle-shaped electrodes. The scale bar is 100 μm.

5.3 4-Pin Microelectrode System

Revolving motion of microparticle was observed in the 4-pin microelectrodes system under a stationary direct current voltage. Fig. 5-3 showed microparticles in the 4-pin microelectrode system when 150 V was applied. As samples, three of the microparticles, (a), (b) and (c), were traced and their trajectories were shown as red, blue and green dotted lines, respectively. These showed that the microparticle were revolving around the center, and the orbit diameter is approximately 1700 μm. The motion direction was counter-clockwise. It was difficult to do the experiment with only one microparticle, in contrast to the two needle-shaped electrode experiments. This is due to the lack of the manipulators.

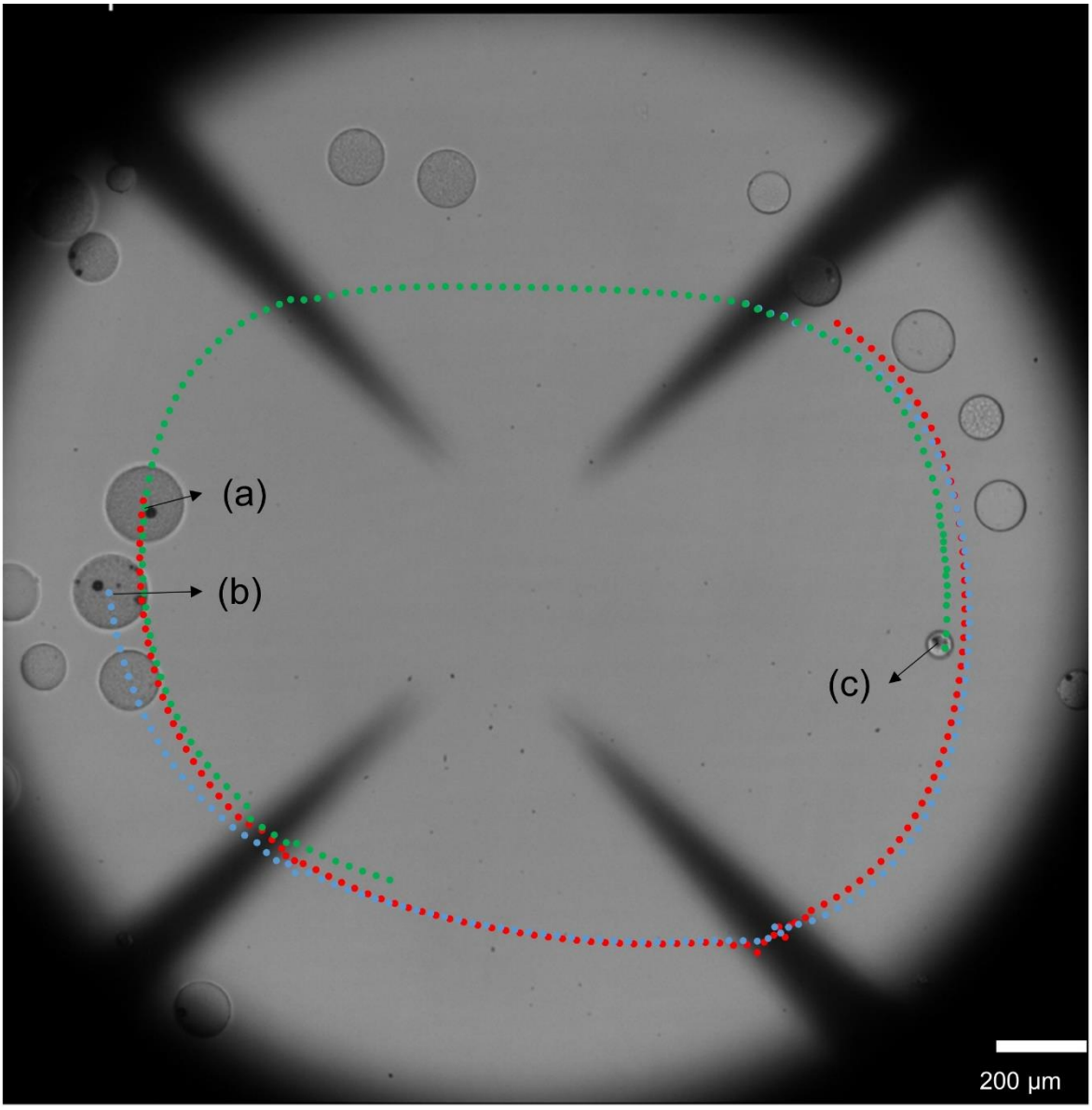

Fig. 5-3 The trajectories of microparticles in 4-pin microelectrodes system. Three of the microparticles (a), (b) and (c), as indicated by black arrows, were tracked, and their motion trajectories were shown as red, blue and greed dotted lines, respectively. The revolving direction was counter-clockwise. The scale bar was 200 μm.

The output power of microparticle a, b and c were P_a = 7.34×10^{-13} J/s, P_b = 7.41×10^{-13} J/s and P_c = 2.67×10^{-13} J/s by eq. 3.3, 3.5 and 3.6. The output power was similar to that in two needle-shaped electrodes system, as demonstrated in Fig. 3.5.

However, it is expected that the 4-pin microelectrode system can generate higher output of the micromotor, if the micromotor can be restricted near the center of the microelectrode system. Fig. 5-4 (a) and (b) showed the electric field distribution in 4-pin microelectrode system and two needle-shaped electrodes system, respectively. The calculation method was identical to that of D. Yamamoto *et al.*[27]. The anionic surfactant that was used in the study flew against the direction of electric field due to the effect of electrophoresis. This electrophoretic flow appeared in the strongest intensity region. Consequently, the compensation stream of surfactant flew along the direction of electric field in the other region. Thus, the surfactant convection was created. Fig. 5-4 (c) and (d) showed the electrophoretic flow (as red arrows) and the compensation flow (as green arrows) in 4-pin microelectrode system and two needle-shaped electrodes system, respectively. Moreover, Fig. 5-4(c) showed that the direction of the electrophoretic convection is the same as that of the revolving motion of microparticles, which indicates that the electrophoretic convection provides the driving force for the microparticles. Therefore, the microparticle must have higher output power under a stronger electric field where electrophoretic convection is faster. Fig. 5-4(a) showed that, near the center of the 4-pin microelectrode system, a stronger electric field region was found. The convection near the center of the system may be too fast for the microparticle, so the microparticle was pushed away from the center due to centrifugal force.

The results of this study suggested that a higher output power is expected for the 4-pin microelectrode system when the microparticle motion can be restricted near

the center of the system, such as building a “wall” around the center of the system. Moreover, future study may be focused onto the generation of better convection by designing geometry of microelectrode system. For example, a 6-pin and 8-pin microelectrode system may be useful for the electrophoresis. Fig. 5-5(a) and (b) showed the electric field distribution calculated for the 6-pin and the 8-pin microelectrode system, respectively, while Fig. 5-5(c) and (d) showed the electrophoretic flow (as red arrows) and compensation flow (as green arrows) in the 6-pin and the 8-pin microelectrode system, respectively.

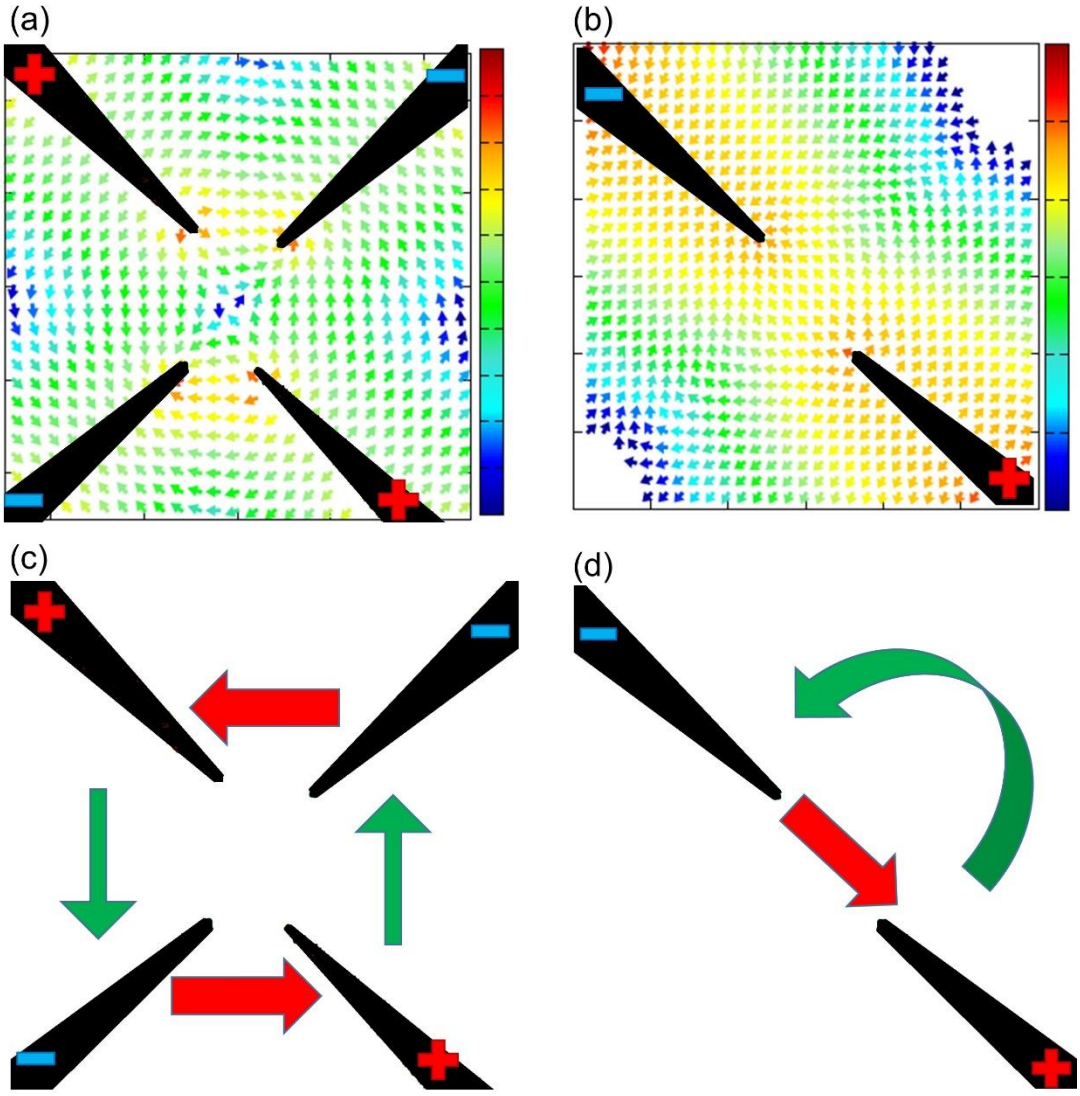

Fig.5-4 The electric field distributions and the surfactant convection in the 4-pin microelectrode system and two needle-shaped electrodes system. (a) and (b) are the electric field distributions of 4-pin microelectrode system and two needle-shaped electrodes system, respectively. (c) and (d) are the surfactant flow due to electrophoresis (as red arrows) and due to compensation (as green arrows) in 4-pin microelectrode system and two needle-shaped electrodes system, respectively.

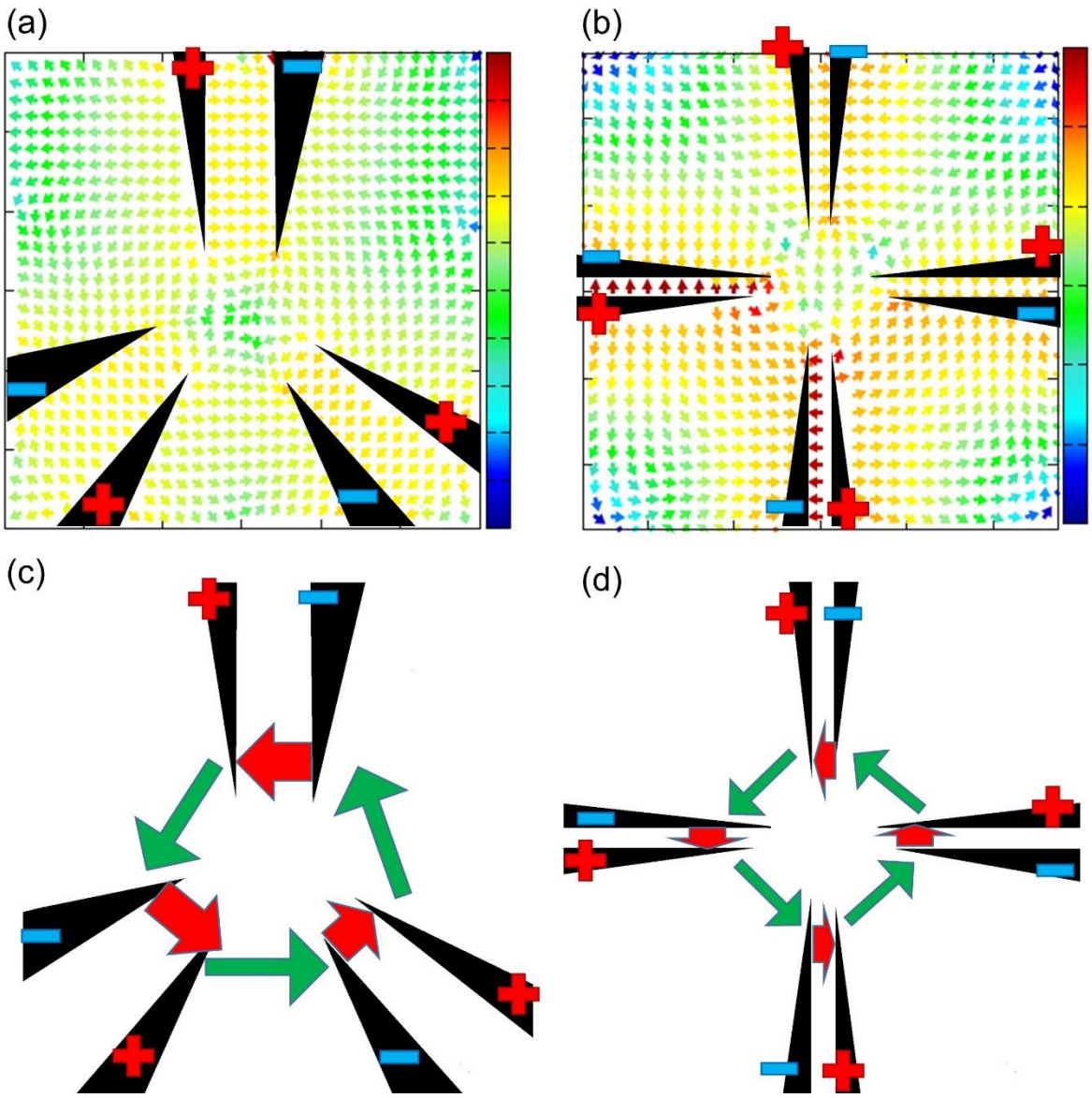

Fig. 5-5 The electric field distribution and surfactant convection of 6-pin and 8-pin microelectrode system. (a) and (b) are the electric field distribution of 6-pin and 8-pin microelectrode system, respectively. (c) and (d) are the surfactant convection with electrophoretic flow (as red arrows) and compensation flow (as green arrows) of 6-pin and 8-pin microelectrode system, respectively.

5.4 Ratchet-Shaped Microparticle

When the ratchet-shaped microparticle, namely “shuriken”, was used in the two needle-shaped electrodes system in the ethanol-added solution (prepared in the same method as explained in chapter 4.2), three types of motions: suspending state, oscillating and spinning motion are found.

Suspending state is when the shuriken particle suspending between the tips of two electrodes. This was considered a motion because the shuriken particle made from steel would sink to the glass slide without the electric field. The particle was suspended only when a DC voltage applied. Fig. 5-6(a) and (b) showed the shuriken particle at electrodes distance of 222 μm and 242 μm, respectively, while (c) showed that the particle was not suspended even when the electrodes distance was large (electrodes distance 245 μm). The applied DC voltage was 100 V. The particle motion may be caused by the balance of attraction from both electrodes.

Oscillating motion means the back-and-forth motion between the tips of the electrodes. Fig. 5-7 showed a sequence of photos of the oscillating motion under a DC voltage of 100 V. The mechanism of this oscillating motion may be due to the metal shuriken particle was charged by the electrodes and moved back-and-forth due to the electrostatic repulsion[28] . Currently, suspending state and oscillating motion are difficult to be controlled separately. Oscillating motion was commonly observed, and suspending state was rare.

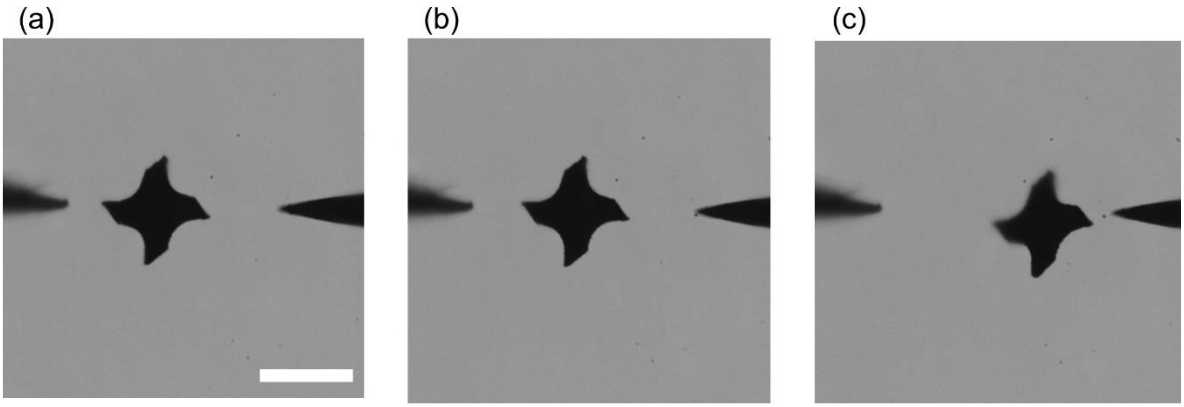

Fig. 5-6 The suspending states of shuriken microparticle in (a) and (b), and the breaking of suspending state in (c). The electrodes distance of (a), (b) and (c) are 222, 242 and 245 μm, respectively. The scale bar is 100 μm.

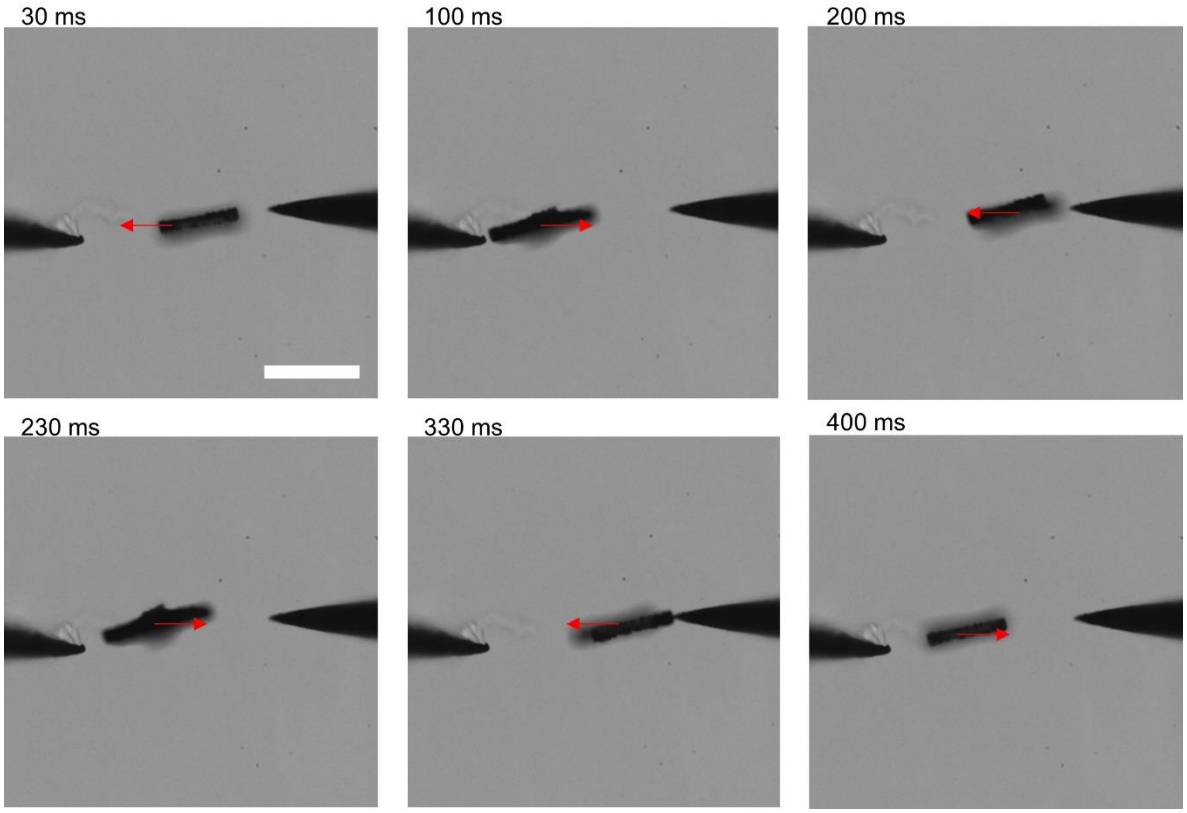

Fig. 5-7 A sequence of photos of shuriken microparticle oscillating between electrodes. The red arrows marked the motion direction. The scale bar is 100 μm.

A spinning motion was observed when the heights of two electrodes are different along the gravitational axis. This motion was stable and lasting over 6 mins. Fig. 5-8(a) showed a sequence of photos of shuriken particle spinning motion, which was shown by tracing one tip of the shuriken particle. The applied DC voltage was 95 V. Fig. 5-8(b) showed a 3D model of this motion between the two needle-shaped electrodes system, where the surfactant electrophoretic flow direction, the surfactant compensation flow direction and the spinning motion direction were showed as red, green and blue arrow, respectively. The direction of spinning motion is the same as that of surfactant convection in the system. Therefore, the spinning motion is probably caused by the electrophoresis of surfactant.

Shuriken particle showed essentially the same motions in ethanol-free solution as well. However, the voltage higher (>200 V) was required, and the reproducibility were poor.

For future application, a prototype of micromotor system (shown in Fig. 5-9) can be applied to the microelectromechanical systems. The ratchet-shaped shuriken microparticle was placed in a closed system with surfactant mixture at the center of the 4-pin microelectrode system. The closed system ensures the particle to stay at the center of the 4-pin electrodes, where the electric field intensity was relatively strong. The fast surfactant convection from the 4-pin microelectrode system will generate a rapid spinning motion of the shuriken particle at the bottom, which will also move the upper microparticle via the bar connecting both microparticles. The upper microparticle can be applied in liquid or in air as a micro-mixer, micropump, etc.

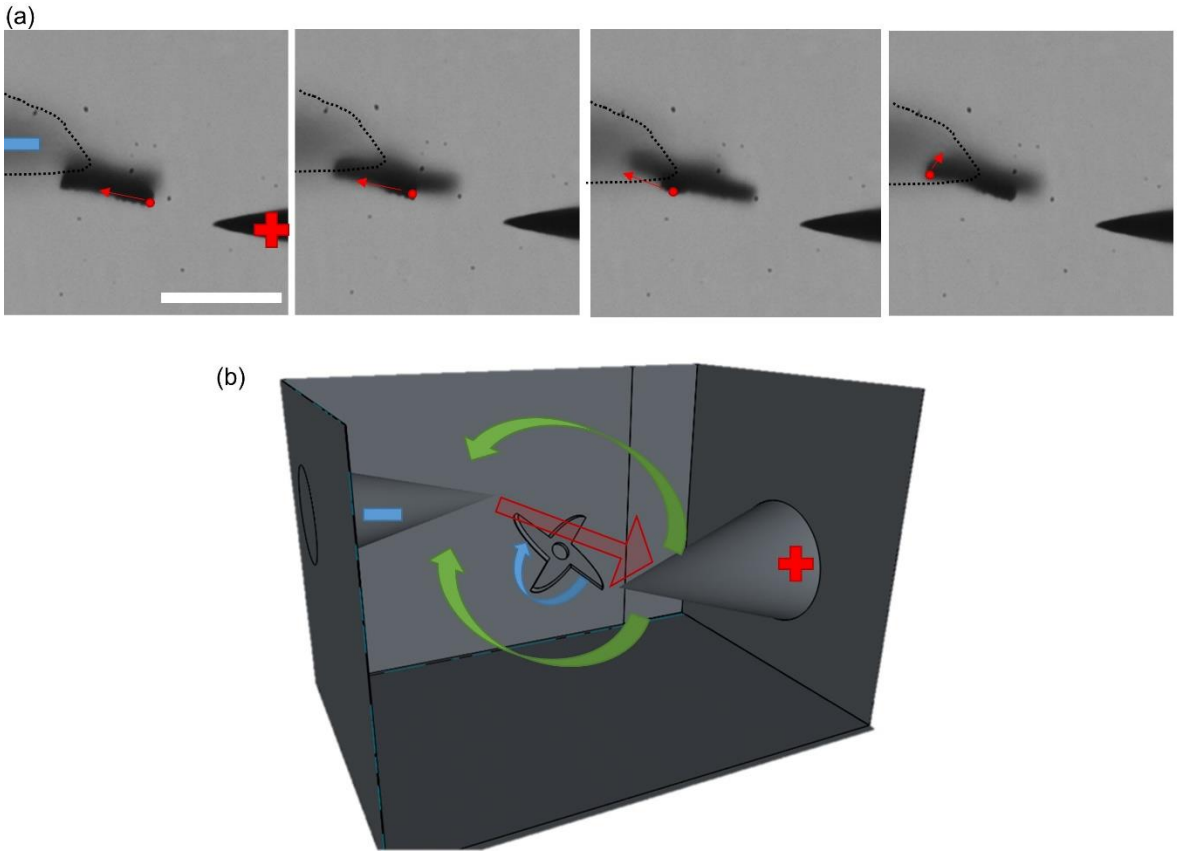

Fig. 5-8 Photos and the 3D model of the microparticle spinning motion. (a) A sequence of photos of the ratchet-shaped microparticle spinning motion. The red dot and the red arrow indicate the tip of the microparticle and the motion direction, respectively. The black dotted lines indicate the cathode that was out of focus. The scale bar was 100 μm. (b) The red arrow and the green arrows in the 3D model indicated the electrophoretic and compensation flow of surfactant, respectively. The blue arrow indicated the spinning motion direction of the microparticle.

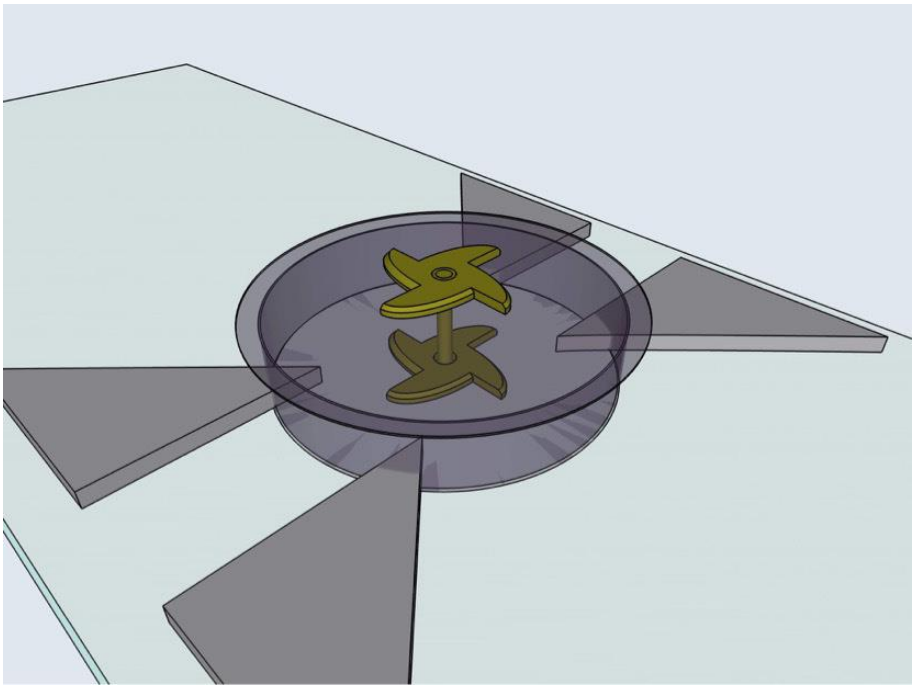

Fig. 5-9 A 3D model of the prototype of micromotor system. Ratchet-shaped microparticle “Typhoon” was placed in a closed system at the center of a 4-pin microelectrode system.

5.5 Conclusion

A 4-pin microelectrode system and a ratchet-shaped microparticle were studied for the future application of the micromotor system. Spherical micromotor was revolving in the 4-pin microelectrode system. This was caused by the electrophoretic convection that was generated by the 4-pin microelectrodes. The output power of the 4-pin this system is expected to be higher than that of two needle-shaped electrodes system, if the micromotor motion can be restricted at the center of the electrodes. the ratchet-shaped microparticle showed three types of motions in the two needle-shaped electrodes system: suspending state, oscillating and spinning motion. The suspending state may be due to the balance of attraction from each electrode. The oscillating motion may be induced by the electrophoresis of the metal microparticle that was charged by the electrodes. The spinning motion direction agree with that of the surfactant electrophoretic convection, which meant that the spinning motion was driven by the surfactant flow. For future application, to place the ratchet-shaped microparticle at the center of the 4-pin microelectrode system may lead to a rapid spinning motion This rapid motion can be applied to micro-mixing or micro-pump in the microdevices.

References:

[1] N.G. Dagalakis, T. LeBrun, J. Lippiatt, Micro-mirror array control of optical tweezer trapping beams, in: Proc. 2nd IEEE Conf. Nanotechnol., IEEE, 2002: pp. 177–180. https://doi.org/10.1109/NANO.2002.1032219.

[2] M. Zrínyi, M. Nakano, Toward Colloidal Motors, Period. Polytech. Chem. Eng. 61 (2017) 15. https://doi.org/10.3311/PPch.10274.

[3] C. Chen, E. Karshalev, J. Guan, J. Wang, Magnesium-Based Micromotors:

Water-Powered Propulsion, Multifunctionality, and Biomedical and Environmental Applications, Small. 14 (2018) 1704252. https://doi.org/10.1002/smll.201704252.

[4] E. Karshalev, B. Esteban-Fernández de Ávila, J. Wang, Micromotors for “Chemistry-on-the-Fly,” J. Am. Chem. Soc. 140 (2018) 3810–3820. https://doi.org/10.1021/jacs.8b00088.

[5] L. Zhang, T. Petit, Y. Lu, B.E. Kratochvil, K.E. Peyer, R. Pei, J. Lou, B.J. Nelson, Controlled Propulsion and Cargo Transport of Rotating Nickel Nanowires near a Patterned Solid Surface, ACS Nano. 4 (2010) 6228–6234. https://doi.org/10.1021/nn101861n.

[6] J. Wang, W. Gao, Nano/Microscale Motors: Biomedical Opportunities and Challenges, ACS Nano. 6 (2012) 5745–5751. https://doi.org/10.1021/nn3028997.

[7] L. Xie, X. Pang, X. Yan, Q. Dai, H. Lin, J. Ye, Y. Cheng, Q. Zhao, X. Ma, X. Zhang, G. Liu, X. Chen, Photoacoustic Imaging-Trackable Magnetic Microswimmers for Pathogenic Bacterial Infection Treatment, ACS Nano. 14 (2020) 2880–2893. https://doi.org/10.1021/acsnano.9b06731.

[8] R. Mundaca - Uribe, B. Esteban - Fernández de Ávila, M. Holay, P. Lekshmy Venugopalan, B. Nguyen, J. Zhou, A. Abbas, R.H. Fang, L. Zhang, J. Wang, Zinc Microrocket Pills: Fabrication and Characterization toward Active Oral Delivery, Adv. Healthc. Mater. 9 (2020) 2000900. https://doi.org/10.1002/adhm.202000900.

[9] W. Zhang, K. Ohara, Y. Okamoto, E. Nawa-okita, D. Yamamoto, A. Shioi, Energy Flux on a Micromotor Operating under Stationary Direct Current Voltage, J. Chem. Eng. Japan. 1 (2020).

[10] D. Yamamoto, A. Shioi, Self-Propelled Nano/Micromotors with a Chemical Reaction: Underlying Physics and Strategies of Motion Control, KONA Powder Part. J. 32 (2015) 2–22. https://doi.org/10.14356/kona.2015005.

[11] C. Maggi, F. Saglimbeni, M. Dipalo, F. De Angelis, R. Di Leonardo, Micromotors with asymmetric shape that efficiently convert light into work by thermocapillary effects, Nat. Commun. 6 (2015) 7855. https://doi.org/10.1038/ncomms8855.

[12] S. Zhan, R.-F. Cui, L.-Y. Qiao, J.-X. Chen, Transport of nanodimers through chemical microchip, Commun. Theor. Phys. 72 (2020) 015601. https://doi.org/10.1088/1572-9494/ab544f.

[13] M. Pacheco, M.Á. López, B. Jurado-Sánchez, A. Escarpa, Self-propelled micromachines for analytical sensing: a critical review, Anal. Bioanal. Chem. 411 (2019) 6561–6573. https://doi.org/10.1007/s00216-019-02070-z.

[14] W. Li, X. Tang, L. Wang, Photopyroelectric microfluidics, Sci. Adv. 6 (2020) eabc1693. https://doi.org/10.1126/sciadv.abc1693.

[15] N. Azizipour, R. Avazpour, D.H. Rosenzweig, M. Sawan, A. Ajji, Evolution of Biochip Technology: A Review from Lab-on-a-Chip to Organ-on-a-Chip, Micromachines. 11 (2020) 599. https://doi.org/10.3390/mi11060599.

[16] C. Tymm, J. Zhou, A. Tadimety, A. Burklund, J.X.J. Zhang, Scalable COVID-19 Detection Enabled by Lab-on-Chip Biosensors, Cell. Mol. Bioeng. 13 (2020) 313–329. https://doi.org/10.1007/s12195-020-00642-z.

[17] N.I. Khan, E. Song, Lab-on-a-Chip Systems for Aptamer-Based Biosensing, Micromachines. 11 (2020) 220. https://doi.org/10.3390/mi11020220.

[18] A. Tsopela, A. Laborde, L. Salvagnac, V. Ventalon, E. Bedel-Pereira, I. Séguy, P. Temple-Boyer, P. Juneau, R. Izquierdo, J. Launay, Development of a lab-

on-chip electrochemical biosensor for water quality analysis based on microalgal photosynthesis, Biosens. Bioelectron. 79 (2016) 568–573. https://doi.org/10.1016/j.bios.2015.12.050.

[19] O. Behrmann, M. Hügle, P. Bronsert, B. Herde, J. Heni, M. Schramm, F.T. Hufert, G.A. Urban, G. Dame, A lab-on-a-chip for rapid miRNA extraction, PLoS One. 14 (2019) e0226571. https://doi.org/10.1371/journal.pone.0226571.

[20] F. Nafian, B. Kamali Doust Azad, S. Yazdani, M.J. Rasaee, N. Daftarian, A lab - on - a - chip model of glaucoma, Brain Behav. (2020) 1–13. https://doi.org/10.1002/brb3.1799.

[21] G. Dame, J. Lampe, S. Hakenberg, G. Urban, Development of a Fast miRNA Extraction System for Tumor Analysis Based on a Simple Lab on Chip Approach, Procedia Eng. 120 (2015) 158–162. https://doi.org/10.1016/j.proeng.2015.08.593.

[22] M. Hügle, G. Dame, O. Behrmann, R. Rietzel, D. Karthe, F.T. Hufert, G.A. Urban, A lab-on-a-chip for preconcentration of bacteria and nucleic acid extraction, RSC Adv. 8 (2018) 20124–20130. https://doi.org/10.1039/C8RA02177E.

[23] H. Shintaku, H. Nishikii, L.A. Marshall, H. Kotera, J.G. Santiago, On-Chip Separation and Analysis of RNA and DNA from Single Cells, Anal. Chem. 86 (2014) 1953–1957. https://doi.org/10.1021/ac4040218.

[24] S. Dekker, P.K. Isgor, T. Feijten, L.I. Segerink, M. Odijk, From chip-in-a-lab to lab-on-a-chip: a portable Coulter counter using a modular platform, Microsystems Nanoeng. 4 (2018) 34. https://doi.org/10.1038/s41378-018-0034-1.

[25] F.W.M. Ling, A.A. Khleif, H.A. Abdulbari, Investigating the effect of micro-

riblets on the flow and micro-mixing behavior in micro-channel, Chem. Eng. Commun. 411 (2020) 1–14. https://doi.org/10.1080/00986445.2020.1715959.

[26] M.K. Masukawa, M. Hayakawa, M. Takinoue, Surfactant concentration modulates the motion and placement of microparticles in an inhomogeneous electric field, RSC Adv. 10 (2020) 8895–8904. https://doi.org/10.1039/D0RA00703J.

[27] D. Yamamoto, K. Kosugi, K. Hiramatsu, W. Zhang, A. Shioi, K. Kamata, T. Iyoda, K. Yoshikawa, Helical micromotor operating under stationary DC electrostatic field, J. Chem. Phys. 150 (2019) 014901. https://doi.org/10.1063/1.5055830.

[28] T. Kurimura, M. Ichikawa, M. Takinoue, K. Yoshikawa, Back-and-forth micromotion of aqueous droplets in a dc electric field, Phys. Rev. E. 88 (2013) 042918. https://doi.org/10.1103/PhysRevE.88.042918.

Chapter 6

Conclusion

A quantification method for the performance and energy conversion efficiency of the micromotor system was proposed, and a micromotor system as a prototype of future adaptation in microelectromechanical systems was discussed.

In a two needle-shaped electrodes system, a water droplet was moving back-and-forth between electrodes under a direct current voltage. Two types of back-and-forth motion modes were observed: oscillating and bouncing. When the diameter of the droplet was larger than 20% of electrodes distance, oscillating-type back-and-forth motion was observed, otherwise, bouncing motion was observed. During the back-and-forth motion of the droplet, the acceleration increased when the droplet moved near the anode/cathode. The volume of the droplet was found to decrease with time when the droplet moved due to electrolysis. A quantification method was proposed to calculated the kinetic energy output of the droplet from Stokes' drag equation and the electric energy input. The energy conversion efficiency was thus quantified, and it has become clear that the efficiency was significantly small. This is attributable to the electrochemical process of electrolysis.

To improve the efficiency of the micromotor system, a solid, chemically inert, spherical micromotor made from polyethylene was used. Revolving and spinning motions were observed for this micromotor. The output power of the revolving and spinning motions was calculated based on viscous drag and viscous torque, respectively. The total output power of a spherical micromotor was assumed to be the sum of these two output powers. The output power increased with an increase in applied voltage. The dependency of the output power on the surfactant concentration indicated an increase in output power in the low concentration, but a decrease was observed in the high concentrations. The increment in the output power of the micromotors was probably due to the effect of surfactant electrophoretic flow, which

was enhanced by higher voltage and higher surfactant concentration. The decrease in the output power was not considered to be the result of the increased viscosity of solutions. An asymptotic tendency of the output power was observed in a highly concentrated surfactant solution compared with the pure surfactant solution, suggesting that the decrease was caused by the high surfactant ratio. Moreover, the electric energy input to the system was calculated. As a result, the energy conversion efficiency of a spherical micromotor system was quantified.

The effect of the additional solvent, ethanol, on the output power and energy conversion efficiency of a spherical micromotor was studied. The output power of the microparticle in the ethanol-added system increased compared to that in the ethanol-free system. However, the electric current increased, which was caused by the higher conductivity of the solution. As a result, the energy conversion efficiency was lower in the ethanol-added system. In the liquid micromotor system, the lower conversion efficiency does not necessarily correspond to lower output power.

In comparison, the output power of water droplet and ethanol-added solid micromotor systems were higher, which means these systems had better performance. However, the energy conversion efficiency of ethanol free micromotor system was higher due to the chemically inert motor and low conductivity solution. Such comparisons were difficult without the quantification method proposed in this study. The quantification method proposed in this study can become a universal tool for micromotor studies. It enables the comparisons between different micromotor systems on energy levels, irrespective of the size, velocity, angular velocity of the micromotors, viscosity of the solution, or types of input energy to the system. The energy conversion efficiency, as a representation of energy flux of the system, also provides guidelines

for micromotor system development and will improve the progress of micromotor systems.

A 4-pin microelectrode system and a ratchet-shaped microparticle were studied for the future application of the micromotor system. Spherical micromotor was revolving in the 4-pin microelectrode system. This was caused by the electrophoretic convection that was generated by the 4-pin microelectrodes. The output power of the 4-pin this system is expected to be higher than that of two needle-shaped electrodes system, if the micromotor motion can be restricted at the center of the electrodes. The ratchet-shaped microparticle showed three types of motions in the two needle-shaped electrodes system: suspending state, oscillating and spinning motion. The suspending state may be due to the balance of attraction from each electrode. The oscillating motion may be induced by the electrophoresis of the metal microparticle that was charged by the electrodes. The spinning motion direction agree with that of the surfactant electrophoretic convection, which meant that the spinning motion was driven by the surfactant flow. For future application, to place the ratchet-shaped microparticle at the center of the 4-pin microelectrode system may lead to a rapid spinning motion This rapid motion can be applied to micro-mixing or micro-pump in the microdevices.

Acknowledgement

Throughout the writing of this dissertation I have received a great deal of support and assistance.

First and foremost, I am extremely grateful to my supervisor, Professor Akihisa Shioi for his advice, continuous support, and patience during my PhD study. Prof. Shioi's immense knowledge and plentiful experience have encouraged me in all the time of my academic research and daily life. His expertise was invaluable in formulating the research questions and methodology. Thank you for your insightful feedback which pushed me to sharpen my thinking and brought my work to a higher level.

My gratitude extends to Prof. Daigo Yamamoto and Prof. Erika Nawa-Okita for their support in my study. Prof. Kenichi Yoshikawa, Prof. Tomokazu Iyoda, and Prof. Katsumi Tsuchiya for their wisdom and patience with me during our discussions. Prof. Mitsuaki Ueda from the Global Resource Management (GRM) Program of Doshisha University, and Prof. Masahiro Takinoue from Tokyo Institute of Technology for the internship opportunities and to the GRM Program for the funding.

I would like to express gratitude to Dr. Yasunao Okamoto for being a great mentor not only to my PhD study but also to my daily life in Japan as a foreign student. To my micromotor research team members Kazuya Hiramatsu, Kento Kosugi, Takahiro Kozaki, Ichiro Kakimoto, Shunsuke Tamura, Hiroki Mimoto, Masahiko Yamada, Kohei Ohara, Yohei Takikawa for a cherished time spent together in the lab. My appreciation also goes out to my friends and colleagues for their encouragement and support all throughout my studies.

I would like to give a special thanks to Elvi "Jojee" Dumayaca and her family. Jojee, thank you for bringing color back to my life four years ago. Thank you for

bringing me flowers that made my days, for singing me songs when I was going through dark times. Thank you for your carrot cakes and sourdough bread when I was too busy writing my dissertation, and for being the one in my life whom I can make silly jokes and also discuss science and philosophy with. Thank you, Mr. and Mrs. Dumayaca, Kuya Joel, JJ and JM for your warm acceptance into your family.

Last but not least, I would like to thank my parents. I would never be who I am today without them. When my father was 13 years old, he and his brothers would start their day at 3 am as construction workers, building the roads in my city brick by brick. When I was 13 years old, he would drive me to school every day on his motorbike in the early morning, and then catch some sleep in his office before work. During our family's difficult times, my mother had to struggle between jobs. She would sell breakfast in the cold winter morning at the bus stations and would still be able to take care of me. Between my father and mother, they had 15 different jobs throughout their lives. I never realized how much I have learned from them until I reached my PhD years. Looking back, I realized the reason for my success, the reason that I have never given up, is because I learned persistence from them. It is like the old saying in Cantonese: "fight through it no matter how hard", my parents never gave up. They keep on fighting for a better life, and so will I.

頂硬上。

To the ones we started out with, thank you. To the ones we end up with, thank you. And to the ones we gain along the way, thank you.

Wenyu Zhang

2021

List of Publications

Chapter 2:

W. Zhang, T. Kozaki, I. Kakimoto, D. Yamamoto, K. Yoshikawa, A. Shioi, Energy consumption and conversion efficiency for a micromotor under DC voltage, Colloids Surfaces A Physicochem. Eng. Asp. 607 (2020) 125496. https://doi.org/10.1016/j.colsurfa.2020.125496.

Chapter 3:

W. Zhang, K. Ohara, Y. Okamoto, E. Nawa-Okita, D. Yamamoto, and A. Shioi, Energy Flux on a Micromotor Operating under Stationary Direct Current Voltage, Colloids Surfaces A Physicochem. Eng. Asp. *In press*.

Chapter 4:

W. Zhang, Y. Okamoto, D. Yamamoto, A. Shioi, Energy Conversion Efficiency of Micromotor System, Chem. Lett, (2021), 50 (2021) 661–663. https://doi.org/10.1246/cl.200753